

DESTRUCTION OF PERCHLORATE AND NITRATE BY STABILIZED ZERO-
VALENT IRON NANOPARTICLES AND IMMOBILIZATION
OF MERCURY BY A NEW CLASS OF IRON
SULFIDE NANOPARTICLES

Except where reference is made to the work of others, the work described in this dissertation is my own or was done in the collaboration with my advisory committee. This dissertation does not include proprietary or classified information.

Zhong Xiong

Certificate of approval:

Mark O. Barnett
Associate Professor
Civil Engineering

Dongye Zhao, Chair
Associate Professor
Civil Engineering

Willie F. Harper Jr.
Associate Professor
Civil Engineering

Ram B. Gupta
Professor
Chemical Engineering

German Mills
Associate Professor
Chemistry and Biochemistry

Joe F. Pittman
Interim Dean
Graduate School

DESTRUCTION OF PERCHLORATE AND NITRATE BY STABILIZED ZERO-
VALENT IRON NANOPARTICLES AND IMMOBILIZATION
OF MERCURY BY A NEW CLASS OF IRON
SULFIDE NANOPARTICLES

Zhong Xiong

A Dissertation

Submitted to

the Graduate Faculty of

Auburn University

in Partial Fulfillment of the

Requirements for the

Degree of

Doctor of Philosophy

Auburn, Alabama
December 17, 2007

DESTRUCTION OF PERCHLORATE AND NITRATE BY STABILIZED ZERO-
VALENT IRON NANOPARTICLES AND IMMOBILIZATION
OF MERCURY BY A NEW CLASS OF IRON
SULFIDE NANOPARTICLES

Zhong Xiong

Permission is granted to Auburn University to make copies of this dissertation at its discretion, upon request of individuals or institutions and at their expense. The author reserves all publication rights.

Signature of Author

Date of Graduation

VITA

Zhong Xiong, son of Bangmin Xiong and Xiaoying Hu, was born in a small village near Nanchang City, Jiangxi Province, China on February 7, 1979. He received a B.S. and a M.S. degree of Environmental Engineering in 2000 and 2003, respectively, both from Chongqing University in Chongqing, China. Starting from January 2004, He has been pursuing his Ph.D. degree at Auburn University. During the four-year stay at Auburn, he has produced two patent-pending technologies, five papers in prominent journals such as Water Research, Industrial Engineering Chemistry Research, Separation Science and Technology, Environmental Science and Technology, and six publications/presentations at various national and international conferences. He feels honored to be selected as a recipient of four eminent awards including the Graduate Student Award in Environmental Chemistry (2007), CH2M HILL Fellowship for Outstanding Ph.D. Students (2006), Third Place Poster Presentation at Alabama Water Resource Conference (2005), and Dean's Fellowship (2004).

DISSERTATION ABSTRACT

DESTRUCTION OF PERCHLORATE AND NITRATE BY STABILIZED ZERO-
VALENT IRON NANOPARTICLES AND IMMOBILIZATION
OF MERCURY BY A NEW CLASS OF IRON
SULFIDE NANOPARTICLES

Zhong Xiong

Doctor of Philosophy, December 17, 2007
(M. S. Chongqing University, China, 2003)
(B. S. Chongqing University, China, 2000)

204 Typed Pages

Directed by Dongye Zhao

This research compares representative standard strong-base anion (SBA) and weak-base anion (WBA) exchangers, a bifunctional resin (A-530E), a class of polymeric ligand exchangers (PLE's), and an ion-exchange fiber (IXF) with respect to perchlorate sorption capacity, kinetics, and regenerability. The sequence of the perchlorate sorption capacity factor (A_f) follows: A-530E >> IRA 900 > DOW 66 > Smopex-103x > DOW 3N-Cu >> WA21J > DOW 3N > XAD1180 3N-Cu >> XAD7HP 3N-Cu \approx IRA 958. The sequence of the ion-exchangers' regeneration efficiency is IRA 958 > WA21J > XAD7HP 3N-Cu > IRA 900 > DOW 3N-Cu > A-530E.

A new class of stabilized zero-valent iron (ZVI) nanoparticles was developed and used for complete destruction of perchlorate in both fresh water and ion-exchange brine.

The stabilized ZVI nanoparticles were prepared successfully using a low-cost and food-grade carboxymethyl cellulose (CMC) as a stabilizer and were used for perchlorate reduction. The mean diameter of stabilized ZVI nanoparticles was 13.7 ± 2.3 nm. Batch kinetic tests showed that at an iron dose of 1.8 g/L and at moderately elevated temperatures (90-95 °C), ~90% of perchlorate in both fresh water and a simulated ion-exchange brine (NaCl=6% (w/w)) was transformed within 7 hours.

The stabilized ZVI nanoparticles were also tested for reductive transformation of nitrate in fresh water and ion-exchange brine. The observed pseudo first-order rate constant (k_{obs}) for nitrate reduction with the stabilized ZVI nanoparticles was more than 5 times greater than that for non-stabilized ZVI particles. With a ZVI-to-NO₃⁻ molar ratio of 2.5, N₂-N accounted for two thirds (66%) of the nitrate reduction products, 30% greater than that with a ZVI-to-NO₃⁻ molar ratio of 3.9.

An innovative *in-situ* mercury (Hg) immobilization technology using stabilized iron sulfide (FeS(s)) nanoparticles was investigated in this study. The FeS(s) nanoparticles were successfully prepared using carboxymethyl cellulose (CMC) as the stabilizer. The particle size of freshly prepared FeS(s) nanoparticles was measured to be 38.5 ± 5.4 nm. Column tests proved that the stabilized FeS(s) nanoparticles reduced the mercury leachability of the Hg-laden sediment by as much as 66.7% and the extracted Hg in TCLP solutions was reduced by 76.9% when the sediments was treated with 0.5 g/L stabilized FeS(s) nanoparticles. Column tests also proved that stabilized FeS(s) nanoparticles were highly mobile in a clay loam sediment and ~100% of FeS(s) nanoparticles passed through the sediment with 18.4 PV's (pore volumes) of 0.5 g/L stabilized FeS(s) nanoparticles.

ACKNOWLEDGEMENTS

First of all, I would like to acknowledge my dissertation advisor Dr. Dongye Zhao for his support, guidance, inspiration, motivation, and friendship. I had trouble getting my visa to enter the U.S. in Summer 2003. Thanks for his continuous and unconditional help, I was able to get into this country and start a new life here at Auburn. He identified important aspects of my research, directed me to translate them into my doctoral dissertation, and secured funding to allow me research them. I have learned a lot from his expertise of environmental engineering and chemistry. Especially, I sincerely appreciate the benefits I get from his input of time and energy helping me on the publications.

I'd like to thank Drs. Mark O. Barnett, Willie F. Harper Jr., Ram B. Gupta, German Mills, and Virginia A. Davis for their services on my Ph.D. committee, inspiring comments and discussion. It is my pleasure working with them. Without the help and support of my labmates, this dissertation would not have been possible. I'd especially like to thank Dr. Feng He and Jinling Zhuang for their experimental and analytical assistance. I would also like to thank Taerwoo Yi, Dr. Yinghui Xu, Dr. Ruiqiang Liu, Byungryul An, Thomas Steinwinder, Chunhui Luo, Man Zhang, Qiqi Liang, Dr. Sushi Kanel, Dr. Sunghee Joo, as well as other members of environmental engineering program here at AU for their research advices and for creating a supportive environment.

Finally, I'd like to thank my wife, Zhenni Li, for her encouragement, support and love. Thanks are also due to other family members for their support during the course of my study.

Style manual or journal used Water Research

Computer software used Microsoft Word & Excel 2002; SigmaPlot 8.0.

TABLE OF CONTENTS

LIST OF TABLES.....	xiii
LIST OF FIGURES.....	xiv
CHAPTER 1. GENERAL INTRODUCTION	1
1.1 Groundwater Contamination.....	1
1.2 Soil Contamination	2
1.3 Objectives	3
1.4 Organization.....	5
CHAPTER 2. REMOVAL OF PERCHLORATE FROM CONTAMINATED WATER BY USE OF ION EXCHANGERS	7
2.1 Introduction.....	7
2.2 Materials and Methods.....	11
2.3 Results and Discussion	16
2.3.1 Equilibrium sorption isotherms.....	16
2.3.2 Fixed bed column run with DOW 3N-Cu.....	26
2.3.3 Sorption kinetics	28
2.3.4 Effect of pH on perchlorate uptake	33
2.3.5 Perchlorate desorption from various resins.....	35
2.3.7 Effect of ethanol on perchlorate desorption.....	37
2.3.8 Effect of pH on perchlorate desorption.....	39

2.3.9 Effects of resin morphology: Porous beads versus fibers	42
2.4 Conclusions.....	44
CHAPTER 3. COMPLETE DESTRUCTION OF PERCHLORATE IN WATER AND ION-EXCHANGE BRINE USING STABILIZED ZERO-VALENT IRON NANOPARTICLES.....	
	46
3.1 Introduction.....	46
3.2 Materials and Methods.....	49
3.3 Results and Discussion	53
3.3.1. Characterization of nanoparticles	53
3.3.2. Kinetics and activation energy of perchlorate reduction	55
3.3.3. Chlorine mass balance and reaction completeness	62
3.3.4. Perchlorate reduction by various iron nanoparticles.....	64
3.3.5. Effect of background chloride or salinity	68
3.3.6. Effect of pH on perchlorate reduction	71
3.3.7 Effect of UV light	73
3.4 Summary and Conclusions	74
CHAPTER 4. RAPID AND CONTROLLED TRANSFORMATION OF NITRATE IN WATER AND BRINE BY STABILIZED ZERO-VALENT IRON NANOPARTICLES.....	
	76
4.1 Introduction.....	76
4.2 Materials and Methods.....	80
4.3 Results and Discussion	82

4.3.1 Nitrate reduction with CMC-stabilized and non-stabilized ZVI nanoparticles	82
4.3.2 Effect of ZVI-to-NO ₃ ⁻ molar ratio on nitrate reduction rate and pathways	88
4.3.3 Effect of metal catalysts.....	95
4.3.4 Effect of stabilizer-to-ZVI molar ratio on reactivity of nanoparticles.....	98
4.3.5 Effect of pH on nitrate reduction	100
4.3.6 Effect of salinity on nitrate reduction	104
4.4 Summary and Conclusions	108
CHAPTER 5. <i>IN-SITU</i> MERCURY IMMOBILIZATION IN SEDIMENT BY STABILIZED IRON SULFIDE NANOPARTICLES	
5.1 Introduction.....	110
5.2 Materials and Methods.....	114
5.3 Results and Discussion	119
5.3.1 Characterization of stabilized FeS(s) nanoparticles and the role of stabilizer	119
5.3.2 Immobilization of mercury by stabilized FeS(s) nanoparticles: batch tests	123
5.3.3 Mobility of stabilized FeS(s) nanoparticles in a sediment column.....	129
5.3.4 Immobilization of mercury by stabilized FeS(s) nanoparticles: column tests	131
5.3.5 Implication to in-situ mercury remediation	137
5.4 Summary and Conclusion.....	137

CHAPTER 6. CONCLUSIONS AND SUGGESTIONS FOR FUTURE	
RESEARCH.....	139
6.1 Summary and Conclusions	139
6.2 Suggestions for Future Work.....	142
REFERENCES	144
APPENDIX A ADDITIONAL EXPERIMENTAL RESULTS.....	170
APPENDIX B KINETIC MODELING OF PERCHLORATE UPTAKE BY DOW 3N-	
CU	181

LIST OF TABLES

Table 2-1. Salient properties of various sorbents used in this study.....	12
Table 2-2. Salient properties of polymeric sorbents used for preparing PLE's.....	13
Table 2-3. Freundlich model parameters, the capacity factor A_f , binary separation factor, and total ion-exchange capacity of various ion-exchangers. (Errors given as standard deviation).	17
Table 3-1. Observed pseudo-first-order rate constant of perchlorate reduction by CMC-stabilized iron nanoparticles at various temperatures.	59
Table 3-2. Physical parameters and perchlorate reduction rate constants for various iron nanoparticles at 110 °C.	66
Table 4-1. Model-fitted pseudo-first-order rate constants of nitrate reduction under various experimental conditions.	86
Table 4-2. Summary of nitrate reduction rate constants by various ZVI particles in the literature.	87
Table 5-1. Composition of the mercury-laden sediments.....	116

LIST OF FIGURES

Figure 2-1a. Perchlorate sorption isotherms for a strong-base polystyrene-based resin (IRA 900), a strong-base polyacrylic resin (IRA 958), and three PLE's (DOW 3N-Cu, XAD7HP 2N-Cu, and XAD1180 3N-Cu). Initial $\text{ClO}_4^- = 10 \text{ mg/L}$, $\text{SO}_4^{2-} = 100 \text{ mg/L}$. Maximum final $\text{Cl}^- = 21-77 \text{ mg/L}$. Solution pH was kept at 7.0 ± 0.1 during the tests. (Symbols: experimental data; Lines: Freundlich model fitting).....	18
Figure 2-1b. Perchlorate sorption isotherms for a bifunctional resin (A-530E), an IXF (Smopex-103x), a chelating resin (DOW 3N), and two WBA resins (DOW 66, WA21J). Initial $\text{ClO}_4^- = 10 \text{ mg/L}$, $\text{SO}_4^{2-} = 100 \text{ mg/L}$. Maximum final $\text{Cl}^- = 21-77 \text{ mg/L}$. Solution pH was kept at 7.0 ± 0.1 during the tests. (Symbols: experimental data; Lines: Freundlich model fitting).....	19
Figure 2-2. Schematic illustration of binding mechanisms of perchlorate with various ion exchangers.....	24
Figure 2-3. Fixed-bed column runs' breakthrough history curves of a multi-component system using DOW 3N-Cu.	27
Figure 2-4. Kinetics of perchlorate sorption by various ion exchangers (A-530E, DOW 66, DOW 3N-Cu, IRA 958, IRA 900, and XAD1180 3N-Cu). Initial $\text{ClO}_4^- = 10 \text{ mg/L}$, $\text{SO}_4^{2-} = 100 \text{ mg/L}$ and pH was kept at 7.0 ± 0.1 . (Symbols: experimental data; Lines: model fitting).	31

Figure 2-5. Comparison of perchlorate sorption rate for an ion-exchange fiber (Smopex-103x) and two ion exchange resins (A-530E, IRA 900). Initial $\text{ClO}_4^- = 10 \text{ mg/L}$, $\text{SO}_4^{2-} = 100 \text{ mg/L}$ and pH was kept at 7.0 ± 0.1 .	32
Figure 2-6. Perchlorate sorption onto DOW 3N-Cu, IRA 900, and WA21J as a function of pH in the presence of competing sulfate ions. Initial $\text{ClO}_4^- = 10 \text{ mg/L}$, $\text{SO}_4^{2-} = 100 \text{ mg/L}$.	34
Figure 2-7. Regeneration of perchlorate-laden ion-exchangers (A530-E, IRA 958, IRA 900, DOW 3N-Cu, and XAD7HP 3N-Cu) with a regenerant containing 12% (w/w) NaCl and 10% (v/v) of ethanol at pH 10.5. Empty bed contact time (EBCT) = 30 min; superficial liquid velocity (SLV) = 0.025 m/hr.	36
Figure 2-8. Regeneration of perchlorate-laden DOW 3N-Cu by a regenerant containing 12% (w/w) NaCl at pH 10.5 and various concentrations of ethanol. EBCT = 30 min; SLV = 0.025 m/hr.	38
Figure 2-9. Regeneration of perchlorate-laden DOW 3N-Cu with a regenerant containing 12% (w/w) NaCl at various pH. EBCT = 30 min; SLV = 0.025 m/hr.	40
Figure 2-10. Regeneration of perchlorate-laden WA21J with a regenerant containing 12% (w/w) NaCl and 10% (v/v) ethanol at various pH. EBCT = 30 min; SLV = 0.025 m/hr.	41
Figure 2-11. Regeneration of perchlorate-laden Smopex-103x with a regenerant containing 12% (w/w) NaCl at neutral pH. EBCT = 30 min; SLV = 0.025 m/hr.	43
Figure 3-1. TEM image of fresh ZVI nanoparticles stabilized with 0.9% (w/w) CMC. The scale bar represents 100 nm.	54

Figure 3-2. Perchlorate reduction by CMC-stabilized ZVI nanoparticles at various temperatures. Initial $[\text{ClO}_4^-] = 10 \text{ mg/L}$, ZVI = 1.8 g/L, CMC = 0.9% (w/w), initial pH (pH_0) = 6.5, and final pH (pH_f) = 7.5-7.8. Control tests were performed at 110 °C with no ZVI. Data plotted as mean of duplicates..... 57

Figure 3-3. Fitting a pseudo-first-order model to the experimental perchlorate reduction rate data of Figure 3-2. Symbols: experimental data; lines: model fittings. 60

Figure 3-4. Linearized Arrhenius plot of the observed first-order rate constant (Table 3-1) as a function of $1/T$ 61

Figure 3-5. Chlorine mass balance during perchlorate reduction by CMC-stabilized ZVI nanoparticles. Initial $[\text{ClO}_4^-] = 10 \text{ mg/L}$, ZVI dose = 1.8 g/L, CMC = 0.9% (w/w), $\text{pH}_0 = 6.6-6.8$ and $\text{pH}_f = 7.7-7.8$. Data plotted as mean of duplicates. 63

Figure 3-6. Perchlorate reduction by various ZVI-based particles. For all cases: ZVI dose = 1.8 g/L, initial $[\text{ClO}_4^-] = 10 \text{ mg/L}$, $\text{pH}_0 = 6.5-6.8$, $\text{pH}_f = 7.5-7.8$, and temperature = 110 °C; for stabilized ZVI nanoparticles, starch or CMC = 0.9% (w/w); for Fe-Pd bimetallic nanoparticles, Pd = 0.3% of Fe (w/w). Data plotted as mean of duplicates. 65

Figure 3-7. Perchlorate reduction by CMC-stabilized ZVI nanoparticles in the presence of various background chloride concentrations at 95 °C. Initial $[\text{ClO}_4^-] = 100 \text{ mg/L}$, ZVI dose = 1.8 g/L, CMC = 0.9% (w/w), $\text{pH}_0 = 6.5-6.8$, and $\text{pH}_f = 7.5-7.8$. Data plotted as mean of duplicates..... 70

Figure 3-8. Effect of pH on perchlorate reduction by CMC-stabilized ZVI nanoparticles in the presence of 6% NaCl (w/w) at 95 °C. Initial $[\text{ClO}_4^-] = 100 \text{ mg/L}$, ZVI dose =

1.8 g/L, CMC = 0.9% (w/w). The pH given refers to initial and final pH. Data plotted as mean of duplicates.....	72
Figure 4-1. Reduction of nitrate by non-stabilized ZVI and CMC-stabilized ZVI nanoparticles. Initial nitrate concentration (C_0) = 200 mg/L, ZVI = 0.7 g/L (ZVI-to- NO_3^- = 3.9), CMC = 0.63% (w/w). Solution pH was controlled at 7.0~7.5 (initial and final) with a 0.05 M HEPES buffer. Data plotted as mean of duplicates.	84
Figure 4-2. Effect of ZVI-to- NO_3^- molar ratios on nitrate reduction by CMC-stabilized ZVI nanoparticles. In all cases, ZVI = 0.7 g/L, CMC = 0.63%. Three initial nitrate concentrations were: NO_3^- = 310 mg/L, 200 mg/L, and 150 mg/L. Solution pH was controlled at 7.0~7.5 (initial and final) with a 0.05 M HEPES buffer. Data plotted as mean of duplicates.	89
Figure 4-3a. Evolution of nitrate and ammonium concentrations (normalized to initial nitrate concentration, C_0) during nitrate reduction by CMC-stabilized ZVI nanoparticles at a ZVI-to- NO_3^- molar ratio of 2.5 (ZVI = 0.7 g/L; NO_3^- = 310 mg/L). CMC = 0.63% and solution pH was controlled at 7.0~7.5 (initial and final) with a 0.05 M HEPES buffer. Data plotted as mean of duplicates.....	93
Figure 4-3b. Evolution of nitrate and ammonium concentrations (normalized to initial nitrate concentration, C_0) during nitrate reduction by CMC-stabilized ZVI nanoparticles at a ZVI-to- NO_3^- molar ratio of 3.9 (ZVI = 0.7 g/L; NO_3^- = 200 mg/L). CMC = 0.63% and solution pH was controlled at 7.0~7.5 (initial and final) with a 0.05 M HEPES buffer. Data plotted as mean of duplicates.....	94
Figure 4-4. Effect of metal catalysts on nitrate reduction by CMC-stabilized ZVI nanoparticles at a ZVI-to- NO_3^- molar ratio of 3.9 (ZVI = 0.7 g/L; NO_3^- = 200 mg/L,	

CMC = 0.63%). Doses of catalysts are given as weight percentage of ZVI (w/w of Fe). Solution pH was controlled at 7.0~7.5 (initial and final) with a 0.05 M HEPES buffer. Data plotted as mean of duplicates..... 97

Figure 4-5. Effect of CMC concentrations (CMC-to-ZVI molar ratios) on nitrate reduction by CMC-stabilized ZVI nanoparticles. Initial nitrate concentration = 150 mg/L and ZVI = 0.7 g/L (ZVI-to-NO₃⁻ = 5.2). Solution pH was controlled at 7.0~7.5 (initial and final) with a 0.05 M HEPES buffer. Data plotted as mean of duplicates. 99

Figure 4-6a. Effect of solution pH on nitrate reduction by CMC-stabilized ZVI nanoparticles during nitrate reduction. Numbers in the parentheses refer to initial and final pH values. ZVI = 0.7 g/L, NO₃⁻ = 200 mg/L (ZVI-to-NO₃⁻ = 3.9), CMC = 0.63%. Data plotted as mean of duplicates. 102

Figure 4-6b. pH evolution during nitrate reduction by CMC-stabilized ZVI nanoparticles. ZVI = 0.7 g/L, NO₃⁻ = 200 mg/L (ZVI-to-NO₃⁻ = 3.9), CMC = 0.63%. Data plotted as mean of duplicates. 103

Figure 4-7. Nitrate reduction by CMC-stabilized ZVI nanoparticles in the presence of various concentrations of NaCl. Initial nitrate concentration = 150 mg/L, ZVI = 0.7 g/L (ZVI-to-NO₃⁻ = 5.2), CMC = 0.63%. Solution pH was controlled at 7.0~7.5 (initial and final) with a 0.05 M HEPES buffer. Data plotted as mean of duplicates. 106

Figure 4-8. Concentration histories of various nitrogenous species during nitrate reduction by CMC-stabilized ZVI nanoparticles in the presence of 6% NaCl (w/w). Initial nitrate concentration = 150 mg/L, ZVI = 0.7 g/L (ZVI-to-NO₃⁻ = 5.2), CMC =

0.63%. All concentration was normalized to C_0 . Solution pH was controlled at 7.0~7.5 (initial and final) with a 0.05 M HEPES buffer. Data plotted as mean of duplicates.	107
Figure 5-1. TEM images of FeS(s) particles prepared without a stabilizer (a), and with 0.2% (w/w) CMC (b). FeS(s) particles were prepared freshly in water and FeS(s) = 0.5 g/L in both cases. The scale bar represents 200 nm.....	121
Figure 5-2. Histogram showing the size distribution of the CMC-stabilized FeS(s) nanoparticles for a random sample of 247 particles.	122
Figure 5-3. Mercury concentration in the aqueous phase when the Hg-laden sediment was treated with various doses (expressed as FeS(s)/Hg molar ratio) of the stabilized FeS(s) nanoparticles for 1 week. The pH was controlled at 7 with 0.1 N HCl and/or 0.1 N HNO ₃ . Control test was also carried out by using a solution containing 0.2% CMC and 0.1 M NaNO ₃ but no FeS(s) nanoparticles. Data plotted as mean of duplicates.	125
Figure 5-4. Mercury concentration in the TCLP extractant from the sediments that were treated with various doses of the stabilized FeS(s) nanoparticles. Data plotted as mean of duplicates.	126
Figure 5-5. The breakthrough curves of a tracer (KBr) and FeS(s) nanoparticles in a clay loam sediment column. The initial KBr concentration was 0.05 g/L and the initial stabilized FeS(s) nanoparticles concentration was 0.5 g/L stabilized with 0.2% CMC. The Empty Bed Contact Time (EBCT) = 30 min and Superficial Liquid Velocity (SLV) = 0.13 cm/min.....	130

Figure 5-6. Mercury leached from a low-Hg content clay loam sediment by an influent with or without the presence of the stabilized FeS(s) nanoparticles. 0.5 g/L FeS(s) nanoparticles stabilized with 0.2% CMC were used to treat the sediment. A solution containing 0.2% CMC and 0.1 M NaNO ₃ was used as a control. EBCT = 30 min and SLV = 0.13 cm/min.....	134
Figure 5-7. Mercury leached from a high-Hg content clay loam sediment by an influent with or without the presence of the stabilized FeS(s) nanoparticles. 0.5 g/L FeS(s) nanoparticles stabilized with 0.2% CMC were used to treat the sediment. A solution containing 0.2% CMC and 0.1 M NaNO ₃ was used as a control. EBCT = 30 min and SLV = 0.13 cm/min.	135
Figure 5-8. Mercury concentration in the TCLP extractant from a low-Hg and a high-Hg content clay loam sediments that was treated with the stabilized FeS(s) nanoparticles or from the control tests. TCLP fluid #1 was used as the extractant and the reaction time was 18 hours. Data plotted as mean of duplicates.	136
Figure A-1. Validation of ion-exchange stoichiometry with DOW3 N-Cu in perchlorate-chloride system.	170
Figure A-2. Plot of regeneration efficiency of exhausted DOW 3N-Cu versus pH grouped by regenerant.....	171
Figure A-3. Plot of percent Cu loss from DOW 3N-Cu versus pH for different regenerants.	172
Figure A-4. Perchlorate elution curves for the regeneration of DOW 3N-Cu, A-530E, A-520E, and P4VP with 12% brines or 11% NaCl/1% NaOH at an EBCT of 21 ± 1 minutes.....	173

Figure A-5. Regeneration efficiency curves for DOW 3N-Cu, A-530E, A-520E, and P4VP with 12% brines and an EBCT of 21±1 minutes.	174
Figure A-6. DOW 3N-Cu regeneration breakthrough and efficiency curves varying salt brine composition regenerated at an EBCT of 20.4 ± 0.4 minutes.	175
Figure A-7. Perchlorate elution and regeneration efficiency curves for DOW 3N-Cu with regenerate solutions composed of 4%NaCl, 2% NaOH and solvents containing a combination of water, Tween 80, and ethanol regenerated at an EBCT of 20.4 ± 0.4 minutes.	176
Figure A-8. Catast effect on ammonium production during nitrate reduction by CMC-stabilized ZVI nanoparticles. Initial nitrate concentration = 200 mg/L, ZVI= 0.7 g/L (ZVI-to-NO ₃ ⁻ = 3.9), CMC = 0.63%. Solution pH was controlled at 7.0~7.5 (initial and final) with a 0.05 M HEPES buffer. Data plotted as mean of duplicates, and errors refer to standard deviation.	177
Figure A-9. Reuse of oxidized ZVI nanoparticles for nitrate reduction in the presence of 6% (w/w) NaCl. A stoichiometric amount of NaBH ₄ was added to produce ZVI nanoparticles after each cycle.	178
Figure A-10. Hysteresis of mercury adsorption onto clay-loam sediment.	179
Figure A-11. Iron content in a clay-loam sediment column treated with 0.5 g/L FeS(s) stabilized with 0.2% NaCMC or a solution containing 0.1 M NaNO ₃ and 0.2% NaCMC.	180

CHAPTER 1. GENERAL INTRODUCTION

1.1 Groundwater Contamination

Underground sources of water make a significant contribution to the annual agricultural, domestic, and industrial needs. The volume of groundwater is estimated to comprise 30.1% of all freshwater resource on earth compared to 0.4% in surface freshwater and atmospheric water, and groundwater makes up about 20% of the world's fresh water supply (Czarra, 2003). Groundwater pollution occurs when hazardous substances come in contact and dissolve in the water that has soaked into the soil (U.S. EPA, 2007). Some of the major sources of groundwater contamination, called contaminants, are storage tanks, septic systems, hazardous waste sites, landfills, industrial discharges, and non-point sources. Although groundwater contamination has occurred for centuries, increased industrialization, population density, and agricultural activities have greatly exacerbated this problem.

As our dependence on groundwater increases, its quality becomes an ever more important issue (Pye and Patrick, 1983). Contaminated groundwater can affect the quality of drinking and other types of water supplies when it reaches the surface (U.S. EPA, 2007) and contaminated groundwater is of concern due to the toxicity towards humans and the ecotoxicity (Piver, 1992). Also, groundwater contamination often results in further migration of contaminants and contamination of drinking water supplies (Langwaldt and

Puhakka, 2000). Perchlorate and nitrate are two major groundwater contaminants.

Perchlorate (ClO_4^-) is a widespread contaminant that has been detected at about 400 sites in groundwater, surface water, soil or public drinking water in more than twenty-five states across the United States with concentrations ranging from 4 $\mu\text{g/L}$ to more than 3.7 million $\mu\text{g/L}$ (U.S. GAO, 2005). When ingested, perchlorate can impede the endocrine function by blocking iodide from entering thyroid gland, thereby reducing the production of thyroid hormones. The adverse health effects were reported to be more profound for newborns, children, and pregnant women (Wolff, 1998).

Nitrate contamination of groundwater has been associated with agricultural land runoff, leaching of nitrogen fertilizers, concentrated animal feeding operations, food processing, and industrial waste effluent discharge (Su and Puls, 2004). The National Research Council (NRC, 1994) reported that there were approximately 300 - 400 thousands of nitrate-contaminated sites in the United States. Ingestion of nitrate in drinking water by infants can cause dangerously low oxygen levels in the blood (Nolan et al., 1997; Fan and Steinberg, 1996). Nitrate-N concentrations of 4 mg/L or more in rural drinking water supplies have been associated with increased risk of non-Hodgkin's lymphoma (Ward et al., 1996).

1.2 Soil Contamination

In the United States, there are 1200 sites on the National Priority List (NPL) for the treatment of contaminated soils, indicating the extensiveness of soil contamination. Approximately 63% of the sites on the NPL include contamination from toxic heavy metals (Hazardous Waste Consultant, 1996). The sources of heavy metals include mining

and smelting, electroplating, painting, fuel production, fertilizer and pesticide application (Alkorta et al., 2004). Heavy metals in soil are not degraded naturally and pose significant risks to human and environmental health. Mercury (Hg) is one of the most pervasive and bio-accumulative contaminants and the remediation of mercury-contaminated soil and sediment is one of the focuses of this research.

Mercury (Hg) contamination is a growing global problem. The annual global input to the atmosphere is estimated to be 5,500-6,000 metric tons (Charles, 2002), of which 50-75% result from human activities (Hansel, 2002). The annual anthropogenic Hg emitted in the U.S. totals 158 metric tons, of which ~33.3% are deposited in the homeland. In addition, the global reservoir adds ~35 tons of Hg annually to the U.S. territory (Sznopak and Goonan, 2002). Mercury is a potent neurotoxin; the most at risk are children and the unborn. According to the Natural Resources Defense Council (NRDC, 2003), one in 12 women of childbearing age has blood mercury levels exceeding the U.S. EPA safe level for protection of the fetus, i.e. ~320,000 babies born annually in the U.S. are at risk for neuro-developmental delays. In wildlife, mercury is a reproductive hazard with harmful effects on a variety of species.

1.3 Objectives

The overall goal of this research is to investigate the feasibility of applying innovative technologies for remediation of ground water and soils contaminated with perchlorate, nitrate, or mercury. The specific objectives of this research are to:

1. Study perchlorate sorption and desorption behaviors of select representative standard anion exchange resins and some newly developed ion exchange materials such as

ion-exchange fiber (IXF), and a class of polymeric ligand exchanger (PLE) is developed for perchlorate removal. The equilibrium sorption capacity, kinetic behaviors, and desorption/regeneration efficiency, of various ion-exchange materials will be investigated. The underlying mechanisms for perchlorate uptake and the effect of resin properties (i.e. functionality and matrices) and solution chemistry on perchlorate sorption and desorption will be elucidated.

2. Test the feasibility of using stabilized zero-valent iron (ZVI) nanoparticles for perchlorate destruction in fresh water, simulated IX regeneration brine, or contaminated saline water. An innovative class of ZVI nanoparticles will be prepared using polysaccharides such as water-soluble starch or carboxymethyl cellulose (CMC) as the stabilizer. The reaction rate and extent of perchlorate reduction by stabilized ZVI nanoparticles will be determined and the influences of temperature, salinity, and pH on the reactivity of the nanoparticles will be characterized.
3. Apply the stabilized ZVI nanoparticles for nitrate reduction and to test the effectiveness of using the CMC-stabilized ZVI nanoparticles for transformation of nitrate in fresh water, simulated IX regeneration brine, or saline water. The rate, extent and pathways of nitrate reduction by the stabilized ZVI nanoparticles will be studied and the influences of ZVI-to- NO_3^- molar ratio, pH, metal catalysts, concentration of stabilizer and salinity on the nitrate reduction rate and pathways will be investigated.
4. Develop stable and dispersive iron sulfide (FeS(s)) nanoparticles using a low-cost, food-grade polysaccharide as a stabilizer and to explore the effectiveness of the stabilized iron sulfide nanoparticles for mercury immobilization in sediment. A new

class of FeS(s) nanoparticles will be prepared using carboxymethyl cellulose (CMC) as a stabilizer and will be characterized with transmission electron microscope (TEM) and dynamic light scattering (DLS). The mobility of the stabilized FeS(s) nanoparticles in sediment and the effectiveness of mercury immobilization using stabilized FeS(s) nanoparticles will be explored.

1.4 Organization

This dissertation includes six chapters. Except for Chapter 1 (General Introduction) and Chapter 6 (Conclusions and Suggestions for Future Research), each chapter of this dissertation is formatted in a stand alone journal paper. Chapter 1 gives a general introduction and overview of this dissertation. Chapter 2 investigates perchlorate sorption affinity, capacity, kinetics, and regenerability with representative standard strong-base anion (SBA) and weak-base anion (WBA) exchangers, a bifunctional resin (A-530E), a class of polymeric ligand exchangers (PLE's), and an ion-exchange fiber (IXF). The mechanisms for perchlorate uptake by ion-exchangers, strategies to improve perchlorate affinity, capacity, and regenerability are investigated. This chapter is based on the information that has been published in *Separation Science and Technology* (Xiong et al., 2006) and to be published in *Industrial & Engineering Chemistry Research* (Xiong et al., 2007a). Chapter 3 describes the synthesis of stabilized zero-valent iron (ZVI) nanoparticles by using polysaccharides as stabilizers and presents the results of complete perchlorate reduction using stabilized ZVI nanoparticles in both fresh water and ion-exchange brine. This chapter is based on the information that has been published in *Water Research* (Xiong et al., 2007b). Chapter 4 investigates the effectiveness of the

stabilized ZVI nanoparticles for reductive transformation of nitrate in both fresh water and ion-exchange regeneration brine. Nitrate reduction by ZVI nanoparticles pathways, mass balance, and effects of experimental parameters are also explored. This chapter is based on the information that has been submitted to Journal of Nanoparticle Research for publication (Xiong et al., 2007c). Chapter 5 reports the development of an innovative class of stabilized FeS(s) nanoparticles using carboxymethyl cellulose (CMC) as the stabilizer and the results for nanoparticles characterization, mobility of FeS(s) nanoparticles, and mercury immobilization in sediment using the stabilized FeS(s) nanoparticles are discussed. The information in this chapter is to be submitted to Environmental Science & Technology (Xiong et al., 2007d). Chapter 6 gives a summary of major conclusions of this research and suggestions for future work.

CHAPTER 2. REMOVAL OF PERCHLORATE FROM CONTAMINATED WATER BY USE OF ION EXCHANGERS

This chapter compares representative standard strong-base anion (SBA) and weak-base anion (WBA) resins, a bifunctional resin (A-530E), a class of polymeric ligand exchangers (PLE's), and an ion-exchange fiber (IXF) with respect to perchlorate sorption affinity, capacity, kinetics, and regenerability. The fundamental mechanisms for perchlorate uptake by ion-exchangers are discussed and effects of the hydrophobicity of resin matrix, solution pH, ethanol, resin morphology on the regeneration of exhausted ion-exchangers are investigated through a series of batch and column tests.

2.1 Introduction

Perchlorate has emerged as a widespread contaminant in groundwater and surface water across the United States (U.S. GAO, 2006) and has also been detected in diary milk and breast milk (Kirk et al., 2005), tobacco (Ellington et al., 2001), leafy vegetables (Sanchez et al., 2005), fruit (Sanchez et al., 2006), plant species (Smith et al., 2004; Urbansky et al., 2000), and bottled water (Snyder et al., 2005). Perchlorate is primarily used as an oxidizer in solid rocket fuels (Urbansky, 1998), and is also found in Chilean nitrate fertilizer, which has been regarded as a semi-natural source for perchlorate (Sridhar et al., 1999; Susalar et al., 1999). Recently, researchers claimed that perchlorate

can also be produced naturally (Bao and Gu, 2004; Dasgupta et al., 2005; 2006). A recent study estimates the perchlorate source strength for solid fuels, Chilean nitrate fertilizer, and natural production to be, respectively, 10.6, 0.75, 0.13~0.64 Gg/year in the United States (Dasgupta et al., 2006). Perchlorate concentrations of 180~220 $\mu\text{g/L}$ in drinking water (Blount et al., 2006) or 2.9 $\mu\text{g/L}$ in urine (Greer et al., 2002) can competitively inhibit iodide uptake, especially to women with lower-iodine level. In February 2005, the National Academy of Sciences (NAS) recommended an RfD (reference dose) of 0.7 $\mu\text{g}/(\text{kg}\cdot\text{d})$, which was translated into a Drinking Water Equivalent Level (DWEL) of 24.5 $\mu\text{g/L}$ by the U.S. EPA (2005). It is generally expected that perchlorate will be regulated in the U.S. in the next few years with a final maximum contaminant level (MCL) in the range of 1-20 $\mu\text{g/L}$. Meanwhile, the state of Massachusetts set a clean up standard of 2 $\mu\text{g/L}$ in 2006 and the Office of Environmental Health Hazard Assessment (OEHHA) of California affirmed a public health goal of 6 $\mu\text{g/L}$.

To mitigate the health risks of perchlorate and to comply with the increasing regulations, cost-effective technologies for perchlorate removal from contaminated water have been intensively explored over the last few years. Of the various technologies tested so far, anaerobic biological degradation (Cang et al., 2004; Logan, 2001; Min et al., 2004; Okeke et al., 2002; Xu et al., 2003) and ion exchange have been identified as the most promising technologies (Logan, 2000). However, anaerobic degradation is a slow process, which typically requires a prolonged hydraulic residence time (HRT) and thus a large reactor volume. Anaerobic processes are also less efficient when used for drinking water treatment, where the concentrations of substrates and nutrients are low.

Ion exchange (IX) offers the following general advantages: 1) is simple in configuration; 2) maintenance and operation are straightforward and can be automated; 3) can reduce perchlorate to very low levels (e.g. $<1 \mu\text{g/L}$); 4) can be readily inserted in an existing treatment scheme or used at the point of use; 5) does not produce harmful by-products such as odors; and 6) resins may be reused for multiple cycles. Tripp and Clifford (2000; 2004; 2006) studied the effect of resin cross-linking, porosity and functional groups on perchlorate selectivity and found that more hydrophobic resins exhibited higher perchlorate affinity. Batista et al. (2000) investigated several SBA and WBA resins to remove perchlorate from water, and observed that both SBA and WBA resins can offer high perchlorate sorption capacity. Gu et al. (2005; 2006) compared perchlorate sorption by some SBA resins and bifunctional resins, and observed that the sorption capacity of the bifunctional resins is orders of magnitude greater than that for the mono-functional SBA resins at low ClO_4^- concentrations (e.g., $<1 \text{ mg/L}$).

In general, sorption selectivity of a resin can be affected by sorbate-sorbent interactions as well as sorbate-solvent interactions. It has been well recognized that resin matrix and functional groups can strongly affect ion exchange capacity and selectivity (Barron and Fritz, 1984; Clifford and Weber, 1983; Li and SenGupta, 1998). On the other hand, uptake of larger and more hydrophobic (low hydration energy) anions by ion exchangers can be enhanced through water structure-enforced ion-pairing (WSEIP) (Diamond, 1963). According to the WSEIP theory, the large and more hydrophobic ions such as ClO_4^- , tend to be driven away by water to the less structured resin phase (Chu et al., 1962; Diamond, 1963).

Based on the latest knowledge, most resins with polystyrene matrices are able to offer practically acceptable perchlorate sorption capacity. However, regeneration efficiency of perchlorate-laden styrenic type resins was found, in general, to be very limited. Conversely, while acrylic resins are generally easier to regenerate, the perchlorate sorption capacity of these more hydrophilic resins is too low for the process to be cost-effective. As a result, in many cases, ion exchange resins have been used on a disposable basis (i.e. resins are used one time and then disposed of or incinerated).

In the search for resins of both great perchlorate capacity and regenerability, Gu et al. (2001) and Bonnesen et al. (2000) developed and characterized a bifunctional anion exchange resin (A-530E) that can remove perchlorate selectively. To reuse the resin, Gu et al. (2001; 2007) and Gu and Brown (2006) prescribed a regenerant consisting of 1M FeCl_3 and 4 M HCl, and they observed that nearly 100% of sorbed ClO_4^- was eluted with ~ 2 BV's of the regenerant. In another study, Gu et al. (2005) reported that strong acid (HCl) alone was ineffective for desorbing perchlorate from the bifunctional resin.

To further exploit the potential of ion exchange technology for perchlorate removal, our knowledge on perchlorate sorption and desorption with various classes of ion-exchangers of different matrices and functional groups needs to be improved. The overall goal of this study was to compare the perchlorate sorption and desorption behaviors of select representative standard anion exchange resins and some newly developed ion exchange materials such as a class of PLE's and an IXF. The specific objectives were to 1) compare the equilibrium sorption capacity, kinetic behaviors, and desorption/regeneration efficiency, of various ion-exchange materials; 2) elucidate the underlying mechanisms for perchlorate uptake; and 3) investigate the effect of resin

properties (i.e. functionality and matrices) and solution chemistry on perchlorate sorption and desorption.

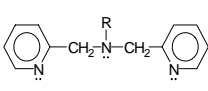
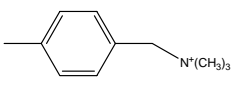
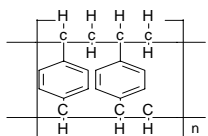
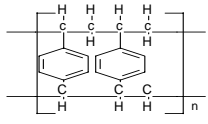
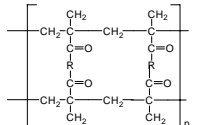
2.2 Materials and Methods

Table 2-1 and **Table 2-2** present salient properties of various sorbents used in this study. Before use, all sorbents except the anion exchange fiber (Smopex-103x) were conditioned following a procedure of cyclic exhaustion with 1 N sodium hydroxide, rinsing successively with deionized (DI) water, 1 N hydrochloric acid, 1 N NaCl, and then air-dried.

An anion exchange fiber (Smopex-103x) in chloride form was obtained from Johnson Matthey Catalysts, West Deptford, NJ, USA. Smopex-103x was supplied as ~2 mm long polyethylene fibers of 10 to 20 μm in diameter (Johnson Matthey, 2006). The material was used as received.

Three PLE's, designated as DOW 3N-Cu, XAD1180 3N-Cu and XAD7HP 3N-Cu, were prepared in our lab and tested in this study. DOW 3N-Cu was prepared based on a commercially available chelating resin (DOW 3N, purchased from Aldrich, Milwaukee, WI, USA) and following the procedure by Zhao and SenGupta (1998) and Zhao et al. (2006). XAD1180 3N-Cu and XAD7HP 3N-Cu were prepared based on a polystyrene sorbent (XAD1180) and polyacrylic matrix (XAD7HP), both obtained from Rohm and Haas, Philadelphia, PA, USA. Functionalization of these polymers was carried out following a procedure by Zhao et al. (2006), which included chloromethylation and amination of the polystyrene-based matrices, and subsequently, immobilization of copper(II) onto the resins.

Table 2-1. Salient properties of various sorbents used in this study.

Sorbent Trade Name	Functional Group*	Description	Matrix	Manufacturer
A-530E	$\begin{array}{c} \text{R} \\ \\ \text{C}_2\text{H}_5-\text{N}^+-\text{C}_2\text{H}_5 \\ \\ \text{C}_2\text{H}_5 \end{array}, \quad \begin{array}{c} \text{R} \\ \\ \text{H}_3\text{C}_6-\text{N}^+-\text{C}_6\text{H}_{13} \\ \\ \text{C}_6\text{H}_{13} \end{array}$	SBA resin	Polystyrene, macroporous	Purolite Co., Bala Cynwyd, PA, USA
Diaion®WA21J	$\begin{array}{c} \text{R} \\ \\ \text{CH}_3-\text{N}^+-\text{H} \\ \\ \text{CH}_3 \end{array}$	WBA resin	Polystyrene, macroporous	Mitsubishi Chemical, Bellefonte, PA, USA
DOW 3N or Dowex M4195		Chelating resin, high copper(II) affinity	Polystyrene, macroporous	DOW Chemical, Midland, MI, USA
DOW 66 or Dowex 66	$\begin{array}{c} \text{R} \\ \\ \text{CH}_3-\text{N}^+-\text{H} \\ \\ \text{CH}_3 \end{array}$	WBA resin	Polystyrene, macroporous	DOW Chemical, Midland, MI, USA
IRA 900	$\begin{array}{c} \text{R} \\ \\ \text{CH}_3-\text{N}^+-\text{CH}_3 \\ \\ \text{CH}_3 \end{array}$	SBA resin	Polystyrene, macroporous	Rohm and Haas Co., Philadelphia, PA, USA
IRA 958	$\begin{array}{c} \text{R} \\ \\ \text{CH}_3-\text{N}^+-\text{CH}_3 \\ \\ \text{CH}_3 \end{array}$	SBA resin	Polyacrylic, macroporous	Rohm and Haas Co., Philadelphia, PA, USA
Smopex-103x		SBA resin	Polyethylene, fibrous	Johnson Matthey Catalysts Co., West Depford, NJ, USA
XAD 4		Non-ionic polymeric sorbent	Polystyrene, macroporous	Rohm and Haas Co., Philadelphia, PA, USA
XAD1180		Non-ionic polymeric sorbent	Polystyrene, macroporous	Rohm and Haas Co., Philadelphia, PA, USA
XAD7HP		Non-ionic polymeric sorbent	Polyacrylic, macroporous	Rohm and Haas Co., Philadelphia, PA, USA

* “R” denotes the repeating units of the polymer matrices.

Table 2-2. Salient properties of polymeric sorbents used for preparing PLE's.

Sorbents	Particle Size, mm	Surface Area, m²/g	Porosity, ml/ml	Medium Pore Size, nm
DOW 3N (macroporous beads) ^a	0.2-1.2	139.01	-	35.9
XAD4 (macroporous beads) ^b	0.49-0.69	≥ 750	≥ 0.50	12.5
XAD7HP (macroporous beads) ^b	0.56-0.71	≥ 380	≥ 0.50	35
XAD1180 (macroporous beads) ^b	0.35-0.60	≥ 500	≥ 0.60	45
Smopex-103x (non-porous polyethylene fiber) ^b	L = 2 mm D = 0.01-0.02 mm	0.014 ^c	0	

a. Property data from Zhao 1997; b. Data from the manufacturer; c. Calculated the length (L) of 2 mm, and a mean diameter (D) of 0.015 mm.

Perchlorate sorption isotherms were constructed for various ion-exchangers through a series of batch equilibrium experiments using a set of 100 mL glass vials fitted with Teflon-lined screw caps. First, known masses of an ion-exchanger (0.0025~0.2000 g) were added into a set of 100 mL solutions containing 10 mg/L ClO_4^- and 100 mg/L SO_4^{2-} at an initial pH of 7.0. Note that mass for all sorbents is given as air-dried mass throughout this work. The mixtures were then equilibrated on an end-to-end shaker (New Brunswick Scientific Co., Edison, NJ, USA) operated at 200 rpm for two weeks, which was proven to be sufficient to reach equilibrium through separate kinetic experiments. Solution pH was kept at 7.0 ± 0.1 through intermittent adjustment using 0.1 N NaOH and/or 0.1 N HCl. At equilibrium, ClO_4^- and SO_4^{2-} in the solution phase were analyzed and the uptake of ClO_4^- and SO_4^{2-} by the sorbents was determined by mass balance calculations.

Fixed-bed column runs were carried out on DOW 3N-Cu to test the breakthrough behavior of this material. The experiment set-up included a Plexiglass column (diameter = 11 mm, length = 300 mm, Omnifit, Cambridge, UK), a HPLC pump and a fraction collector (Eldex Laboratories, Napa, CA). The empty bed contact time (EBCT) was 10 minutes and the superficial liquid velocity (SLV) was 0.51 cm/min. A simulated wastewater solution containing 0.2 mg/L ClO_4^- , 50 mg/L SO_4^{2-} , 35.5 mg/L Cl^- and 30.5 mg/L HCO_3^- at pH 7.2 was used as inflow.

Batch equilibrium tests were also carried out at a final solution pH ranging from 2 to 12, which was maintained through intermittent acid or base addition, to study the pH effect on perchlorate sorption. For each fixed pH, ~0.015 g of a sorbent was added into 50 mL of a solution containing 10 mg/L ClO_4^- and 100 mg/L SO_4^{2-} . The mixtures were

then equilibrated on an end-to-end shaker (New Brunswick Scientific Co., Edison, NJ, USA) operated at 200 rpm. After two weeks, solution samples were taken and analyzed for perchlorate and sulfate.

Batch kinetic tests were carried out in 4-liter glass bottles. In each test, a known amount of a sorbent was added into 4 L solution containing 10 mg/L ClO_4^- and 100 mg/L SO_4^{2-} at pH 7.0 ± 0.1 . The following sorbent mass was used in the tests: A-530E = 0.21 g, DOW 3N-Cu = 0.61 g, DOW 66 = 0.55 g, IRA 900 = 0.61 g, IRA 958 = 0.62 g, XAD1180 3N-Cu = 0.60 g. The reactors were agitated on an end-to-end shaker (New Brunswick Scientific Co., Edison, NJ, USA) operated at 200 rpm. At predetermined time intervals, 4 mL water samples were taken for analysis. Solution pH was kept neutral with intermittent adjustment with 0.1 N NaOH and/or 0.1 N HCl during the tests.

For perchlorate desorption tests, air-dried ion-exchangers were first loaded with perchlorate by equilibrating ~10 mL (3.8~6.5 g) of an ion-exchanger in a solution ($V \approx 4$ L) containing 100~150 mg/L of ClO_4^- and 100 mg/L of SO_4^{2-} at a controlled pH 7.0 ± 0.1 for two weeks under mixing on an end-to-end shaker (New Brunswick Scientific Co., Edison, NJ, USA) operated at 200 rpm. The initial and final perchlorate concentrations were measured and used to determine the perchlorate uptake by the ion exchangers through mass balance calculations.

Desorption of perchlorate was then carried out in a fixed-bed configuration including a Plexiglas column (inner diameter = 11 mm, length = 300 mm, Omnifit, Cambridge, UK), a HPLC pump and a fraction collector (Eldex Laboratories, Napa, CA, USA). Typically, 1.2 mL of a perchlorate-loaded ion-exchanger was packed in the column. Following a brief rinse using 5 to 10 bed volumes of DI water, a regenerant

solution was passed in the down flow mode through the resin bed at an Empty Bed Contact Time (EBCT) of 30 minutes and a Superficial Liquid Velocity (SLV) of 0.025 m/hr. Regenerants containing 12% (w/w) NaCl and various concentrations of ethanol (0-30%, v/v) at pH ranging from 9.06 to 13.44 were tested in this study. The regeneration efficiency was measured by comparing total perchlorate eluted and perchlorate initially loaded to an ion-exchanger.

Cl^- , ClO_4^- and SO_4^{2-} were analyzed with a Dionex Ion Chromatography (DX-120) equipped with a suppressed conductivity detector. The eluent flow rate was set at 1.0 ml/min. For ClO_4^- , an AS16 column, an AG16 guard column, and a 1000 μL sample loop were employed; and a degassed 50 mM sodium hydroxide solution was used as the eluent. The detection limit for perchlorate was 4 $\mu\text{g/L}$. For Cl^- and SO_4^{2-} , an AS14 column, an AG14 guard column, and a 100 μL sample loop were used. In this case, a solution containing 3.5 mM sodium carbonate and 1.0 mM sodium bicarbonate was used as the eluent. HCO_3^- was analyzed as Inorganic Carbon (IC) using a TOC Analyzer (Phoenix 8000, TEKMAR DOHRMANN). Cu^{2+} was analyzed by a Varian SpectrAA 220 FS.

2.3 Results and Discussion

2.3.1 Equilibrium sorption isotherms

Figure 2-1 presents the experimental (symbols) and fitted (lines) isotherms for various ion exchangers under otherwise identical conditions. To facilitate comparison of the sorption capacities, the classical single-component Freundlich model (Michel et al., 2007) was used to interpret the experimental data:

$$q_e = K_f C_e^n \quad (2-1)$$

where K_f is the Freundlich capacity coefficient $[(\text{mg}\cdot\text{g}^{-1})/(\text{mg}\cdot\text{mL}^{-1})^n]$, n is the Freundlich exponent reflecting the site energy distribution and sorption intensity, q_e is the solid-phase concentration (mg/g), and C_e is the equilibrium aqueous-phase concentration (mg/L). **Table 2-3** lists the fitted K_f and n values.

Table 2-3. Freundlich model parameters, the capacity factor A_f , binary separation factor, and total ion-exchange capacity of various ion-exchangers. (Errors given as standard deviation).

Ion Exchanger	$K_f, (\text{mg}\cdot\text{g}^{-1})/(\text{mg/L})^n$	n	R^2	$A_f, \text{mg}^2/(\text{g}\cdot\text{L})$	$\alpha_{P/S}^*$	Total capacity, meq/g dry wt.**
A-530E	91±5.5	0.29±0.04	0.91	711	386±8.4	2.2
DOW 3N-Cu	19±0.7	0.47±0.02	0.99	180	33±5.1	3.0
DOW 3N	15±2.1	0.37±0.08	0.92	128	7±0.8	3.0
DOW 66	25±3.5	0.44±0.09	0.90	229	14±1.2	4.0
IRA 900	25±2.1	0.49±0.06	0.97	242	7±1.0	4.2
IRA 958	5±0.5	0.31±0.05	0.95	40	0.4±0.1	3.3
Smopex-103x	17±1.9	0.65±0.06	0.97	198	12±1.8	2.5
WA21J	13±1.2	0.72±0.11	0.96	165	12±1.5	5.8
XAD1180 3N-Cu	10±0.6	0.55±0.07	0.97	104	14±0.9	1.25
XAD7HP 3N-Cu	5±0.7	0.34±0.03	0.96	41	0.5±0.1	0.94

* $\alpha_{P/S}$ refers to the binary perchlorate-to-sulfate separation factor.

** Total capacity for PLE's was determined in our lab based on copper loaded; For other resins, it was obtained from the manufacturers.

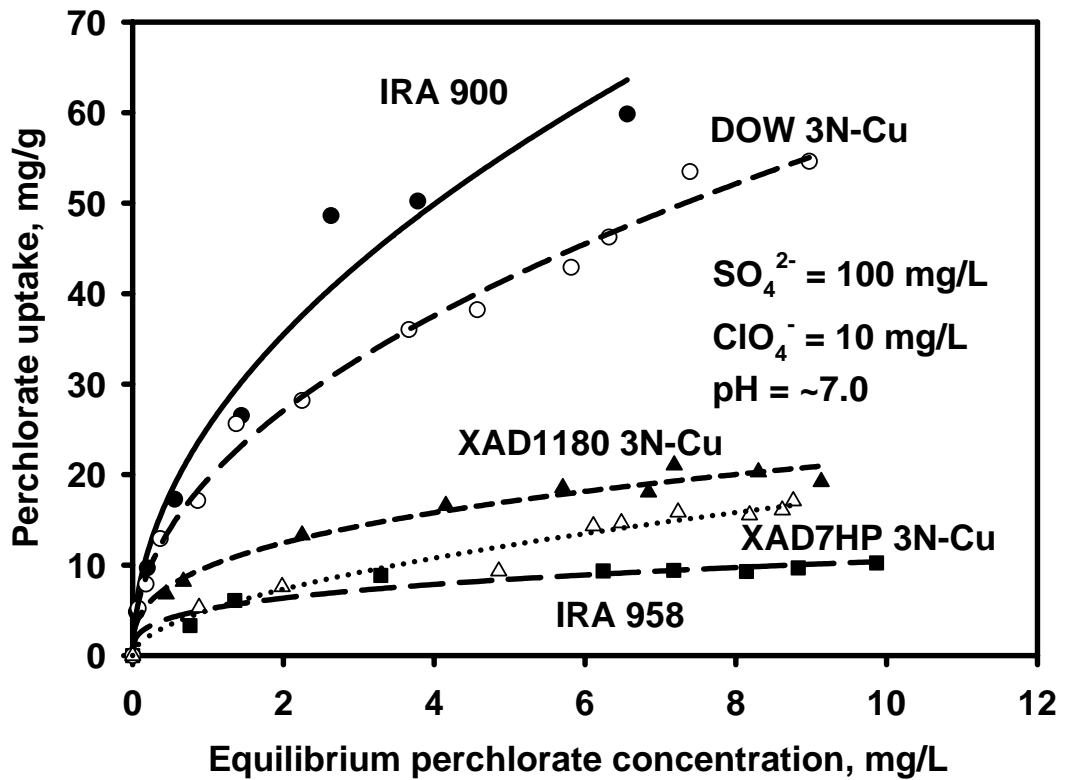


Figure 2-1a. Perchlorate sorption isotherms for a strong-base polystyrene-based resin (IRA 900), a strong-base polyacrylic resin (IRA 958), and three PLE's (DOW 3N-Cu, XAD7HP 2N-Cu, and XAD1180 3N-Cu). Initial ClO₄⁻ = 10 mg/L, SO₄²⁻ = 100 mg/L. Maximum final Cl⁻ = 21-77 mg/L. Solution pH was kept at 7.0±0.1 during the tests. (Symbols: experimental data; Lines: Freundlich model fitting).

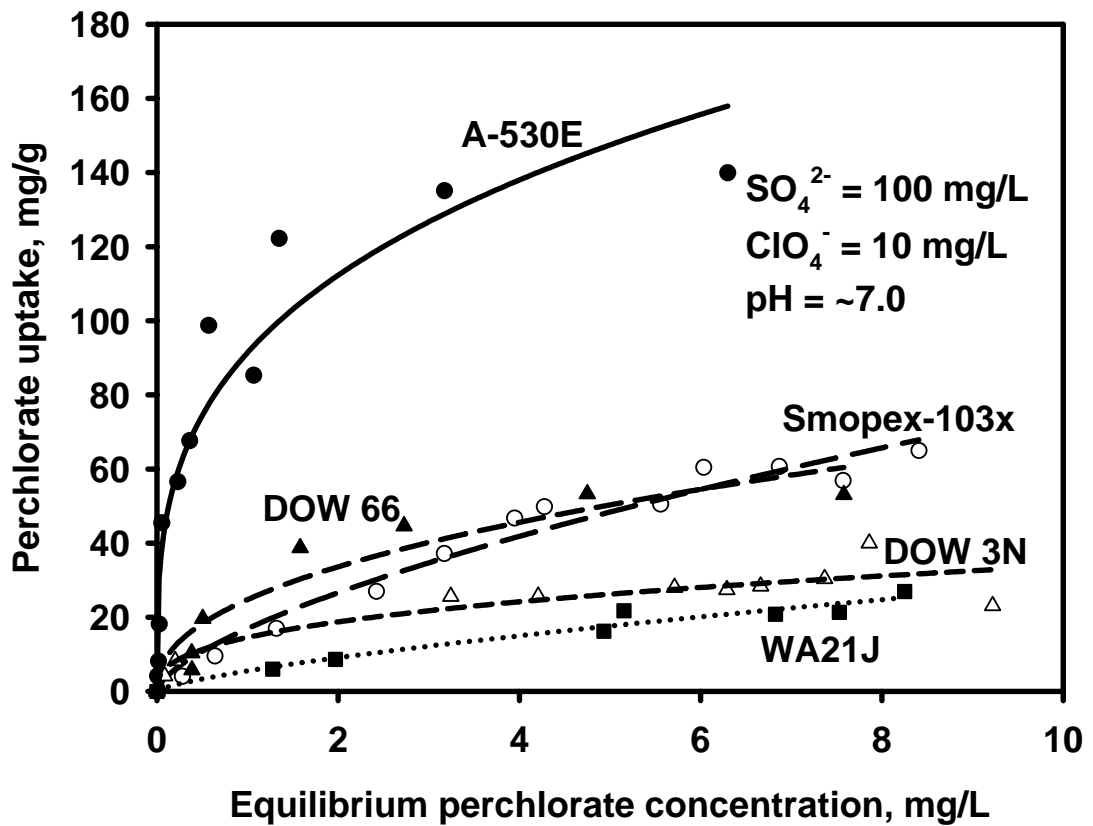


Figure 2-1b. Perchlorate sorption isotherms for a bifunctional resin (A-530E), an IXF (Smopex-103x), a chelating resin (DOW 3N), and two WBA resins (DOW 66, WA21J). Initial ClO₄⁻ = 10 mg/L, SO₄²⁻ = 100 mg/L. Maximum final Cl⁻ = 21-77 mg/L. Solution pH was kept at 7.0±0.1 during the tests. (Symbols: experimental data; Lines: Freundlich model fitting).

To facilitate a fair comparison of the perchlorate sorption capacity, an area-based capacity parameter (A_f) was defined and calculated based on the best-fitted Freundlich equation for each resin, i.e.

$$A_f = \int_0^6 K_f C_e^n dC_e \quad (2-2)$$

where the integration was carried out in the concentration range of 0 to 6 mg/L based on the experimental data. While the Freundlich parameters K_f and n reflect the sorption capacity and affinity, respectively, the capacity parameter A_f manifests the overall sorption capacity behavior over a given concentration range, and thus, serves as a more reasonable parameter to compare the overall sorption capacity of various resins. Based on the A_f values in **Table 2-3**, the perchlorate sorption capacity follows the order of: A-530E >> IRA 900 > DOW 66 > Smopex-103x > DOW 3N-Cu > WA21J > DOW3N > XAD1180 3N-Cu > IRA 958 \approx XAD7HP 3N-Cu.

To compare the perchlorate selectivity, the mean binary perchlorate-to-sulfate separation factor ($\alpha_{P/S}$) for each ion-exchanger was calculated based on the equilibrium isotherm data and via Eq. (2-3) (Zhao and SenGupta, 1998):

$$\alpha_{P/S} = \frac{q_P}{C_P} \times \frac{C_S}{q_S} \quad (2-3)$$

where q (mg/g) and C (mg/L) represent the concentration in solid phase and aqueous phase, respectively; and the subscripts P and S denote perchlorate and sulfate, respectively.

Based on the separation factor values in **Table 2-3**, all ion-exchangers with polystyrene and polyethylene matrices offered greater affinity for perchlorate over sulfate (i.e. $\alpha_{P/S} > 1$) regardless of their functional groups or physical form (porous beads or fine

fibers). In contrast, the two acrylic resins, IRA 958 and XAD7HP 3N-Cu, showed greater affinity toward sulfate over perchlorate ($\alpha_{P/S} < 1$). This difference can be attributed to the low hydration energy of perchlorate and the different hydrophobicity of the matrices. Perchlorate ions exist as monovalent anions and are known to have much lower hydration energy (i.e. more hydrophobic) (-259 kJ/mol) than most of common anions such as sulfate (-1,103 kJ/mol), chloride (-338 kJ/mol) and bicarbonate (-388 kJ/mol) (Brown et al., 2000). On the other hand, polyacrylic matrices tend to undergo greater hydration and imbibe more water molecules on the polymer surface (Li and SenGupta, 1998). SenGupta and Clifford (1986) observed that the water content of an air-dried IRA 958 was 2.8 times that of IRA 900. This thicker hydration water layer of IRA 958 constitutes a more profound, rigid barrier on the resin's surface, abating the ion pairing between perchlorate and the functional amine groups of the resin. In contrast, for polystyrene-based resins, the more hydrophobic matrix reduces the hydration barrier, which results in an enhanced ion pairing interactions between perchlorate and the functional amine groups of the resins. **Figure 2-2** provides a schematic illustration of binding mechanisms of perchlorate with various ion exchange resins (IRA 900, IRA 958, DOW 3N and DOW 3N-Cu).

The bifunctional resin A-530E displayed the greatest capacity and a perchlorate selectivity of more than one order of magnitude greater than other resins (**Table 2-3**). The enhanced perchlorate selectivity of A-530E is attributed to its unique structure of the trialkylammonium functional groups, where each nitrogen (the binding site) is surrounded by three extended alkyl chains (Gu et al., 2000). The extended chain structure creates a more hydrophobic local environment and hinders sorption of hydrophilic ions such as sulfate. It was reported that this type of functionalities is highly specific for

anions with large size and low hydration energy (such as ClO_4^- , TcO_4^-) (Gu et al., 2000; 2001).

IRA 900 is a standard Type I SBA resin with a polystyrene matrix and quaternary amine functional groups. As shown in **Figure 2-1a** and **Table 2-3**, IRA 900 exhibited a relatively high perchlorate uptake capacity and moderate perchlorate selectivity ($\alpha_{P/S}=7$). DOW 66 and WA21J are typical WBA resins with polystyrene matrices and tertiary amine functional groups. They also exhibited good selectivity toward perchlorate over sulfate ions and presented a perchlorate uptake capacity comparable to that of IRA 900. Earlier, Batisa et al. (2000) also reported that both SBA and WBA resins can offer high perchlorate sorption capacity.

However, when a non-functionalized polystyrene sorbent, XAD4, was tested for perchlorate removal, no perchlorate uptake (data not shown) was observed. Given that both XAD4 and IRA 900 share similar hydrophobic polystyrene matrix and divinylbenzene cross-linking (**Table 2-1**), this observation reveals that while the hydrophobic matrix greatly enhance the ion pairing or Lewis acid-base interactions, the hydrophobic matrix alone is not able to bind perchlorate ions.

The PLE, DOW 3N-Cu, also showed a fairly high perchlorate uptake capacity comparable to the SBA or WBA resins, and a selectivity nearly five times greater than that for IRA 900. Unlike conventional anion exchangers, the PLE's employ transition metal (Cu^{2+}) ions as functional groups and was reported to effectively remove oxyanions such as arsenate, chromate, and phosphate (An et al., 2005; Henry et al., 2004; Zhao, 1997; Zhao and SenGupta, 2000). Although perchlorate is known as a weak ligand in homogeneous systems, solution phase complexation of perchlorate with transition metals,

such as Cu, Ni, Co, and Sn in the presence of organic compounds such as CH₃CN, or pyridyl nitrogen has been reported (Mendiratta et al., 2000). For PLE's with a polystyrene matrix, enhanced Ion-pairing and Lewis acid-base interactions between the fixed Cu(II) functional groups and ClO₄⁻ are expected (**Figure 2-2**). Considering that each Cu(II) bears six primary coordination sites, two of which are occupied by the two pyridyl nitrogen donor atoms in the polymer phase, which results in the firm immobilization of Cu(II) onto the polymer surface (Xiong et al., 2006; Zhao and SenGupta, 2000). The remaining four coordination sites are available for binding ligands. Evidently, this enhanced Lewis acid-based interaction can greatly enforce the selectivity for perchlorate. For instance, although the total sorption capacity of IRA 900 is 3 times greater than XAD1180 3N-Cu, the perchlorate selectivity of XAD1180 3N-Cu is two times greater than that of IRA 900 (**Table 2-3**). On the other hand, fixed-bed column runs showed that more than 12,000 bed volumes (BV's) of perchlorate-free (< 4 µg/L) water can be obtained when DOW 3N-Cu was used to treat a simulated contaminated water containing 200 µg/L ClO₄⁻, 50 mg/L SO₄²⁻, 35.5 mg/L Cl⁻, and 30.5 mg/L HCO₃⁻ at pH 7.2 (Xiong et al., 2006).

DOW 3N, the parent resin for DOW 3N Cu, is a weak base chelating resin with a polystyrene matrix and di(2-picolyl)amine functional groups. Under the prevailing experimental pH of 6.5~7.5, a small fraction of the resin's amine groups is expected to be protonated, and thus, the enhanced electrostatic interaction (**Figure 2-2**) is operative in the same way as other standard WBA resins (e.g. DOW 66 and WA21J). When no copper is loaded, DOW 3N gives a capacity factor (A_f) of 128 mg²/(g·L) and a separation factor of 7 (**Table 2-3**). Upon copper loading, however, the A_f value and the separation factor

are increased to $180 \text{ mg}^2/(\text{g}\cdot\text{L})$ and 33, respectively. Evidently, this enhanced perchlorate uptake by the PLE results from the added positive charges of Cu(II) as well as the enhanced Lewis acid-base and ion pairing interactions.

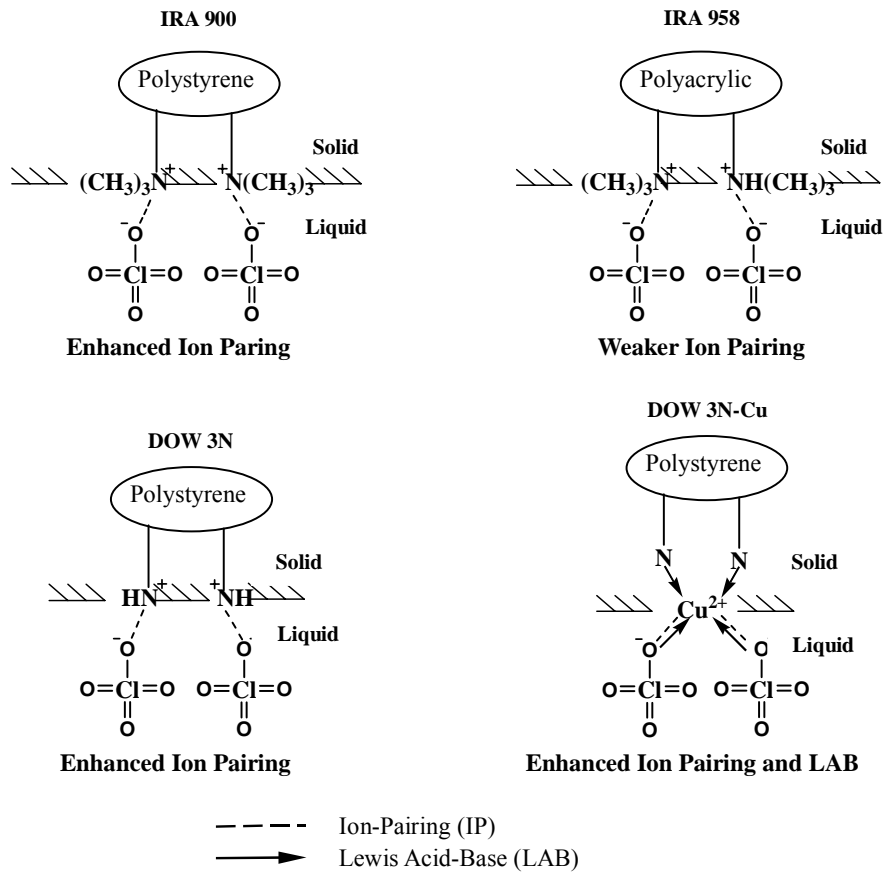


Figure 2-2. Schematic illustration of binding mechanisms of perchlorate with various ion exchangers.

To investigate the effect of matrix on PLE's perchlorate sorption capacity and regenerability, two other PLE's (XAD1180 3N-Cu and XAD7HP 3N-Cu) were synthesized in our lab. Two non-functionalized polymers, XAD1180 and XAD7HP, were selected as the matrices due to their greater surface area ($380 \text{ m}^2/\text{g}$ for XAD7HP and 500

m²/g for XAD1180) than that (139 m²/g) of DOW 3N (**Table 2-2**). However, results in **Figure 2-1a** and **Table 2-3** indicate that PLE's based on these hypo-crosslinked polymers offered a perchlorate sorption capacity much lower than that of macroporous styrenic resins such as DOW 3N-Cu or IRA 900. The A_f value for XAD1180 3N-Cu and XAD7HP 3N-Cu is only 58% and 23%, respectively, of that for DOW 3N-Cu. One reason is that the amount of copper ions, which serve as the functional groups of the PLE's, loaded onto these two sorbents was much (>42%) lower than that for DOW 3N-Cu (**Table 2-3**). However, this observed perchlorate capacity difference also suggests that despite the much greater surface area for the parent XAD resins, a great portion of the sites are inaccessible for large ions such as perchlorate after the resins were subjected to functionalization processes (i.e. chloromethylation, amination, and copper loading).

Ion-exchange fibers (IXF's) have been used in water treatment to remove contaminants such as arsenate, fluoride, nitrate, and phosphate (Liu et al., 2002; Passounaud et al., 2000). Compared to standard beads-form ion exchangers, IXF is known to offer much faster ion exchange kinetics because of their unique physical properties. Smopex-103x is based on a non-porous polyethylene fiber functionalized with quaternary amine groups. As indicated by the octanol-water partition coefficient (K_{ow}) for ethylene and styrene monomers ($\log(K_{ow}) = 1.13$ for ethylene, and 2.95 for styrene) (ATSDR, 1992; Hansch et al., 1995), the matrix of this Smopex-103x is less hydrophobic than polystyrene. Consequently, the hydrophobicity effect is weaker for Smopex-103x than for styrenic SBA resins such as IRA 900. However, the perchlorate capacity factor (A_f) for Smopex-103x is 82% of that for IRA 900 although the total capacity for Smopex-103x is only 59% of that for IRA 900, and the binary separation factor for Smopex-103x

is >1.7 times greater than that for IRA 900. This enhanced perchlorate selectivity for the Smopex-103x is attributed to, at least in part, its non-porous fibrous structure, which warrants a much easier access to the ion exchange sites by the rather large perchlorate ions than for porous resin beads such as IRA 900.

2.3.2 Fixed bed column run with DOW 3N-Cu

Figure 2-3 shows the multi-component breakthrough histories from a fixed-bed column run with DOW 3N-Cu and with an influent containing a trace concentration of perchlorate (0.2 mg/L) and much higher concentrations of competing bicarbonate (30.5 mg/L), sulfate (50 mg/L), and chloride (35.5 mg/L) ions. A superficial liquid velocity (SLV) = 0.51 cm/min and an empty bed contact time (EBCT) = 10 minutes were used in this test. It is noteworthy that complete sulfate breakthrough happened at 633 BV's and complete bicarbonate breakthrough happened at 4,026 BV's, while 10% perchlorate (20 µg/L) breakthrough took place at 12,338 BV's. Also, chromatographic elution was observed for sulfate and bicarbonate, i.e., effluent sulfate and bicarbonate concentration, immediately after breakthrough, became greater than their influent concentrations. Considering that chloride ions are present in the initial form of DOW 3N-Cu, the following affinity sequence can be inferred for DOW 3N-Cu: $\text{ClO}_4^- > \text{HCO}_3^- > \text{SO}_4^{2-} > \text{Cl}^-$. Similar column tests on commercial SBA and WBA resins have also been reported with similar breakthrough histories (Gu et al., 2000; 2003). The lagged perchlorate breakthrough in comparison to other anions proves the preference of monovalent perchlorate over divalent sulfate toward DOW 3N-Cu and commercial resins.

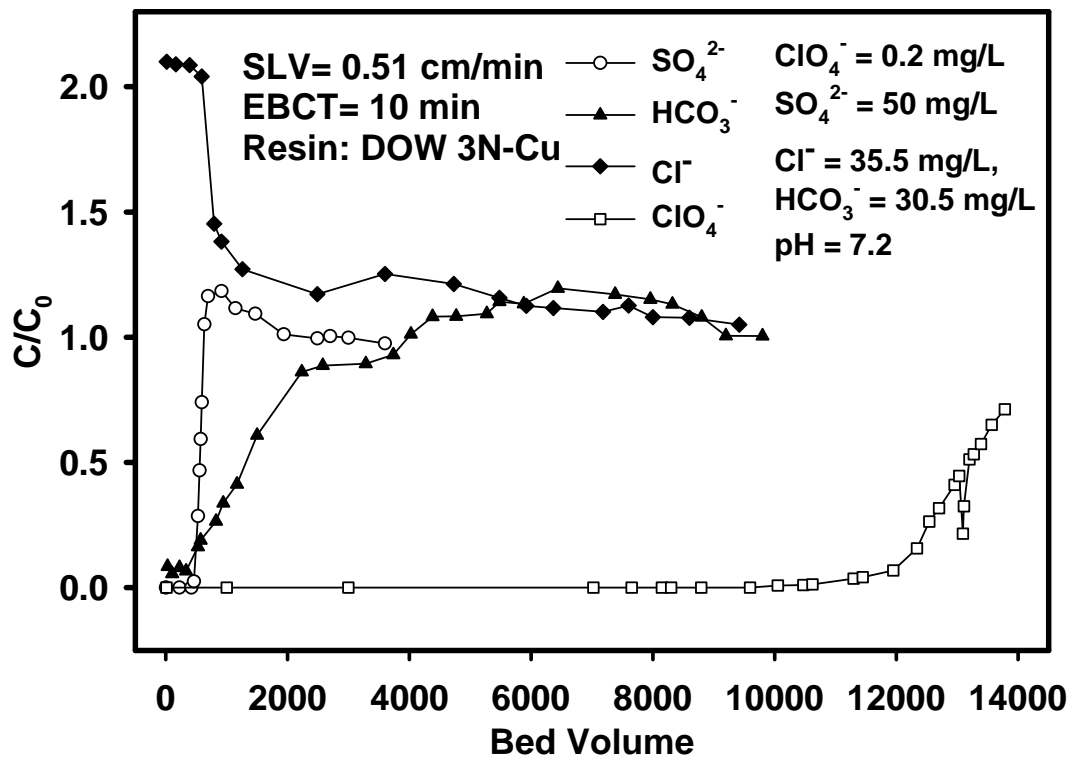


Figure 2-3. Fixed-bed column runs' breakthrough history curves of a multi-component system using DOW 3N-Cu.

2.3.3 Sorption kinetics

Batch kinetic tests in a perchlorate-sulfate binary system were conducted to determine overall intraparticle diffusion coefficients (D) (cm²/min) for various ion-exchange resins. For spherical particles such as the IX resin beads, perchlorate uptake rate during the sorption step can be expressed as follows (Crank, 1975; Helfferich, 1962):

$$\frac{\partial q}{\partial t} = D \left(\frac{\partial^2 q}{\partial r^2} + \frac{2}{r} \frac{\partial q}{\partial r} \right) \quad (2-4)$$

where r (cm) is the radial coordinate (i.e., distance from the bead center) and $q(t, r)$ (mg/g) is the polymer-phase perchlorate concentration at time t (min). Under the experimental conditions, the following initial and boundary conditions apply:

$$q(0, r) = 0 \text{ at } 0 \leq r \leq a, \quad (2-5)$$

$$\frac{\partial q}{\partial r} = 0 \text{ at } r = 0, \quad (2-6)$$

$$\frac{\partial q}{\partial r} \frac{3DM}{a} = -V \frac{\partial C}{\partial t} \text{ at } r = a \quad (2-7)$$

where a (cm) is the mean radius of the resin beads (**Table 2-4**), M (g) is the mass of a resin added, $C(t)$ (mg/L) is perchlorate concentration in the aqueous phase at time t , and V (L) is the solution volume, which is 4 L in these experiments.

The above system conforms to the scenario where diffusion takes place in a well-stirred solution of limited volume. The fractional attainment of equilibrium, F , for perchlorate is then given by the following algebraic equation (Crank, 1975):

$$F = \frac{q(t)}{q_0} = 1 - \sum_{m=1}^{\infty} \frac{6\alpha(\alpha+1) \exp(-Dq_n^2 t / a^2)}{9 + 9\alpha + q_n^2 \alpha^2} \quad (2-8)$$

where q_o is the perchlorate ion uptake by DOW 3N-Cu at equilibrium (calculated using data after 100 h of equilibration), q_n is the non-zero root of Eq (2-9):

$$\tan q_n = \frac{3q_n}{3 + \alpha q_n^2} \quad (2-9)$$

where parameter α is expressed in terms of the final fractional uptake of perchlorate ion by IX resins according to the relation:

$$\frac{q_o}{V_o C_o} = \frac{1}{1 + \alpha} \quad (2-10)$$

where V_o and C_o are initial solution volume and perchlorate ion concentration in solution, respectively.

The experimental values of $q(t)$ at a given time during the kinetic study were determined from the following mass-balance equation:

$$Mq(t) = V[C_o - C(t)] \quad (2-11)$$

A Fortran code was written based on Eqs. (2-4)~(2-11) to facilitate the model fitting to the experimental data and to yield the best fitted diffusivity value of D .

Figure 2-4 shows the observed (symbols) and model-simulated (lines) kinetic data during the sorption of perchlorate ion by representative ion exchange resins. **Table 2-4** gives the resultant diffusivity values. The intra-particle diffusion coefficient (D) of the resins studied ranges from $2.5E-7$ to $7.5E-6$ cm^2/min . The relatively slower rate for DOW 3N-Cu is likely due to the narrowed pore size of the parent DOW 3N resin upon copper loading (Zhao, 1997). The other copper-loaded PLE, XAD1180 3N-Cu, offered a greater diffusivity but a much smaller perchlorate ion sorption capacity (**Table 2-3**) than DOW 3N-Cu, indicating XAD1180 3N-Cu possesses fewer but more readily accessible

sites. Although the capacity factor (A_f) value for IRA 900 was only 36% of that for A-530E, the diffusivity for the two resins was nearly the same.

Because of different resin morphology, the above model is not applicable to ion exchange fibers. Nonetheless, the unparalleled kinetic advantage of Smopex-103x as compared to IRA 900 and A-530E is easily revealed by the plots shown in **Figure 2-5**. Under the otherwise identical experimental conditions (sorbent weight = 0.15 g, solution volume = 4 L, $\text{ClO}_4^- = 100 \text{ mg/L}$, $\text{SO}_4^{2-} = 100 \text{ mg/L}$), ion-exchange equilibrium for Smopex-103x was reached within 1.5 hours, as compared to 23 hours for IRA 900 and 18 hours for A-530E, which were calculated based on the above kinetic model. The much faster kinetics of Smopex-103x is not surprising given that ion exchange sites on the fiber are much more easily accessible than those imbedded inside the micropores of an ion exchange bead (**Table 2-2**).

Table 2-4. Intraparticle diffusion coefficients of perchlorate for various resins.

Resins	Particle Size*, cm	D, cm^2/min
A-530E	0.205-0.042	1.25E-6
DOW 3N-Cu	0.020-0.120	2.50E-7
DOW 66	0.030-0.120	7.50E-6
IRA 900	0.030-0.120	1.00E-6
IRA 958	0.030-0.120	2.5E-6
XAD1180 3N-Cu	0.035–0.060	3.0E-6

*Particle size was from manufacturers. Mean particle size was used in model fittings.

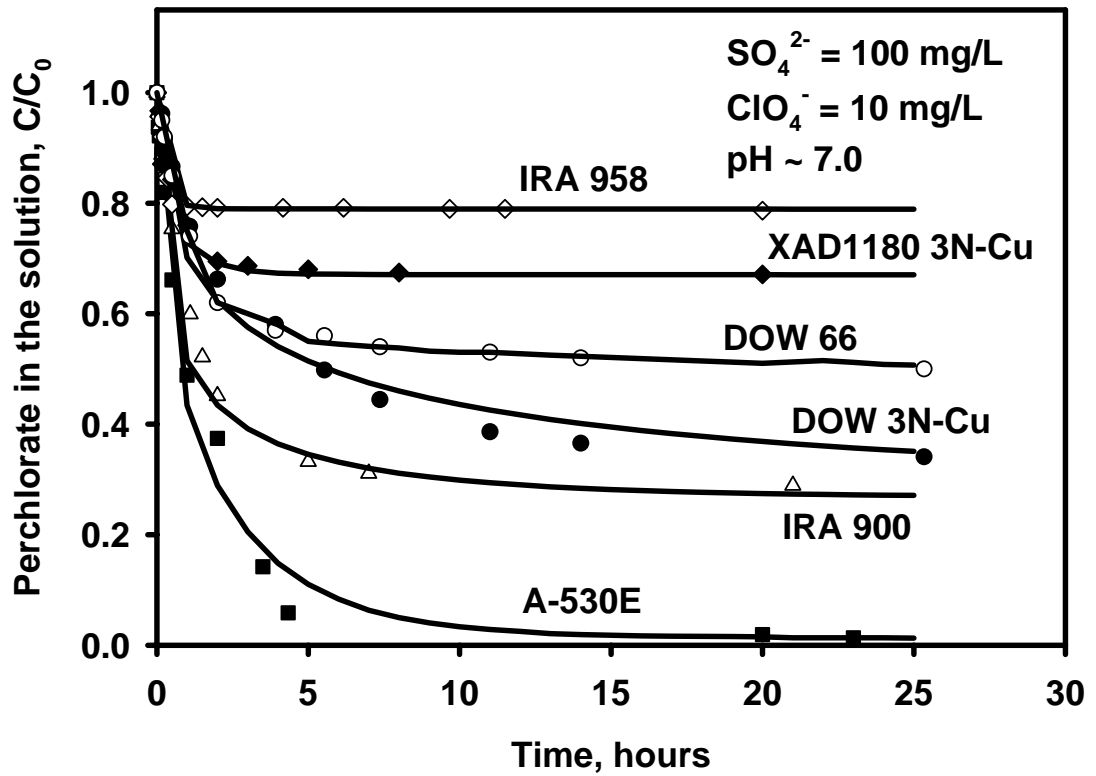


Figure 2-4. Kinetics of perchlorate ion sorption by various ion exchangers (A-530E, DOW 66, DOW 3N-Cu, IRA 958, IRA 900, and XAD1180 3N-Cu). Initial ClO₄⁻ = 10 mg/L, SO₄²⁻ = 100 mg/L and pH was kept at 7.0±0.1. (Symbols: experimental data; Lines: model fitting).

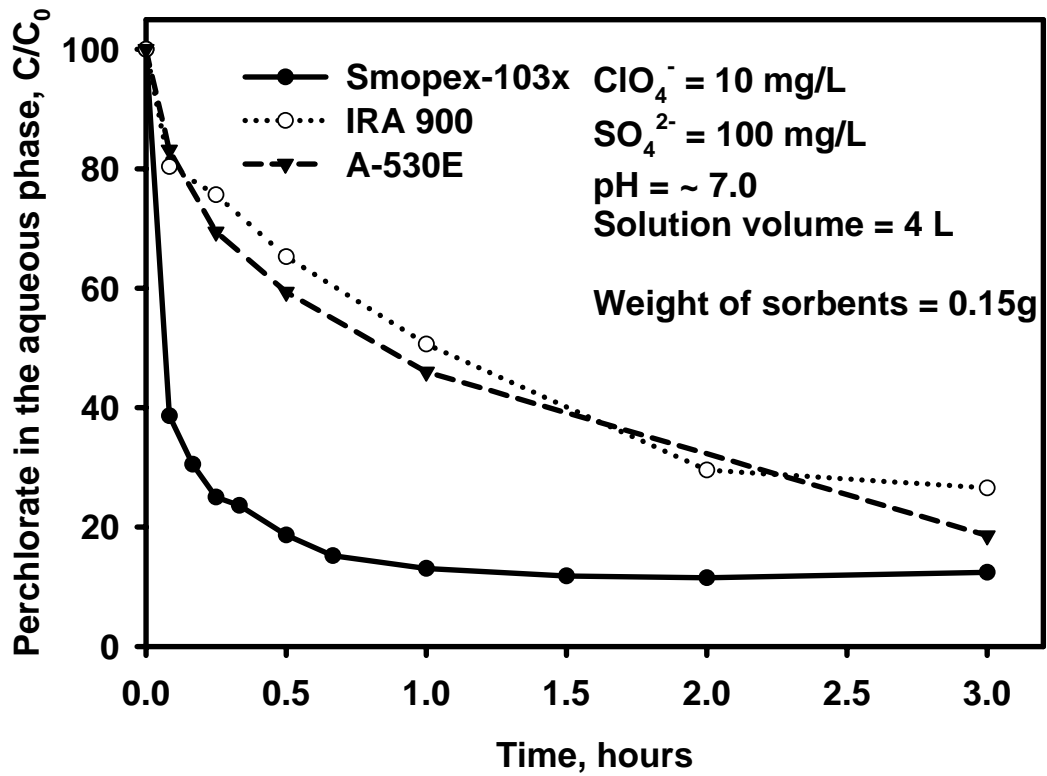


Figure 2-5. Comparison of perchlorate ion sorption rate for an ion-exchange fiber (Smopex-103x) and two ion exchange resins (A-530E, IRA 900). Initial $\text{ClO}_4^- = 10 \text{ mg/L}$, $\text{SO}_4^{2-} = 100 \text{ mg/L}$ and pH was kept at 7.0 ± 0.1 .

2.3.4 Effect of pH on perchlorate uptake

Figure 2-6 shows equilibrium perchlorate uptake as a function of equilibrium solution pH in a perchlorate/sulfate binary system for DOW 3N-Cu, IRA 900, and WA21J, respectively. As expected, perchlorate sorption onto the SBA resin IRA 900 was nearly independent of solution pH over a broad pH range of 2 to 12. For DOW 3N-Cu, perchlorate uptake remained constant below pH 8, and then dropped abruptly as pH increased from 8.0 to 10.5. The observed pH dependence of DOW 3N-Cu results from the competition from hydroxide ions, which are much stronger ligands than perchlorate. At elevated pH, hydroxyl anions become formidable competitors for the functional Cu(II) ions, and greatly diminish sorption of perchlorate. The pH dependence of the WBA resin, WA21J, is as expected. At pH>6, the resin's tertiary amine groups become deprotonated, thereby losing its anion exchange capacity.

From a regeneration viewpoint, the observed pH dependence suggests that PLE's or WBA resins may offer the advantage of being regenerated more efficiently by simply adjusting solution pH.

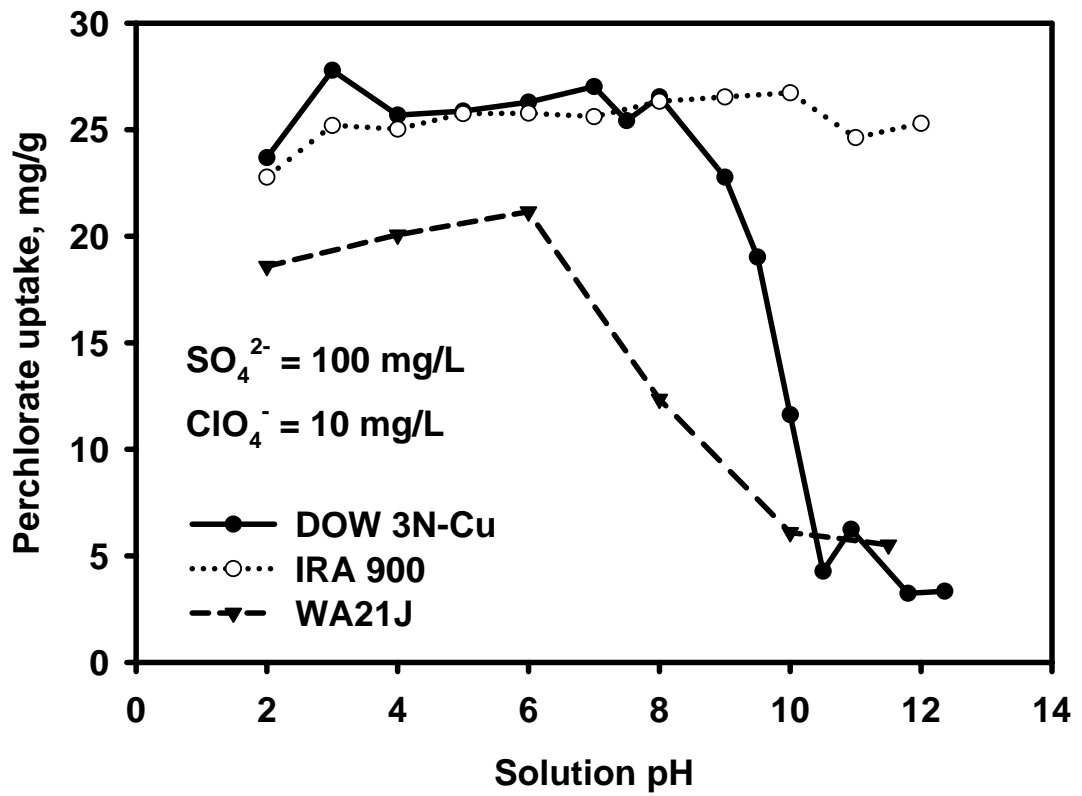


Figure 2-6. Perchlorate sorption onto DOW 3N-Cu, IRA 900, and WA21J as a function of pH in the presence of competing sulfate ions. Initial ClO₄⁻ = 10 mg/L, SO₄²⁻ = 100 mg/L.

2.3.5 Perchlorate desorption from various resins

Regeneration of perchlorate-laden A-530E, DOW 3N-Cu, XAD7HP-Cu, IRA 900 and IRA 958 using a regenerant containing 12% NaCl and 10% ethanol at pH 10.5 was carried out to elucidate the effect of ion-exchange matrices and functional groups on perchlorate desorption under otherwise identical conditions. The two PLE's (DOW 3N-Cu and XAD7HP-Cu) both carry the same functional groups (Cu^{2+}), but different matrices (polystyrene versus polyacrylic). Likewise, for the three SBA resins, A-530E and IRA 900 are more hydrophobic than IRA 958, and A-530E has the highest perchlorate selectivity and sorption capacity. As shown in **Figure 2-7**, ion exchangers with hydrophilic matrices exhibited a >25% greater regeneration efficiency than those with hydrophobic matrix, and the most perchlorate-selective A-530E exhibited the least regeneration efficiency. Within the 45 BV's of the regenerant, the mass of perchlorate desorbed was 94% for IRA 958, 89% for XAD7HP 3N-Cu, 65% for IRA 900, 62% for DOW 3N-Cu, and 27% for A-530E. The observation is consistent with the general notion that sorption of perchlorate to acrylic resins are much more reversible than to styrenic resins. Bastista et al. (2000) reported that 96% of perchlorate was recovered for an acrylic SBA resin during regeneration with 13 bed volumes of 12% NaCl, compared to only 17% for a styrenic SBA resin. Tripp and Clifford (2006) compared the regeneration efficiency of perchlorate-saturated polyacrylic and polystyrene resins using 1N NaCl, and found that the polyacrylic resin required 9 equiv Cl/equiv resin (40 lb/ft^3) to achieve 90% elution of perchlorate, while it would require >17 times more regenerant for a polystyrene-based resin to achieve the same efficiency. Evidently, regardless of types of functionalities, more hydrophobic matrices can greatly enhance sorption capacity and affinity for

perchlorate, which however, also results in much reduced regeneration efficiency with conventional regenerants. As mentioned before, a specialty regenerant (1M FeCl₃ and 4 M HCl) was needed to efficiently regenerate A-530E (Gu and Brown, 2006).

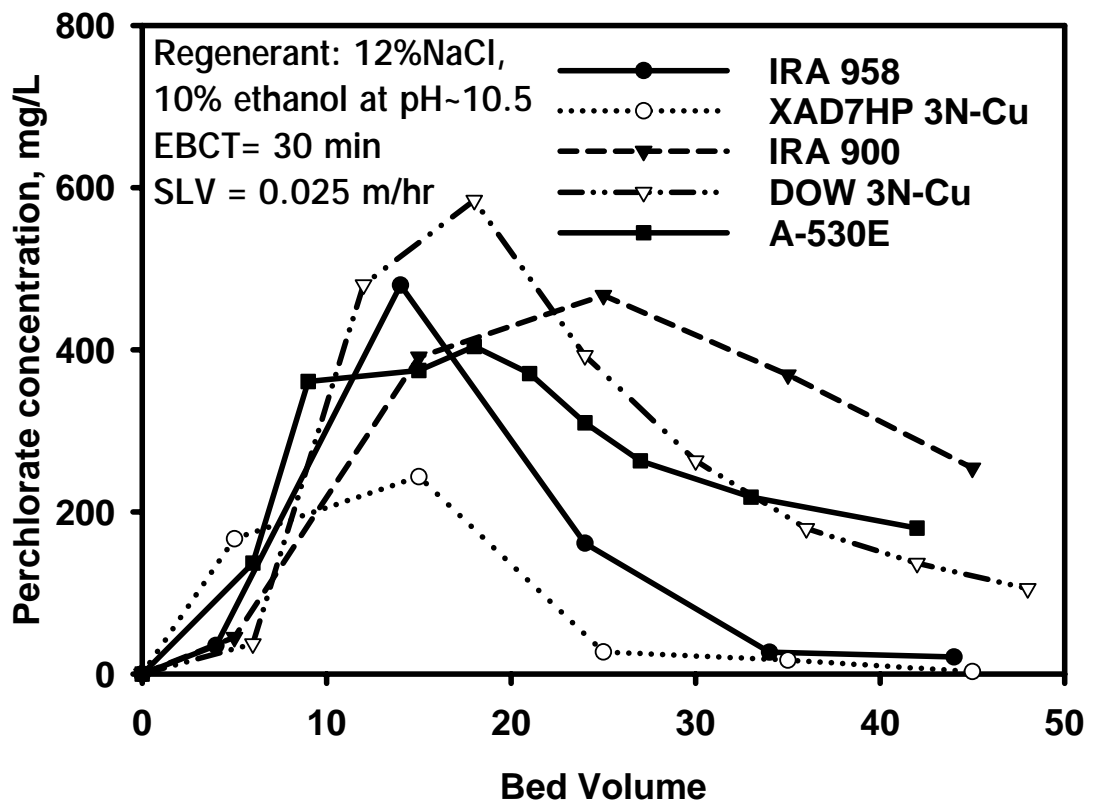


Figure 2-7. Regeneration of perchlorate-laden ion-exchangers (A530-E, IRA 958, IRA 900, DOW 3N-Cu, and XAD7HP 3N-Cu) with a regenerant containing 12% (w/w) NaCl and 10% (v/v) of ethanol at pH 10.5. Empty bed contact time (EBCT) = 30 min; superficial liquid velocity (SLV) = 0.025 m/hr.

2.3.7 Effect of ethanol on perchlorate desorption.

Because of the important roles of the sorbate-solvent interaction for perchlorate sorption, addition of a water-miscible organic solvent such as ethanol is expected to enhance desorption of perchlorate from hydrophobic resins. **Figure 2-8** shows the perchlorate ion concentration in the regenerant as the ethanol content in the regenerant increases. With 48 bed volumes of a regenerant containing 12% NaCl at pH 10.5, the mass of perchlorate desorbed increased steadily when the content of ethanol was increased: 58% when ethanol = 0, 59% with 5% ethanol, 62% with 10% ethanol, 66% with 20% ethanol, and 90% with 30% ethanol. Li and SenGupta (1998) studied the regeneration of IRA 900 loaded with pentachlorophenol (PCP) using regenerants containing NaCl and methanol and observed that sodium chloride solution alone or methanol alone was unable to desorb PCP, however, the combination of methanol and sodium chloride was able to recover 82% of PCP in 15 bed volumes. It was suggested that both ion exchange (due to the presence of chloride anions) and an enhanced nonpolar moiety-solvent interaction (due to reduced solvent dielectric constant) are the mechanisms for the increased regeneration of PCP.

Likewise, the addition of ethanol in the regenerant solution enhanced the perchlorate-regenerant interaction, thereby promoting the regeneration of perchlorate-laden DOW 3N-Cu. In addition, the addition of ethanol was also found to improve resin swelling. For instance, when exposed to 12% NaCl solution, the volume of DOW 3N-Cu bed was observed to increase 5% after 24 hrs; however, when the same bed was immersed in a solution of 12% NaCl and 30% ethanol, the same resin bed was increased by 20%. Consequently, the desorption activation energy is lowered and mass transfer in

the micropores in the resin is enhanced, resulting in improved ion exchange kinetics and regeneration efficiency.

The spent brine can be further treated through physico-chemical (e.g. reduction using zero-valent iron nanoparticles (Xiong et al., 2007a)) or biological processes (Cang et al., 2004; Gingras and Batista, 2002; Logan et al., 2001) where ethanol can be used as a substrate for the growth of bacteria (Kato et al., 1997).

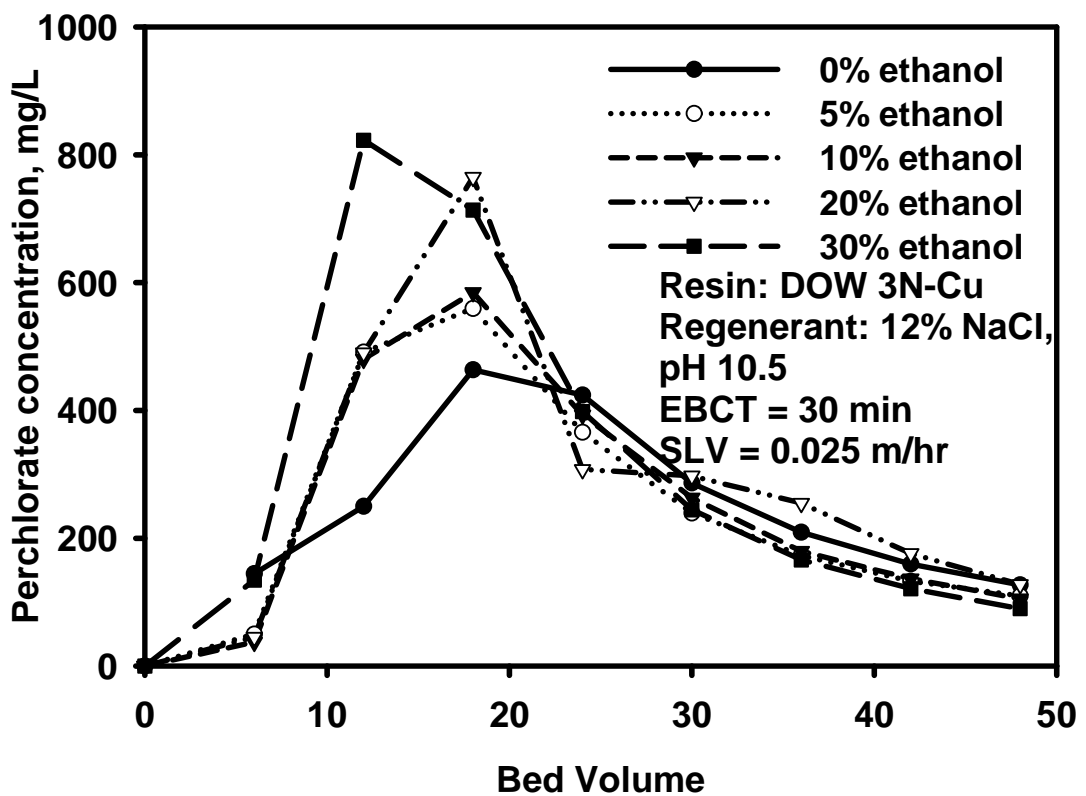


Figure 2-8. Regeneration of perchlorate-laden DOW 3N-Cu by a regenerant containing 12% (w/w) NaCl at pH 10.5 and various concentrations of ethanol. EBCT = 30 min; SLV = 0.025 m/hr.

2.3.8 Effect of pH on perchlorate desorption

As previously discussed, sorption of perchlorate to PLE's and WBA resins is a pH-dependent process. This observation warrants the convenience that sorption and desorption of perchlorate may be manipulated by simply controlling the solution pH. **Figure 2-9** and **Figure 2-10** show that the regeneration becomes more efficient for both DOW 3N-Cu and WA21J, respectively, as the regenerant pH was increased. With 36 bed volumes of a regenerant containing 12% NaCl at various pH, the mass of perchlorate desorbed from the perchlorate-laden DOW 3N-Cu was 49% at pH 9.06, 57% at pH 10.53, 68% at pH 11.96, 74% at pH 13.44, which shows that the regeneration efficiency of perchlorate-laden DOW 3N-Cu was increased by 25% when the regenerant pH was increased from 9.06 to 13.44. The regeneration efficiency was nearly doubled for the WBA resin (WA21J) when the regenerant pH was increased from 7.0 to 10.5 (**Figure 2-10**). The results indicate that for WBA resins, raising pH appears to be a simple and effective method to improve the regeneration efficiency.

It should be noted that for DOW 3N-Cu, up to 4% of initially immobilized copper in the resin was also washed off when the regenerant pH was increased to 12 (Xiong et al., 2006). Thus, caution should be exercised in regeneration of PLE's at elevated pH.

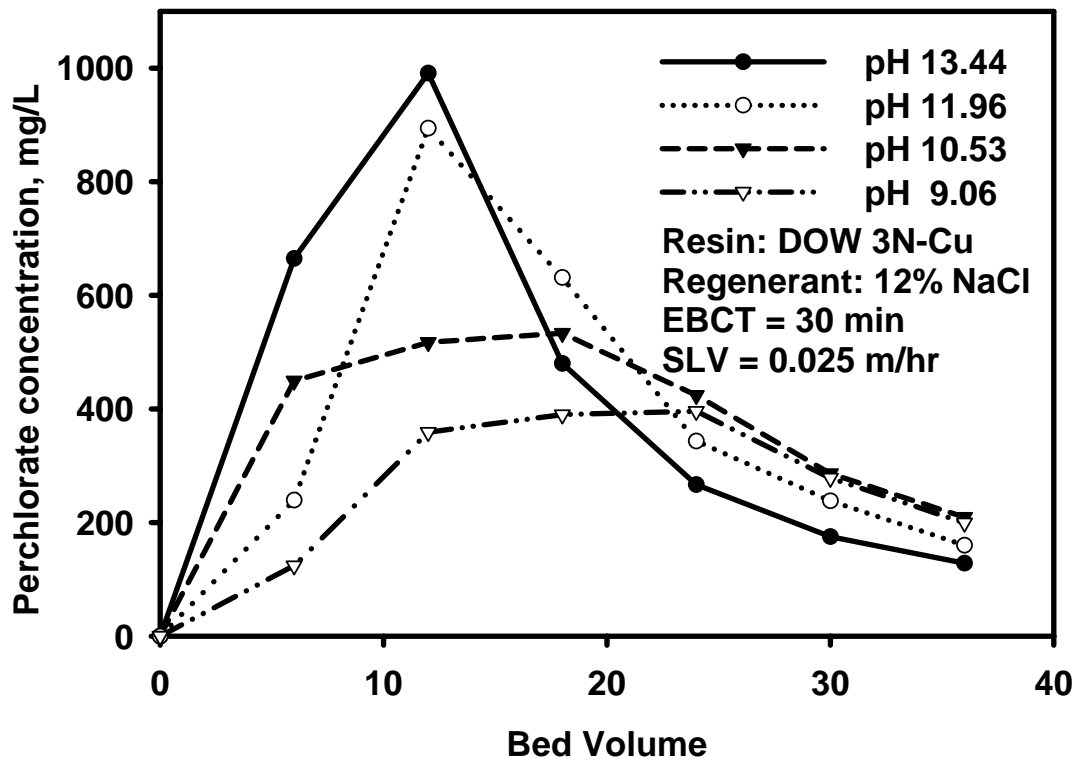


Figure 2-9. Regeneration of perchlorate-laden DOW 3N-Cu with a regenerant containing 12% (w/w) NaCl at various pH. EBCT = 30 min; SLV = 0.025 m/hr.

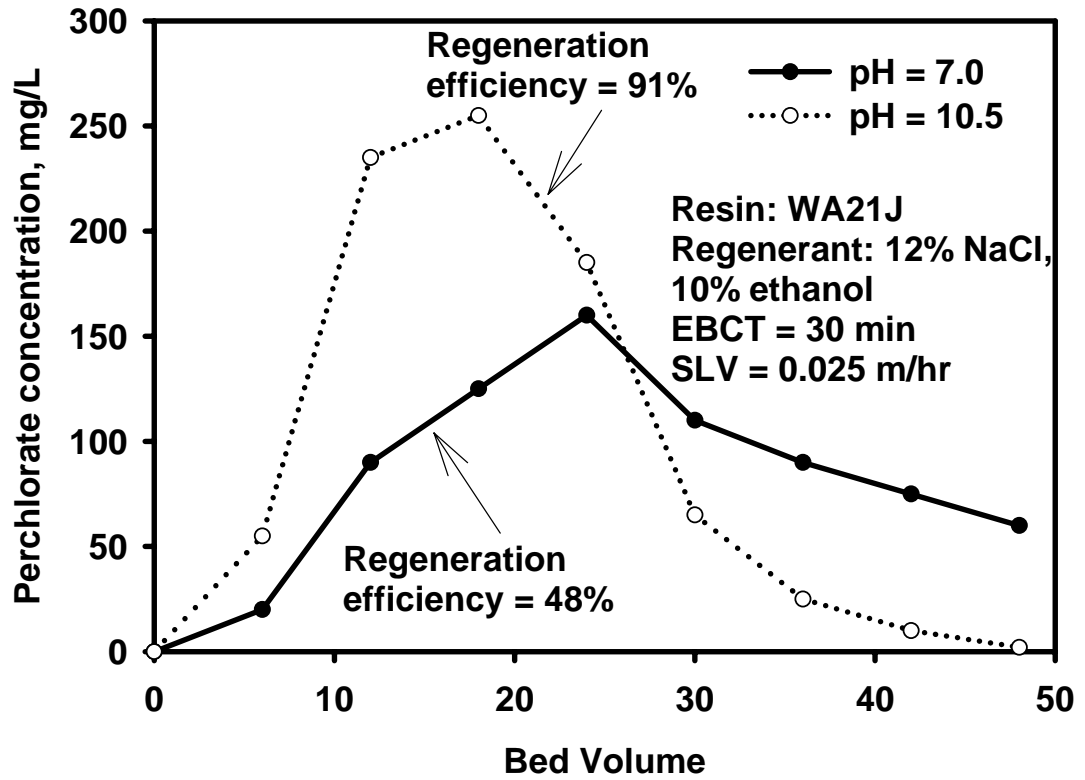


Figure 2-10. Regeneration of perchlorate-laden WA21J with a regenerant containing 12% (w/w) NaCl and 10% (v/v) ethanol at various pH. EBCT = 30 min; SLV = 0.025 m/hr.

2.3.9 Effects of resin morphology: Porous beads versus fibers.

Figure 2-11 shows the perchlorate elution profile and regeneration efficiency during regeneration of the IXF, Smopex-103x. More than 85% of the ion-exchange capacity was recovered with ~38 bed volumes of a brine-only (12% NaCl) solution. Note that under the same conditions the regeneration efficiency for IRA 900 was only 15% (data not shown). This greatly improved regeneration efficiency of Smopex-103x is attributed to the ‘shallow’ and more accessible ion exchange sites of this material. This observation also suggests that the poor regeneration efficiency of standard ion exchange beads is, at least, partially limited by site accessibility, and the profound intraparticle mass transfer resistance during regeneration. When perchlorate sorption capacity, kinetics and regeneration are all considered, IXF such as the Smopex-103x appears to be a promising alternative sorbent over conventional ion exchange resins.

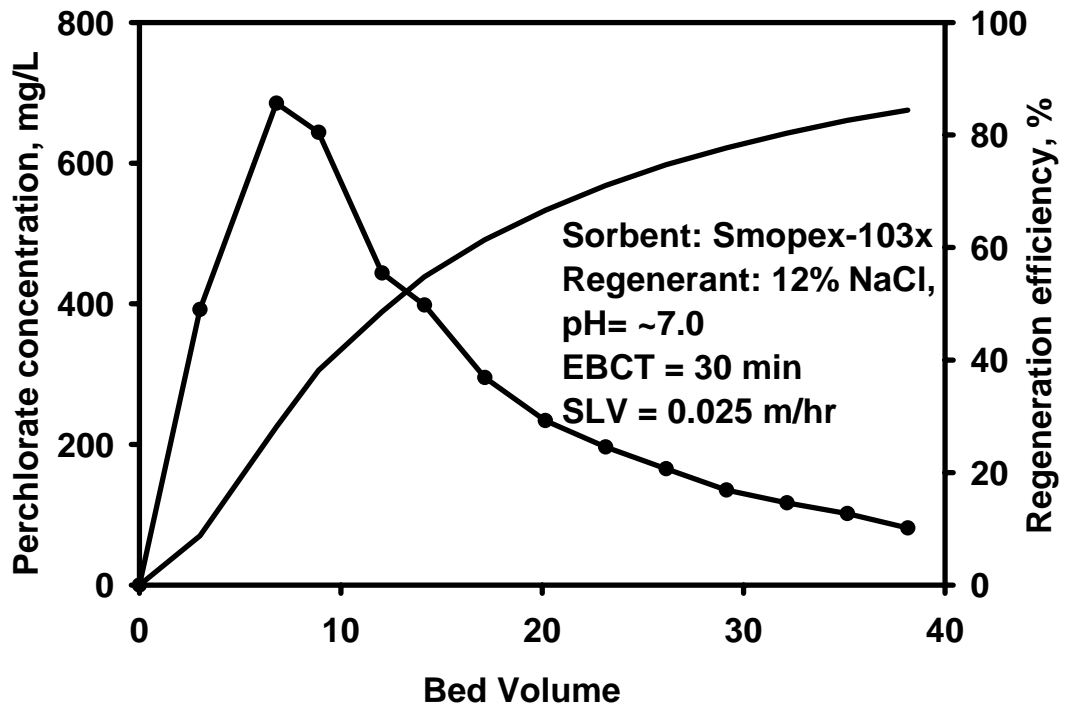


Figure 2-11. Regeneration of perchlorate-laden Smopex-103x with a regenerant containing 12% (w/w) NaCl at neutral pH. EBCT = 30 min; SLV = 0.025 m/hr.

2.4 Conclusions

This study offered a systematic and fair comparison of various classes of ion exchange materials. The acquired findings may enable designers or water utilities to select the most suitable sorbent. This comparison also revealed some important insights into the mechanisms governing the sorption and desorption of perchlorate with various types of sorbents, including standard SBA and WBA resins, a new class of PLE's, and an IXF. The main conclusions from this study are summarized as follows:

1). Styrene-based macroporous resins (A530E, IRA 900, DOW 66, and DOW 3N-Cu) and IXF (Smopex-103x) offer practically acceptable perchlorate sorption capacity and perchlorate selectivity. Among the ion-exchangers tested in this study, the bifunctional A-530E resin exhibited the greatest perchlorate sorption capacity and selectivity, owing to its extended, and thus, more hydrophobic structures at the ion exchange sites. The sequence of the perchlorate sorption capacity factor (A_f) follows: A-530E >> IRA 900 > DOW 66 > Smopex-103x > DOW 3N-Cu >> WA21J > DOW 3N > XAD1180 3N-Cu >> XAD7HP 3N-Cu \approx IRA 958. The enhanced perchlorate selectivity of styrene-based resins results from their hydrophobic nature and enhanced electrostatic interactions. For PLE's, a hydrophobicity-enforced Lewis acid-base interaction between the PLE's metal functional groups and perchlorate ion is also operative. In contrast, resins with polyacrylic matrix (IRA 958 and XAD7HP 3N-Cu) showed much lower perchlorate sorption capacity and were more selective for sulfate over perchlorate ions. Conversely, regeneration of acrylic resins was much more efficient than styrenic resins. The sequence of the ion-exchangers' regeneration efficiency is IRA 958 > WA21J > XAD7HP 3N-Cu > IRA 900 > DOW 3N-Cu > A-530E. Note that the WBA resin

(WA21J) showed a comparable perchlorate ion sorption capacity to that for the styrene-based SBA resin (IRA 900), yet, a much greater regeneration efficiency (comparable to the acrylic resins such as IRA 958).

Kinetic tests revealed that the intraparticle diffusion coefficients (D) of various ion-exchangers are in the sequence: DOW 66 > XAD1180 3N-Cu > IRA 958 > A-530E > IRA 900 > DOW 3N-Cu. However, the difference in perchlorate diffusivity was within one order of magnitude, except for DOW 3N-Cu.

2). In addition to the matrix hydrophobicity, the pore accessibility of a sorbent also plays an important role in both sorption and desorption of perchlorate. Although XAD-based resins offer much greater surface area, the ion exchange sites of these hypocrosslinked materials are poorly accessible for perchlorate uptake. As a result, PLE's prepared based on XAD resins, regardless of matrix type, were not as effective as DOW 3N-Cu, which was prepared based on a macroporous chelating resin.

3). The IXF, Smopex-103x, displayed a perchlorate sorption capacity ~5 times greater than acrylic resins such as IRA 958, and yet, this fibrous sorbent offers unparalleled perchlorate sorption kinetics with a half life of 4 minutes and equilibrium time of 90 minutes. Moreover, the fibrous morphology also grants Smopex-103x much greater regeneration efficiency than styrenic resins. More than 85% of its ion-exchange capacity was recovered after using 38 bed volumes of a brine-only solution (12% NaCl at pH ~7.0).

CHAPTER 3. COMPLETE DESTRUCTION OF PERCHLORATE IN WATER AND ION-EXCHANGE BRINE USING STABILIZED ZERO-VALENT IRON NANOPARTICLES

In this chapter, a new class of stabilized zero-valent iron (ZVI) nanoparticles is prepared and used for complete degradation of perchlorate in both water and ion-exchange brine. The stabilized ZVI nanoparticles are successfully prepared by using polysaccharides such as water-soluble starch and carboxymethyl cellulose (CMC) as stabilizers, and the prepared nanoparticles are characterized with transmission electron microscope (TEM) and dynamic light scattering (DLS). Perchlorate destruction with the stabilized ZVI nanoparticles is carried out in batch tests and effects of reaction temperature, solution pH, metal catalysts, and solution salinity are investigated.

3.1 Introduction

Perchlorate (ClO_4^-) has been primarily used in solid rocket fuels. It is also widely used in firework powder, roadside flares, airbag inflators, and fertilizers imported from Chile (Urbansky, 1998). Past massive use of perchlorate has left a contamination legacy that perchlorate has been detected at about 400 sites in groundwater, surface water, soil or public drinking water in more than 25 states across the United States with concentrations ranging from 4 $\mu\text{g/L}$ to more than 3.7 million $\mu\text{g/L}$ (U.S. GAO, 2005). Recently, perchlorate was also detected in milk (Kirk et al., 2005) and bottled water

(Snyder et al., 2005). To reduce the effects of this anion in human health, especially to thyroid gland (Wolff, 1998; Blount et al., 2006), the U.S. EPA adopted a Drinking Water Equivalent Level (DWEL) of 24.5 $\mu\text{g/L}$. Meanwhile, California adopted a public health goal of 6 $\mu\text{g/L}$ and Massachusetts set the nation's first drinking water standard of 2 $\mu\text{g/L}$ for perchlorate.

Perchlorate is highly water-soluble, non-complexing, non-volatile, and chemically stable ion (Urbansky, 1998). Because of the unique chemistry of this anion, removal of perchlorate ions from water by traditional water treatment approaches is unefficient (Hatzinger, 2005). In recent years, various treatment technologies have been developed and/or tested for perchlorate removal, including biological processes (Logan et al., 2002; Min et al., 2004; Xu et al., 2003), ion-exchange (IX) (Gu et al., 2001; 2003; Tripp and Clifford, 2000; 2004; 2006; Xiong et al., 2006; 2007b), tailored activated carbon sorption (Chen et al., 2005; Parette et al., 2005), filtration (Yoon et al., 2003), dendrimer sorption (Diallo et al., 2007), and chemical reduction (Moore et al., 2003; Gu et al., 2006). However, these technologies are limited by some critical technical and/or economic drawbacks such as slow degradation kinetics and production of large volumes of concentrated process waste residuals. For instance, IX has been considered as one of the best available technologies for perchlorate removal (Gingras and Batista, 2002; Logan, 2000), and many commercial IX resins can offer high perchlorate sorption capacity (Xiong et al., 2007b). However, the regeneration efficiency of the IX resins has been found to be prohibitively poor. As a result, current IX processes are either used on a disposable basis (i.e. the resin is disposed of after only one service run) or, when resin regeneration is practiced, this process yields large volumes of spent regenerant brine.

Spent IX brine is typically characterized with high salinity, concentrated perchlorate, and/or mixtures of concentrated acids and salts (1 M FeCl₃ and 4 M HCl) (Gu et al., 2001). Because of the highly stressful conditions, biological treatment of the spent brine is rather challenging. Consequently, cost-effective technologies that can destroy perchlorate in fresh water and IX regenerant brine are in dire need.

In recent years, ZVI has attracted increasing interest for abiotic dechlorination of chlorinated organic compounds (Wang and Zhang, 1997), removal of nitrate (Huang and Zhang, 2004; Yang and Lee, 2005), reduction of chromate (Wilkin et al., 2005), and sorption of arsenic (Kanel et al., 2006). ZVI was also tested for perchlorate reduction using iron filings (Moore et al., 2003; Moore and Young, 2005), metallic iron and UV (Guroi and Kim, 2000), cast iron (Oh et al., 2006a; 2006b), and non-stabilized iron nanoparticles (Cao et al., 2005).

Because ZVI-based reactions are surface-mediated processes, increasing the surface area of ZVI was found to increase reaction rates (Wang and Zhang, 1997). Decreasing the size of ZVI particles to the nanoscale can greatly enhance the reaction rates for perchlorate reduction (Cao et al., 2005) and nitrate removal (Yang and Lee, 2005). However, because nanoscale ZVI particles tend to agglomerate rapidly (in a few minutes) (He and Zhao, 2005; He et al., 2007), the “nanoparticles” without a stabilizer are actually micro-sized agglomerates or flocs of ZVI particles.

To maximize the reactivity of ZVI nanoparticles, He and Zhao (2005) and He et al. (2007) modified the conventional water-based approach for preparing ZVI nanoparticles by applying a food-grade water-soluble starch or sodium carboxymethyl cellulose (CMC) as a stabilizer. Compared to conventional non-stabilized ZVI

“nanoparticles”, the stabilized nanoparticles displayed much greater surface area, superior physical stability and much faster TCE-dechlorination rates.

This present study aims to test the feasibility of using the starch- or CMC-stabilized ZVI nanoparticles for perchlorate destruction in fresh water or in spent IX regenerant brine or contaminated saline water. The specific objectives are to: 1) determine the rate and extent of perchlorate reduction by stabilized ZVI nanoparticles; and 2) characterize the influences of temperature, metal catalyst, salinity, and pH on the reactivity of the nanoparticles.

3.2 Materials and Methods

The following chemicals were used as received: 4-(2-Hydroxyethyl)-1-piperazineethane ethanesulfonic acid (HEPES, $C_8H_{18}N_2O_4S$) (Fisher, Fair Lawn, NJ, USA); cobalt chloride ($CoCl_2 \cdot 6H_2O$) (Fisher); cupric chloride ($CuCl_2 \cdot 2H_2O$) (Fisher); ferrous sulfate ($FeSO_4 \cdot 7H_2O$) (Acros Organics, Morris Plains, NJ, USA); methyltrioxorhenium (VII) ($MeReO_3$, 98%) (Strem Chemicals, Newburyport, MA, USA); nickel chloride ($NiCl_2 \cdot 6H_2O$) (Fisher); potassium hexachloropalladate (K_2PdCl_6 , 99%) (Acros Organics); sodium borohydride ($NaBH_4$) (MP Biomedicals, Aurora, OH, USA); sodium carboxymethyl cellulose (M.W. = 90,000, D.S. = 0.7) (Acros Organics); sodium chloride (NaCl) (Fisher); sodium chlorate ($NaClO_3$, lab grad) (Fisher); sodium chlorite ($NaClO_2$, 80%) (Fisher); sodium hypochlorite ($NaClO$) (Acros Organics); sodium perchlorate ($NaClO_4$, >98%), (Aldrich, St. Louis, MO, USA); water-soluble starch (Alfa Aesar, Ward Hill, MA, USA).

Stabilized ZVI nanoparticles were prepared following a procedure reported previously (He and Zhao, 2005; He et al., 2007). In brief, the preparation was carried out in a 500 mL flask attached to a vacuum line. A solution containing 1% (w/w) starch or 1% CMC was prepared by dissolving a water soluble starch or CMC with deionized (DI) water and then the solutions were purged with purified N₂ for half an hour to remove dissolved oxygen (DO). Stock solutions of 0.1-0.2 M FeSO₄•7H₂O were also prepared with DI water. In a typical preparation, a FeSO₄•7H₂O stock solution was added to the starch or CMC solution through a burette to yield a desired concentration of iron and the stabilizer. The mixture was purged with N₂ for half an hour to remove DO and to mix the solution. Fe(II) ions were then reduced to Fe(0) nanoparticles by adding a stoichiometric amount of sodium borohydride to the mixture. To ensure efficient use of the reducing agent, the reactor system was operated under continuous exposure to vacuum. The flask was hand-shaken intermittently during the preparation. When gas (hydrogen) evolution ceased (after 15 min), the ZVI nanoparticles were ready for use. To test the effect of metal catalysts, a second metal (Co, Cu, Ni, or Pd) solution was added at 0.3% (w/w) of Fe to the ZVI nanoparticles to yield a class of stabilized bimetallic nanoparticles. To test the catalytic effect of rhenium (Re), various masses of solid methyltrioxorhenium (MeReO₃) were dissolved into selected Fe-Pd suspensions to achieve desired catalyst concentrations. For comparison, non-stabilized ZVI nanoparticles were also prepared following the same procedure but without the addition of a stabilizer.

Transmission electron micrograph (TEM) images were obtained using a Zeiss EM10 transmission electron microscope (Zeiss, Thornwood, NJ) operated at 25 and 40 kV. The TEM image was analyzed using a specialty image processing software ImageJ to

obtain the particle size. Detailed procedures on the sample preparation and analyses were reported elsewhere (He and Zhao, 2005).

Dynamic light scattering (DLS) tests were performed with a Nicomp 380 Submicron Particle Sizer (PSS, Santa Barbara, CA) at a measurement angle of 90° (Internal He-Ne laser, wavelength 633 nm). DLS measures the dynamic particle size distribution of the nanoparticles in situ (aqueous solution). The particle size was measured based on number weighting; and the minimum particle diameter was set at 1 nm. The viscosity of various nanoparticle suspensions was measured with a Gilmont falling ball viscometer and then used to correct the influence of viscosity on particle mobility. Before the measurements, freshly prepared nanoparticle suspensions were first diluted to 0.1 g/L with nitrogen-purged 0.2 % CMC or starch solutions. Samples were placed in the machine for 5 minutes prior to start of the measurements. Each sample was measured three times (10 minutes each) on 1 mL of the diluted sample. The DLS data were then processed with a software package (CW380) to yield the number-weighted size distributions.

Batch kinetic tests for perchlorate degradation by the nanoparticles were carried out using 25 mL glass vials. The reduction was initiated by mixing 2.5 mL of a perchlorate stock solution (1.0–10.0 mM) and 22.5 mL of a certain type of ZVI nanoparticle suspension (2 g/L Fe), which resulted in an initial ClO_4^- concentration of either 10 or 100 mg/L. These initial concentration values are within the range of reported perchlorate levels, especially in the source zones (USGAO, 2005) or in spent IX brine, and are comparable to those studied by other researchers (Cao et al., 2005; Hurley and Shapley, 2007; Moore et al., 2003; Oh et al., 2006a; 2006b). In all cases, a ZVI dose of

1.8 g/L was tested and this iron dose amounts to the lower end of the range (1.0–20.0 g/L of non-stabilized ZVI) tested by Cao et al. (2005). Higher concentrations of ZVI were also prepared, but this required the stabilizer concentration to be increased accordingly. Our tests indicated that when the CMC exceeded 1.2% (w/w), the solution turned into a gel upon heating, and thus was no longer suitable for the desired uses. The vials were then sealed with Teflon-lined caps, and placed in an oven (Thelco model 28, Gca/Precision Scientific), which was set at a desired temperature. We observed that stirring at 40 rpm on a rotator (Glas-Col, Terre Haute, IN, USA) at 80 °C showed no significant effect on perchlorate reduction kinetics. Therefore, no stirring was employed in our tests. At predetermined times, duplicate sample vials were sacrificed for analyzing remaining perchlorate and reduction products. Typically, ~0.5 mL sample was diluted with acidified deionized water (pH=3) by 10-100 times to convert the remaining ZVI nanoparticles to soluble Fe(II), and then analyzed for perchlorate and reduction by-products such as chlorate, chlorite, hypochlorite and chloride. Control experiments were carried out without ZVI nanoparticles but under otherwise identical conditions.

To test pH effects, the degradation experiments were carried out at an initial pH ranging from 5.1 to 8.5 adjusted with 0.1 N NaOH and/or 0.1 N HCl, or under a constant pH 7.4 by adding 5 mM HEPES buffer solution to the vials.

ClO_4^- , ClO_3^- , ClO_2^- , ClO^- , and Cl^- were analyzed using a Dionex Ion Chromatography (DX-120) equipped with a suppressed conductivity detector. ClO_4^- was analyzed using an AS16 column, an AG16 guard column, and a 1000 μL sample loop. A degassed 50 mM sodium hydroxide solution was used as the eluent. The detection limit for perchlorate was 4 $\mu\text{g/L}$. ClO_3^- , ClO_2^- , ClO^- , and Cl^- were analyzed using an AS14

column, an AG14 guard column, and a 100 μL sample loop. Detection limits for ClO_3^- , ClO_2^- , ClO^- , Cl^- were 0.1 mg/L, 0.1 mg/L, 0.05 mg/L, 0.05 mg/L, respectively. A solution containing 3.5 mM sodium carbonate and 1.0 mM sodium bicarbonate was used as the eluent. The eluent flow rate was set at 1.0 mL/min.

3.3 Results and Discussion

3.3.1. Characterization of nanoparticles

Figure 3-1 shows a TEM image of the ZVI nanoparticles prepared at 2 g/L Fe and stabilized with 0.9% CMC. The stabilized ZVI nanoparticles appeared as discrete nanoparticles and remained dispersed in water for more than one week. Five TEM images including 1,711 particles were analyzed for estimating the particle size. The mean size of the freshly prepared CMC-stabilized nanoparticles was estimated to be 11.2 ± 7.9 nm (standard deviation). Meanwhile, DLS tests were also carried out to obtain the dynamic ‘wet’ particle size distribution. The DLS results gave a particle diameter of 13.7 ± 2.3 nm (99.9% particles by number), which appears to agree with TEM-based ‘dry’ particle size. Based on a mean diameter of 13.7 nm, the surface area was calculated to be $55.6 \text{ m}^2/\text{g}$ following the method by He and Zhao (2005). DLS tests were also carried out for the starch-stabilized ZVI nanoparticles. A mean particle diameter of 22.6 ± 2.8 nm (99.9% by number) was obtained, which translates into a surface area of $33.7 \text{ m}^2/\text{g}$.

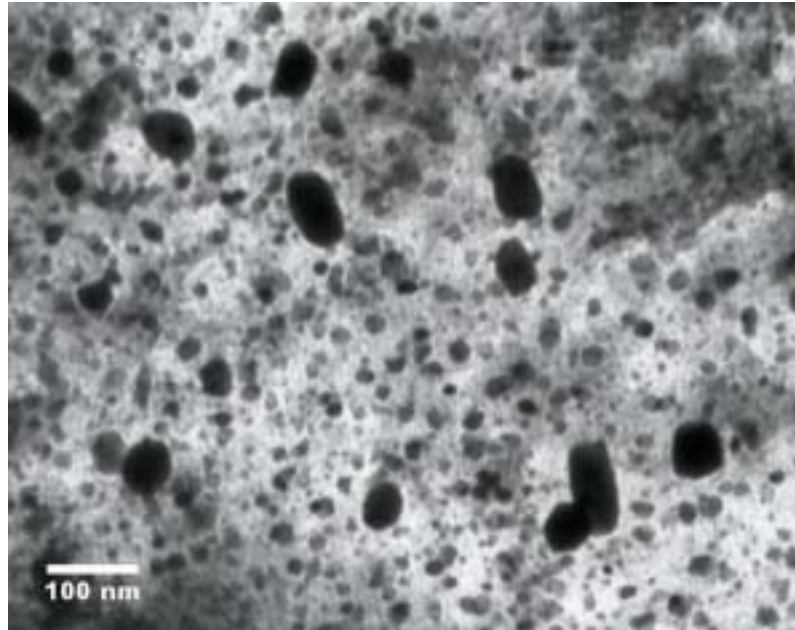
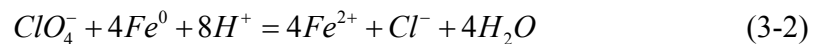


Figure 3-1. TEM image of fresh ZVI nanoparticles stabilized with 0.9% (w/w) CMC.

The scale bar represents 100 nm.

3.3.2. Kinetics and activation energy of perchlorate reduction

Figure 3-2 shows the perchlorate reduction kinetics using 1.8 g/L ZVI nanoparticles stabilized with 0.9% CMC (w/w) at temperatures ranging from 25 °C to 110 °C. The initial pH was ~6.5 and the final pH was 7.5-7.8 after 6 hours. At 25 °C, the degradation proceeded slowly with only 23% of perchlorate reduced in 6 hours. When the temperature was raised to 50 °C, 80 °C, 95 °C, and 110 °C, respectively, the reaction was accelerated progressively. At 95 °C, 97% perchlorate was eliminated in 6 hours, and at 110 °C, complete perchlorate degradation was achieved within only 2 hours. It is noteworthy that the perchlorate reduction (except at 110 °C) displayed a rapid initial drop, and then bounced back up briefly before perchlorate was further degraded. Similar kinetic profile was also observed by Moore et al. (2003) and Moore and Young (2005) who tested the effectiveness of commercial iron filings for perchlorate degradation. In the perchlorate laden solution, the ZVI nanoparticles undergo the following competitive reactions (Gu et al., 2003; Cao et al., 2005):



As the reactions proceed, the surface of the ZVI nanoparticles is progressively oxidized to iron oxides. In the experimental pH range (6.5-7.8), the resultant iron oxides can rapidly adsorb ClO_4^- from water, resulting in the observed rapid drop in perchlorate concentration in the solution phase. However, the concurrent rapid adsorption and reduction of perchlorate rapidly depletes the perchlorate chemical potential in the solution phase such that the concentration gradient between the particle surface and the

solution phase was reversed, and the sorbed perchlorate started releasing back into the solution. The perchlorate desorption was even further promoted as the concentration of chloride ions resulting from the reduction of perchlorate increases. At elevated temperatures (e.g. 110 °C), the perchlorate sorption became thermodynamically less favored whereas the perchlorate reduction was overwhelmingly enhanced. As a result, the “dipping” effect was less significant at higher temperatures. As discussed later in the chlorine mass balance study, the sorption/desorption process was a rather short-lived process and became negligible after 100 minutes of the reaction.

The degradation kinetics data can be interpreted using a pseudo-first-order rate model, Eq. (3-3), following the approach by Johnson et al. (1996):

$$\frac{d[ClO_4^-]}{dt} = -k_{SA}a_s\rho_m[ClO_4^-] = -k_{obs}[ClO_4^-] \quad (3-3)$$

where $[ClO_4^-]$ is the perchlorate concentration (mg/L) in water at time t (min), k_{SA} is the specific reaction rate constant based on surface area of the nanoparticles (L/(min·m²)), a_s is the specific surface area of the nanoparticles (m²/g), ρ_m is the mass concentration of the nanoparticles (g/L), and k_{obs} is the observed pseudo-first-order rate constant (min⁻¹). Because the model describes only reactive degradation of perchlorate, it is only used for the degradation data after the perchlorate concentration was recovered from the sorption/desorption perturbation step. Similar data-fitting approach was also used by Moore et al. (2003) to determine to perchlorate reduction rates by ZVI filings.

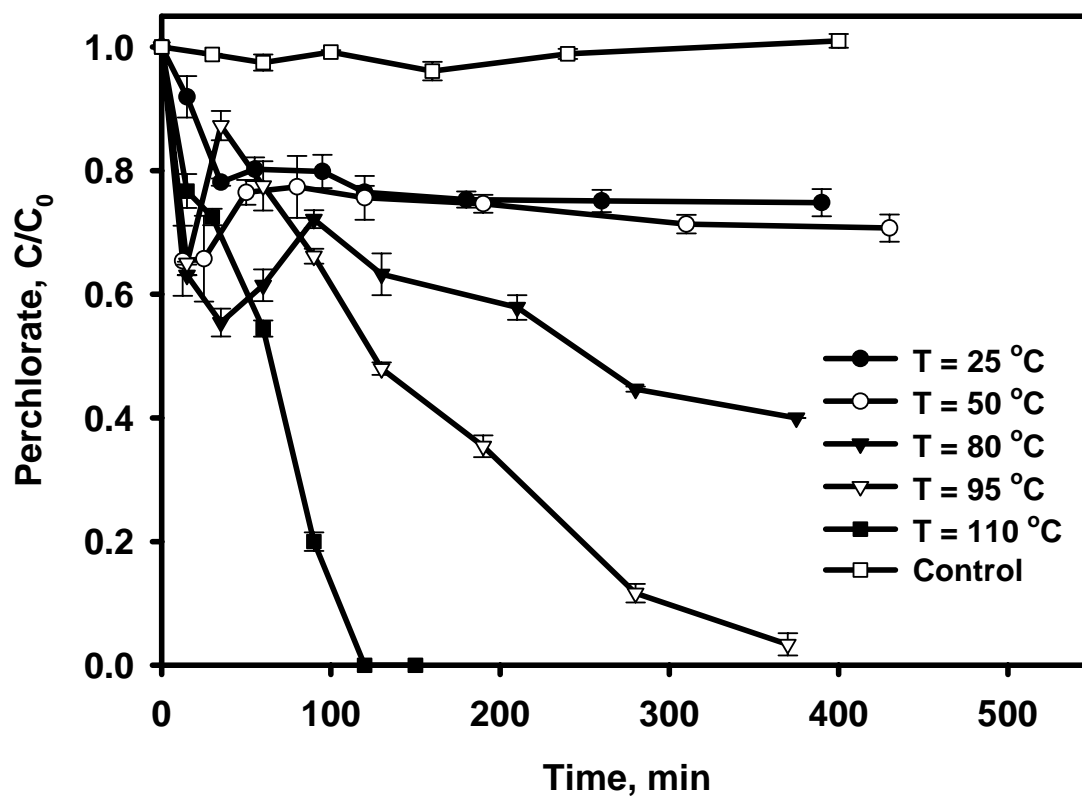


Figure 3-2. Perchlorate reduction by CMC-stabilized ZVI nanoparticles at various temperatures. Initial $[\text{ClO}_4^-] = 10 \text{ mg/L}$, ZVI = 1.8 g/L, CMC = 0.9% (w/w), initial pH (pH_0) = 6.5, and final pH (pH_f) = 7.5-7.8. Control tests were performed at 110 °C with no ZVI. Data plotted as mean of duplicates.

Figure 3-3 shows the linearized plots ($\ln(C/C_0')$ vs time) of the experimental and model-simulated kinetic data, where C_0' denotes the perchlorate concentration right after the perchlorate concentration profile was recovered from the initial sorption/desorption dip and where the perchlorate concentration began to drop again. **Table 3-1** gives the fitted model parameters. Fairly good model fitting ($R^2 > 0.90$) was obtained. Evidently, the observed pseudo-first-order rate constant (k_{obs}) was improved by 82 times when the temperature was increased from 25 °C to 110 °C.

The degradation enhancement at elevated temperatures can be easily explained when the experimental data are plotted in accordance with the linearized Arrhenius equation:

$$\ln k_{obs} = \ln A - \frac{E_a}{RT} \quad (3-4)$$

where A is a constant, E_a is the activation energy (kJ/mol), R is the universal gas constant (8.314 J/(K·mol)), and T is the absolute temperature (K).

Figure 3-4 also gives an activation energy (E_a) of 52.59 ± 8.41 kJ/mol and an A value of 194,075 at a ZVI dose of 1.8 g/L. This relatively high level of activation energy is associated with the unique chemistry of perchlorate. Although the chlorine in perchlorate is at its highest oxidation state (+7), and thus, reduction of perchlorate is thermodynamically favorable, perchlorate is quite inert toward most of reducing agents due to the high kinetic barrier (Urbansky, 1998). However, the activation energy (E_a) determined in this study is much lower than those reported by others. For example, Gu et al. (2003) reported an activation energy of 120 ± 5 kJ/mol when ferrous iron was used to reduce a perchlorate waste residual containing ferric chloride and hydrochloric acid at

elevated temperatures (up to 200 °C) and/or pressure (~20 atm). Cao et al. (2005) reported an activation energy of 79.02 ± 7.75 kJ/mol for reduction of perchlorate (200 mg/L) by non-stabilized ZVI particles at various ZVI doses (1.0-20.0 g/L). The ZVI nanoparticle serve as both a reactant (electron donor) and a catalyst (Lowry and Liu, 2006). Accordingly, the much lower activation energy for the CMC-stabilized ZVI can be attributed to two factors. First, the presence of CMC greatly enhances the surface reactivity of the ZVI nanoparticles. As will be illustrated later on, the surface-normalized rate constant (K_{SA}) for CMC-stabilized ZVI is 3.3 times greater than that for non-stabilized ZVI. Second, the presence of CMC may also boost the catalytic activity of the ZVI nanoparticles. Both enhanced surface reactivity and elevated catalytic activity can result in a reaction pathway of much lower activation energy for perchlorate degradation.

Table 3-1. Observed pseudo-first-order rate constant of perchlorate reduction by CMC-stabilized iron nanoparticles at various temperatures.

Temperature (°C)	k_{obs} (min ⁻¹)	R ²
25	0.0002	0.96
50	0.0003	0.94
80	0.0021	0.97
95	0.0096	0.97
110	0.0164	0.90

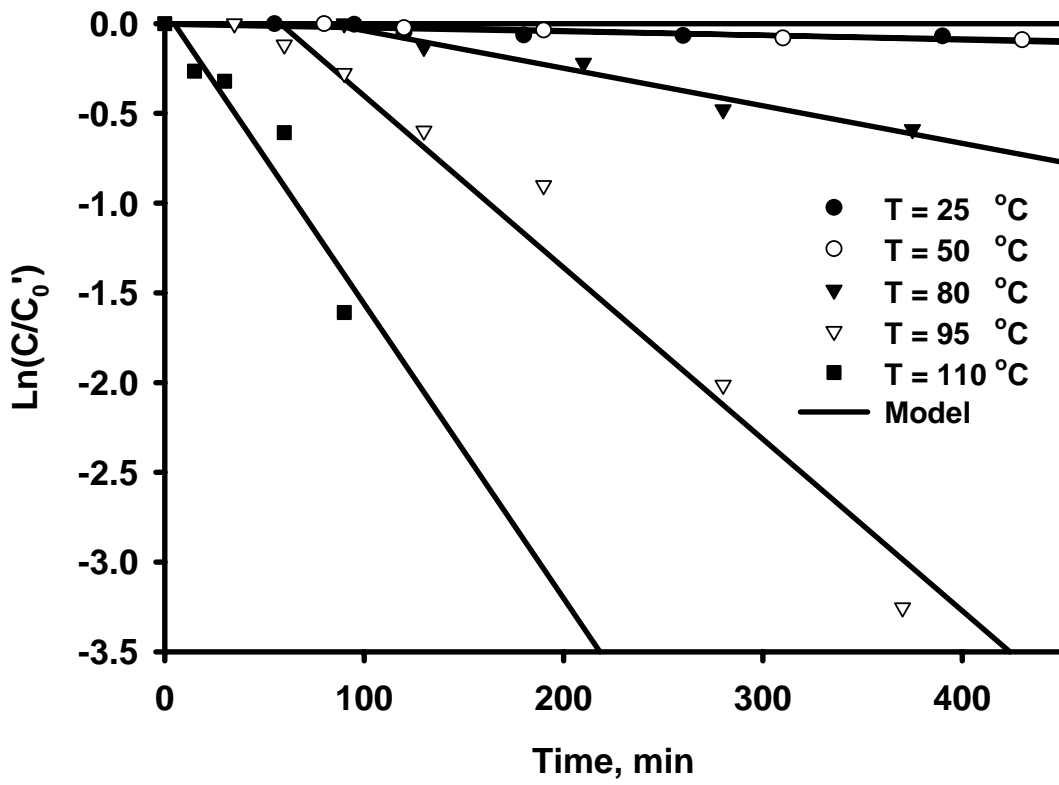


Figure 3-3. Fitting a pseudo-first-order model to the experimental perchlorate reduction rate data of Figure 3-2. Symbols: experimental data; lines: model fittings.

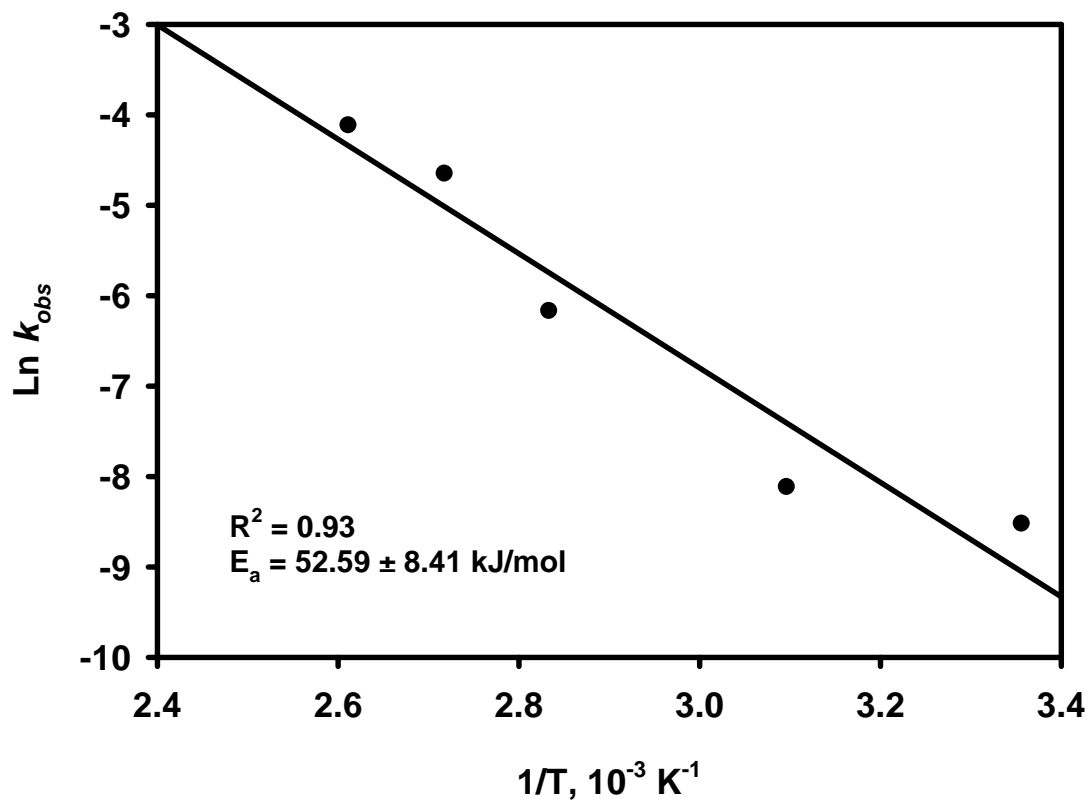


Figure 3-4. Linearized Arrhenius plot of the observed first-order rate constant (Table 3-1) as a function of $1/T$.

3.3.3. Chlorine mass balance and reaction completeness

Perchlorate reduction follows the sequential reactions below (Rikken et al., 1996; Gu et al., 2003; Cao et al., 2005):



Thus, the completeness of perchlorate reduction can be revealed by following the production of chlorate, chlorite, hypochlorite, and chloride in the system. The concentration of chlorine-containing species (ClO_4^- , ClO_3^- , ClO_2^- , ClO^- , and Cl^-) was measured during a set of batch kinetic experiments. **Figure 3-5** shows the concentrations of ClO_4^- and Cl^- as well as the total chlorine-containing species against reaction time under a temperature of 95 °C. Because ClO_3^- , ClO_2^- and ClO^- were not detected during the tests, the total chlorine-containing species was actually the sum of ClO_4^- and Cl^- .

While chloride production increased steadily with time, perchlorate displayed an initial concentration dip due to the initial sorption/desorption effect. Because of the initial rapid adsorption, the measured total chlorine species at ~20 min accounted for only 72% of the total ClO_4^- initially added in the system, which suggests that a significant fraction of perchlorate added was initially adsorbed to the nanoparticles without being degraded. After ~60 min, when the effect of sorption/desorption became less significant, the sum of ClO_4^- and Cl^- accounted for 93%-101% of total ClO_4^- initially added in the system. The nearly perfect mass balance indicates that: 1) the initially strong sorption and desorption of perchlorate became negligible after ~60 min; and 2) perchlorate was nearly completely reduced to chloride without production of significant amounts of intermediate products such as ClO_3^- , ClO_2^- and ClO^- .

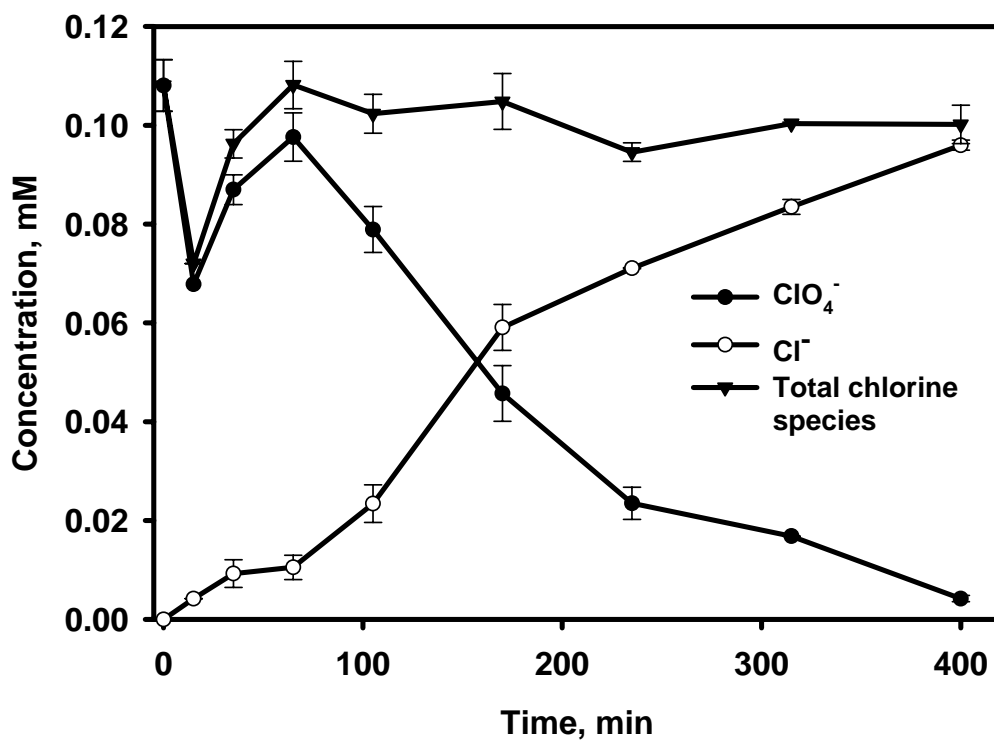


Figure 3-5. Chlorine mass balance during perchlorate reduction by CMC-stabilized ZVI nanoparticles. Initial $[\text{ClO}_4^-] = 10 \text{ mg/L}$, ZVI dose = 1.8 g/L, CMC = 0.9% (w/w), $\text{pH}_0 = 6.6\text{-}6.8$ and $\text{pH}_f = 7.7\text{-}7.8$. Data plotted as mean of duplicates.

3.3.4. Perchlorate reduction by various iron nanoparticles

He and Zhao (2005) and He et al. (2007) reported that both water-soluble starch and CMC can stabilize ZVI nanoparticles. In addition, they reported that addition of a metal catalyst such as Pd on the ZVI nanoparticles can greatly catalyze degradation of chlorinated hydrocarbons. To test the effect of the stabilizer type and metal catalysts on the perchlorate degradation, parallel kinetic tests were carried out using non-stabilized ZVI particles, starch- or CMC-stabilized ZVI nanoparticles, and stabilized nanoparticles with a metal catalyst (i.e. Cu, Co, Ni, Pd, and Re).

Figure 3-6 compares perchlorate degradation rates for various particles at 110 °C under otherwise identical conditions. Again, Eq. (3-3) was used to interpret the experimental data, and **Table 3-2** gives the fitted model parameters. Based on the k_{obs} values, starch- and CMC-stabilized ZVI nanoparticles degraded perchlorate 1.8 and 5.5 times, respectively, faster than non-stabilized ZVI particles did. Based on the surface-area normalized rate constant k_{SA} , starch- and CMC-stabilized ZVI nanoparticles degraded perchlorate 1.8 and 3.3 times, respectively, faster than non-stabilized ZVI particles did. This improved k_{SA} values suggest that stabilizers not only increased the surface area of the nanoparticles (because of the much smaller particle size), but also resulted in more reactive particle surface. On the other hand, the k_{SA} value for CMC-stabilized ZVI nanoparticles is more than 2 orders of magnitude greater than that for a cast iron (surface area = 1.29 m²/g) reported by Oh et al. (2006a).

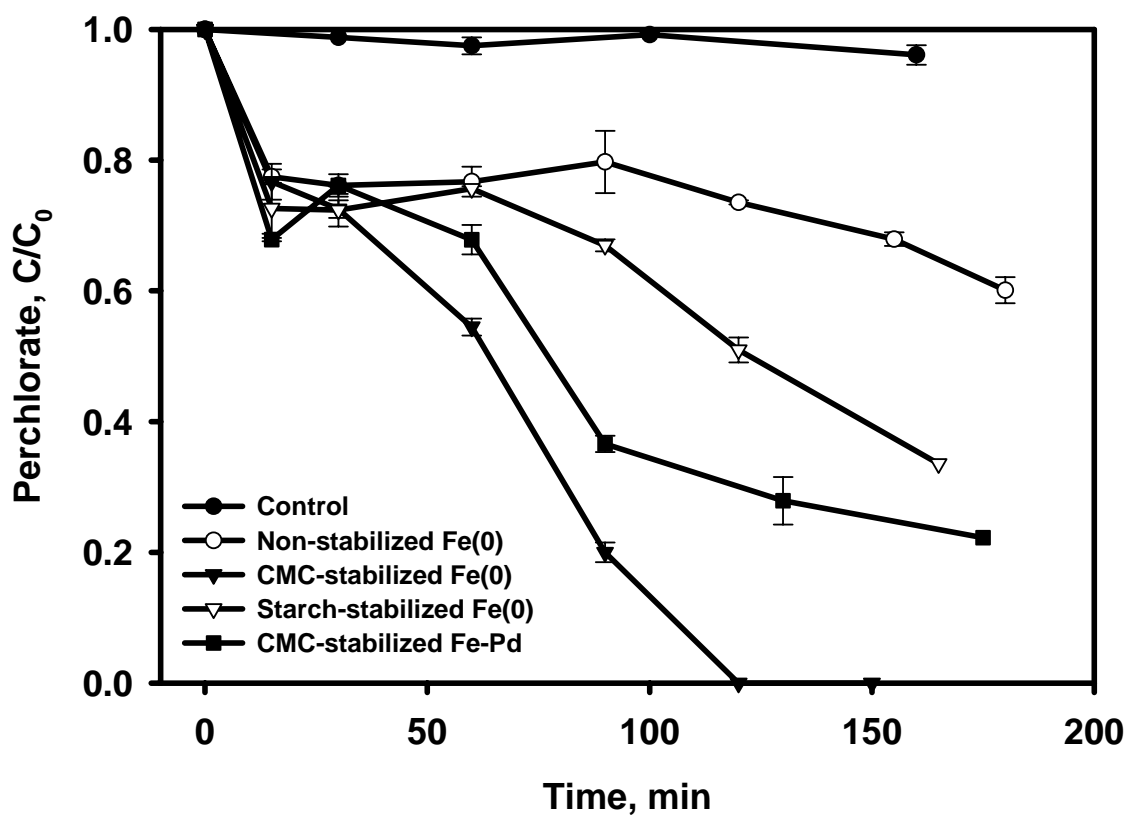


Figure 3-6. Perchlorate reduction by various ZVI-based particles. For all cases: ZVI dose = 1.8 g/L, initial $[\text{ClO}_4^-] = 10 \text{ mg/L}$, $\text{pH}_0 = 6.5\text{-}6.8$, $\text{pH}_f = 7.5\text{-}7.8$, and temperature = 110 °C; for stabilized ZVI nanoparticles, starch or CMC = 0.9% (w/w); for Fe-Pd bimetallic nanoparticles, Pd = 0.3% of Fe (w/w). Data plotted as mean of duplicates.

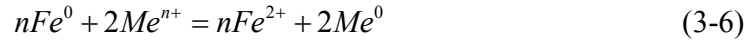
Table 3-2. Physical parameters and perchlorate reduction rate constants for various iron nanoparticles at 110 °C.

Type of Nanoparticles	a_s (m ² /g)	ρ_m (g/L)	k_{obs} (min ⁻¹)	k_{SA} (10 ⁻⁵ ·L/(min·m ²))
Non-stabilized Fe	33.5*	1.8	0.0030	5.0
Starch-stabilized Fe	33.7	1.8	0.0055	9.1
CMC-stabilized Fe	55.6	1.8	0.0164	16.4
CMC-stabilized Fe/Pd	55.6	1.8	0.0091	9.1

* From Wang and Zhang (1997).

The k_{obs} and k_{SA} for CMC-stabilized nanoparticles are 3.0 and 1.8 times, respectively, greater than that for starch-stabilized nanoparticles. This observation indicates that CMC is a more efficient stabilizer than starch, i.e. CMC gives not only smaller but also more reactive ZVI nanoparticles. The more effective particle stabilization of CMC is attributed to its carboxymethyl groups that interact with Fe(II) as well as the nanoparticles more strongly than the hydroxyl groups of starch (He et al., 2007).

Interestingly, the presence of a second metal (e.g. Pd added at 0.3% of Fe) reduced the k_{obs} and k_{SA} by 44.5%. Similar inhibitive effects were also observed when other metals such as Co, Cu, and Ni were used (data not shown). When a second metal is added to the ZVI suspensions, the following redox reaction will take place,



However, this reaction should not decrease the reducing power of the ZVI nanoparticles to any appreciable extent given the minimal amount of the second metal added. The significant drop in perchlorate reduction rate with the additional metals is then primarily attributed to the fact that the metal catalysts can catalyze the corrosion reaction of the ZVI nanoparticles (Eq. 3-1). This accelerated side reaction rendered significant loss in the reducing power of the ZVI nanoparticles toward perchlorate. Cao et al. (2005) reported that addition of Pd or Ag to non-stabilized ZVI particles showed no performance enhancement for perchlorate degradation.

Rhenium has been well recognized to be able to catalyze perchlorate reduction through an oxygen transfer reaction (Cai and Espenson, 2005; Abu-Omar et al., 2000;

2006). A recent study reported that perchlorate was reduced completely to chloride within 24 hours by hydrogen (40 psig) in the presence of methyltrioxorhenium (MeReO_3 , 0.5 mM) and palladium (0.5 mM) as catalysts (Hurley and Shapley, 2007). However, in our study, when MeReO_3 (0.5 mM) and Pd (0.5 mM) were also added to the CMC-stabilized ZVI nanoparticles, no improvement in perchlorate degradation was observed.

3.3.5. Effect of background chloride or salinity

As discussed early, chloride is one of the key products in perchlorate degradation, and will accumulate as the reaction proceeds. Moore et al. (2003) reported the presence of 28.2 mM (or 1.0 g/L) of chloride nearly ceased perchlorate degradation by commercial iron filings (size = 20-100 mesh). On the other hand, it is practically very desirable to destroy perchlorate in saline water or spent ion exchange brine, where high concentrations of perchlorate are co-present with high concentrations of chloride and/or other salts (Gingras and batista, 2002; Xiong et al., 2006; 2007b).

Figure 3-7 shows the degradation kinetics of perchlorate in the presence of chloride (added as NaCl) from 0.1 g/L to 36.4 g/L (0.02% to 6% w/w as NaCl). The degradation profile with 0.1 g/L of Cl^- nearly coincided with that when no chloride was added (with the same k_{obs} of 0.0018 min^{-1}). When chloride concentration was increased to higher levels (1.0 g/L and 10 g/L), perchlorate reduction was actually enhanced. For example, the k_{obs} value was 0.022 min^{-1} and 0.0027 min^{-1} at $\text{Cl}^- = 1.0 \text{ g/L}$ and 10 g/L , respectively, a 22% and 50% increase compared with that when Cl^- was absent. On the other hand, Gotpagar et al. (1999) reported that pretreatment of iron surface by chloride ions was able to enhance the initial degradation rate of trichloroethylene with ZVI.

Johnson et al. (1998) observed that addition of chloride ions increased the rate of CCl_4 dechlorination with ZVI by as many as four times.

The reaction enhancement by chloride can be attributed to two factors. First, the addition of chloride ions can enforce the breakdown of the thin film of iron (hydr)oxides on ZVI surface. Hard Lewis bases ions (such as Cl^- , Br^- , I^-) were reported to be especially aggressive toward the passivating oxide layers to form strong complexes with iron centers (Gotpagar et al., 1999; Johnson et al., 1998). As the oxide layers are broken down by these diffusing anions, a fresh ZVI surface becomes available for perchlorate reduction, resulting in improved perchlorate degradation. Second, chloride ions can promote localized corrosion on iron resulting in pit with irregular shapes, and pitting on iron surface provides added reactive sites for perchlorate reduction (Gotpagar et al., 1999; Prinz and Strehblow, 1998).

However, when the chloride ion concentration was increased from 10 g/L to 36.4 g/L, k_{obs} was decreased only by 23% to 0.0023 min^{-1} although this value is still 27% greater than that when no NaCl was added. This observation indicates that at the extremely high concentration of chloride ions, these anions outcompete perchlorate ions for the sorption sites and the beneficial effects of salinity are lost. Nonetheless, **Figure 3-7** shows that in the presence of 6% NaCl 87.4% of 100 mg/L ClO_4^- was transformed by 1.8 g/L the CMC-stabilized ZVI nanoparticles at 95 °C in 450 minutes, indicating that the stabilized ZVI nanoparticles can highly effectively reduce perchlorate in typical ion-exchange brine.

As indicated by Eq. 2-2, as perchlorate is converted to chloride, Fe is oxidized to Fe^{2+} . The resultant ferrous ions are non-toxic and can be either reused or removed. For

example, in case of IX brine treatment, the added chloride from perchlorate reduction actually enhances the regenerating power of the brine, and thus it is desirable to reuse the brine for regeneration. As perchlorate is re-concentrated in the reused brine, new ZVI nanoparticles can be produced in situ by reducing the existing Fe^{2+} ions in the brine with borohydride. Given the fairly low solubility of Fe^{2+} (e.g. 44 mg/L at pH 8.0), ferrous ion can be removed, if desired, either by slightly raising the pH or by converting these cations to even less insoluble Fe^{3+} ions under ambient conditions.

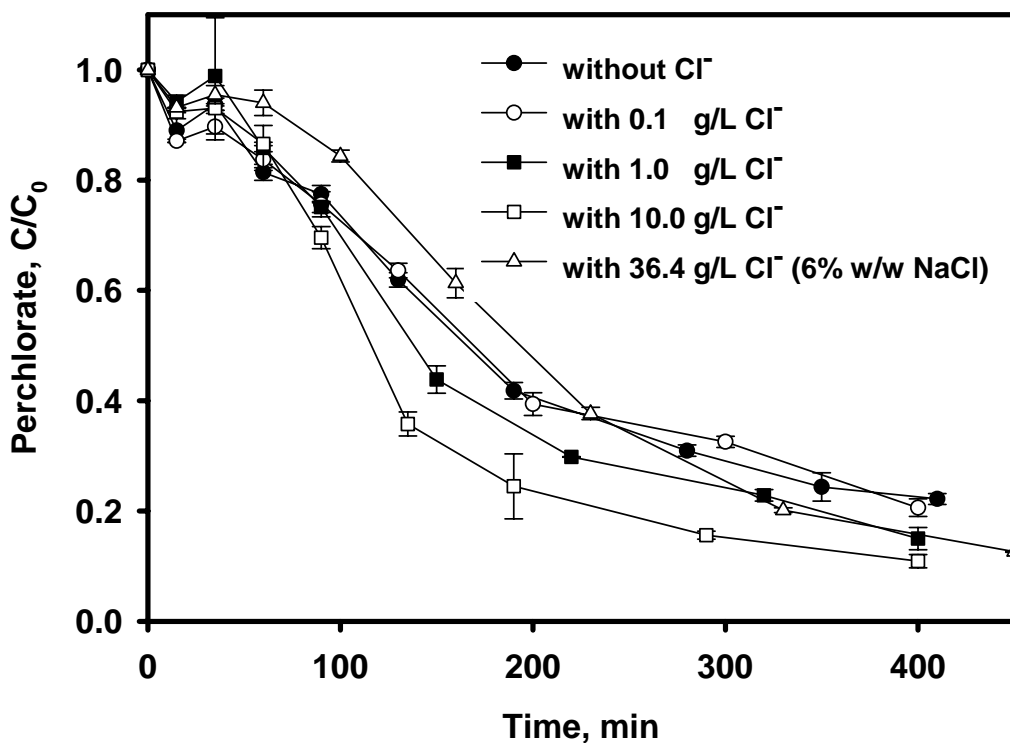


Figure 3-7. Perchlorate reduction by CMC-stabilized ZVI nanoparticles in the presence of various background chloride concentrations at 95 °C. Initial $[\text{ClO}_4^-] = 100 \text{ mg/L}$, ZVI

dose = 1.8 g/L, CMC = 0.9% (w/w), $\text{pH}_0 = 6.5\text{-}6.8$, and $\text{pH}_f = 7.5\text{-}7.8$. Data plotted as mean of duplicates.

3.3.6. Effect of pH on perchlorate reduction

As revealed by Eqs. (3-1) and (3-2), hydrogen activity (pH) can affect corrosion of iron as well as degradation of perchlorate. **Figure 3-8** shows the perchlorate reduction using 1.8 g/L CMC-stabilized ZVI nanoparticles in the presence of 6% (w/w) NaCl at 95 °C and at various solution pH. When the initial pH was 8.5, only 27.4% perchlorate was removed after 400 minutes with a k_{obs} of 0.0010 min^{-1} , which is 56.5% lower than that at an initial pH 6.8 ($k_{obs}=0.0023 \text{ min}^{-1}$). The observed decrease in perchlorate degradation rate can be attributed to the formation of ferrous hydroxide and/or ferric hydroxide precipitates on the ZVI nanoparticles surface at elevated pH. The precipitates hinder the contact between ZVI nanoparticles surface and perchlorate, resulting in slower perchlorate reduction. Indeed, red precipitates were observed when the reacted ZVI solution at pH 8.5 was filtered through 0.22 μm membrane filter. In contrast, faster perchlorate reduction kinetics ($k_{obs} = 0.0054 \text{ min}^{-1}$) was observed when the initial pH was lowered to 5.1. Because a lower pH promotes both iron corrosion (Eq. 3-1) and perchlorate reduction (Eq. 3-2), this observation suggests that overall perchlorate reduction by ZVI nanoparticles is favored at lower pH. When a buffer (5 mM HEPES) was used to hold the solution pH in the range of 7.0-7.4, the degradation rate was greatly improved ($k_{obs}=0.0092 \text{ min}^{-1}$).

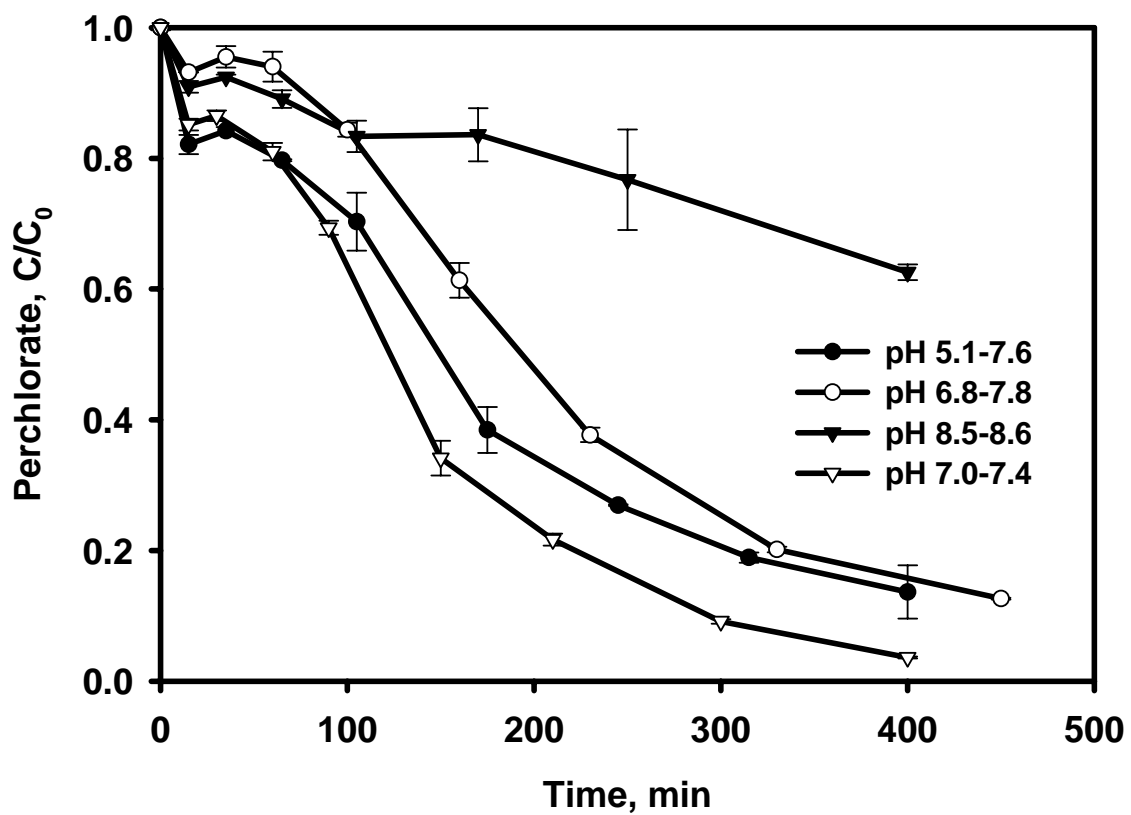


Figure 3-8. Effect of pH on perchlorate reduction by CMC-stabilized ZVI nanoparticles in the presence of 6% NaCl (w/w) at 95 °C. Initial $[\text{ClO}_4^-] = 100 \text{ mg/L}$, ZVI dose = 1.8 g/L, CMC = 0.9% (w/w). The pH given refers to initial and final pH. Data plotted as mean of duplicates.

3.3.7 Effect of UV light

UV light has been reported to promote perchlorate reduction. For example, Gurol and Kim (2000) reported that 77% removal of perchlorate was achieved with 100 g/L of electrolytically-produced 100 mesh metallic iron particles (certified grade, 95%; Fisher; surface area = 0.74 m²/g) and with UV light illumination (wavelength = 254 nm). In this study, UV light was introduced to promote perchlorate reduction by stabilized ZVI nanoparticles (1.8 g/L with 0.9% CMC). The experiments were carried using a UV source present in the department of chemistry at Auburn University and the experiment setup was reported previously (Korchev et al., 2005). In brief, uniform illumination of the optical tubes was achieved by positioning them at mid-height inside a Rayonet 100 circular illuminator that generated photons with a wavelength = 350 ± 15 nm by means of 16 RPR-3500A lamps. The temperature inside the illuminated Rayonet was 29 °C; an Aberchrome 540 was used to determine the light intensity and a maximum light intensity of 3.2 × 10¹⁶ hv/s was used in this study. Parallel experiments of perchlorate (100 mg/L) reduction by stabilized ZVI nanoparticles (1.8 g/L with 0.9% CMC) at 29 °C with or without UV light illumination were carried out. However, after 12 hours, no improvement in the rate of perchlorate reduction was detected in the presence of UV light. The possible reasons for this result are that 1) the lamps used in this study that generates light at 350 nm are not efficient for ClO₄⁻ excitement and it was reported that ClO₄⁻ absorbs light at wavelengths shorter than 185 nm (Gurol and Kim, 2000); 2) the light intensity (3.2 × 10¹⁶ hv/s) used in this study may not be enough for ClO₄⁻ excitation.

3.4 Summary and Conclusions

Major findings and conclusions from this study are summarized as follows:

1). Perchlorate in both fresh water and brine can be rapidly and completely destroyed by low concentrations of stabilized ZVI nanoparticles at moderately elevated temperatures. Based on the surface-area normalized rate constant k_{SA} , starch- and CMC-stabilized ZVI nanoparticles degraded perchlorate 1.8 and 3.3 times, respectively, faster than non-stabilized ZVI particles did. The activation energy (E_a) for the reaction was determined to be 52.59 ± 8.41 kJ/mol. The nanoparticles were able to completely reduce perchlorate to chloride without accumulation of any intermediate products.

2). Temperature was found to be a critical factor for perchlorate reduction. The observed pseudo-first-order rate constant (k_{obs}) increased by 82 times (from 0.0002 to 0.0164 min^{-1}) when the temperature was increased from 25 °C to 110 °C.

3). Unlike degrading chlorinated organics, the presence of trace amounts (0.3% of Fe) of a metal catalyst (Co, Cu, Ni, Pd, or Re) yield no improvement in the reaction rate. On the contrary, the presence of Pd reduced the reaction rate by 44.5%. The inhibitive effect is attributed to the accelerated corrosion of ZVI nanoparticles, which diminished the reducing power of the nanoparticles for perchlorate.

4). The stabilized ZVI nanoparticles can highly effectively transformed perchlorate in saline water or IX regeneration brine. The presence of high concentrations of NaCl (up to 6% w/w) increased perchlorate reduction rates by as high as 53%.

5). Solution pH can also affect the perchlorate reduction by ZVI nanoparticles. When the initial solution pH was lowered from 6.8 to 5.1, the perchlorate reduction rate was increased by 2.3 times. When a buffer solution (5 mM HEPES) was used to keep pH

in the range of 7.0-7.4, the reaction rate was increased by ~4 times as compared to that without pH control.

The stabilized ZVI nanoparticles may offer an alternative means for complete reduction of perchlorate in water that is small in volume and high in concentration such as perchlorate in source zones or ion-exchange brine.

CHAPTER 4. RAPID AND CONTROLLED TRANSFORMATION OF NITRATE IN WATER AND BRINE BY STABILIZED ZERO-VALENT IRON NANOPARTICLES

The data presented in the previous chapter demonstrated that perchlorate can be completely reduced in both fresh water and ion-exchange (IX) regeneration brine by stabilized ZVI nanoparticles. Like perchlorate, nitrate is another widespread groundwater contaminant and IX is one of the best available technologies for nitrate removal from groundwater. In this chapter, the stabilized ZVI nanoparticles are studied for nitrate reduction in both fresh water and IX regeneration brine. Effects of ZVI-to-NO₃⁻ molar ratio, metal catalysts, CMC-to-ZVI molar ratio, pH, and salinity are studied.

4.1 Introduction

Nitrate (NO₃⁻) contamination of groundwater is a widespread environmental problem, and has been associated with agricultural runoff, leaching of nitrogen fertilizers, concentrated animal feeding operations, food processing, and industrial waste effluent discharge (Su and Puls, 2004). Ingestion of nitrate in drinking water by infants can cause dangerously oxygen deficit in the blood, i.e. the 'blue baby' syndrome (Fan and Steinberg, 1996; Nolan et al., 1997). To limit the health impact of nitrate ions in drinking water, the U.S. EPA (1995) established a maximum contaminant level (MCL) of 10 mg/L as NO₃⁻-N. Although nitrate ion concentration in natural groundwater is generally less than 2 mg/L as NO₃⁻-N (Mueller and Helsel, 1996), concentrations exceeding the MCL has been

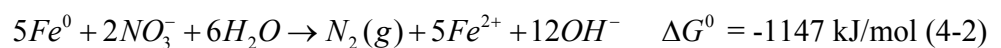
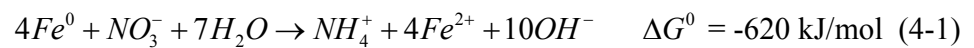
detected in 10%~25% of the water-supply wells in many parts of the western, mid-western, and northeastern U.S. (Nolan et al., 1997; Smith et al., 2005).

Because of our tremendous dependence on groundwater, cost-effective remediation of nitrate-contaminated groundwater has been consistently sought for decades. Among the most cited technologies for nitrate removal are IX (Clifford and Liu, 1993a; Kim and Benjamin, 2004), biological denitrification (Nuhoglu et al., 2002), reverse osmosis (RO), electrodialysis reversal (EDR) (Rautenbach et al., 1986), and chemical reduction (Peel et al., 2003). Although IX, RO and EDR are designated as the best available technologies (BAT) by the U.S. EPA, IX has been the most widely employed technology due to the associated lower cost and easier operation and maintenance (Clifford, 1999). Since nitrate-selective resins became commercially available in the 1980s, IX has gained growing popularity. However, application of IX has been limited by its relatively high costs of regenerant as well as brine disposal (Van der Hoek et al., 1988). Consequently, treatment and reuse of IX brine is highly desirable, which is becoming more compelling as more stringent environmental regulations on brine disposal are emerging and more water utilities are forced into compliance. Similar concerns also apply to the RO process, where disposal of nitrate-laden rejects remains costly challenge (Cox et al., 1994; Smith et al., 2005).

Compared to nitrate ion removal from fresh water, research on nitrate reduction in saline water has been much limited. Biological denitrification has been found effective to eliminate nitrate ions from seawater (Labelle et al., 2005) and from IX brine containing 1%~12.5% NaCl (Clifford and Liu, 1993b; Peyton et al., 2001; Okeke et al., 2002;). However, Clifford and Liu (1993b) reported a 10% drop in denitrification rate in 0.5 N

NaCl than that in fresh-water controls. Earlier, Van der Hoek et al. (1987) reported that denitrification was inhibited by the presence of high concentrations (10~30 g/L) of NaCl. Peyton et al. (2001) reported a specific nitrate reduction rate constant in a range from 1.20×10^{-2} (L·h⁻¹ mg TSS) to 5.54×10^{-3} (L·h⁻¹ mg TSS) depending on carbon sources in the presence of 12.5% (w/w) NaCl at pH 9. Glass and Silverstein (1999) tested effectiveness of bench-scale sequencing batch reactors (SBR) for denitrification in a wastewater containing 36 g/L NO₃⁻ at an ionic strength up to 3.0 (18% total dissolved solids), and they observed that both nitrite and nitrate reduction rates were reduced with increasing salinity.

In recent years, a number of studies have been reported on the reduction of nitrate using ZVI particles (Huang et al., 1998; Choe et al., 2000; Alowitz and Scherer, 2002; Huang and Zhang, 2004; Mishra and Farrell, 2005; Sohn et al., 2006). According to these studies, nitrate is reduced by ZVI following two general pathways below (Kielemoes, et al., 2000):



where ΔG^0 (kJ/mol) is the standard Gibb's free energy change. Eq. (4-1) was invoked by Alowitz and Scherer (2002) who tested commercial iron powders (18~35 mesh) and iron fillings (40 mesh) to reduce nitrate under controlled solution pH (5.5~9.0); and Eq. (4-2) was proposed by Choe et al. (2000) to be the primary nitrate reduction pathway when non-stabilized (or agglomerated) ZVI nanoparticles (BET specific surface area = 31.4 m²/g) were used in an anaerobic system under ambient conditions without pH control. To

the best of our knowledge, there have been no reported studies on abiotic nitrate reduction by ZVI in saline water or IX brine.

Several strategies have been developed to enhance nitrate reduction by ZVI including 1) pretreatment of iron with hydrogen gas (Liou et al., 2005a); 2) addition of metal cations such as Fe^{3+} , Al^{3+} , and Cu^{2+} (Huang and Zhang, 2005); and 3) deposition of a metal catalyst such as Cu on the iron surface (Liou et al., 2005b). In addition, reducing the ZVI particle size to the nanometer scale greatly increases the specific surface area, and thus, the reduction reactivity (Choe et al., 2000; Liou et al., 2005b; Yang and Lee, 2005). However, non-stabilized ZVI nanoparticles, which are typically prepared following the classical borohydride reduction of ferrous or ferric ions in aqueous solution (Glavee et al., 1995), tend to agglomerate to large flocs (micrometer to millimeter scale). As a result, the unique advantage (e.g. high surface area and high reactivity) of nanoscale iron particles is diminished.

To prevent agglomeration of ZVI nanoparticles, He and Zhao (2005) and He et al. (2007) developed a technique for synthesizing highly stable/dispersible ZVI nanoparticles by using environment-friendly and low-cost starch, or food-grade cellulose (known as sodium carboxymethyl cellulose, CMC), as stabilizers. More recently, He and Zhao (2007a) demonstrated that the ZVI particle size can be manipulated by applying stabilizers of with different molecular weights or by tuning the stabilizer-to-ZVI molar ratio. The stabilized nanoparticles displayed both superior physical stability and much greater reactivity than their non-stabilized counterparts when used for degradation of chlorinated hydrocarbons (He et al., 2007) and perchlorate (Xiong et al., 2007a).

The overall goal of this present study is to test the effectiveness of using CMC-stabilized ZVI nanoparticles for the transformation of nitrate in both fresh and saline waters (or simulated IX brine). The specific objectives are to: 1) determine the rate, extent and pathway of nitrate reduction by the stabilized ZVI nanoparticles; 2) characterize the influences of ZVI-to-NO₃⁻ molar ratio, pH, metal catalysts, concentration of stabilizer and salinity on the nitrate reduction rate and pathways.

4.2 Materials and Methods

The following chemicals (analytical grade) were used as received: 4-(2-Hydroxyethyl)-1- Piperazineethanesulfonic acid (HEPES, C₈H₁₈N₂O₄S) (Fisher Scientific, Fair Lawn, NJ, USA); 4-Morpholinoethanesulfonic acid (MES, C₆H₁₃NO₄S·xH₂O) (Fisher); Ammonium nitrate (NH₄NO₃) (Fisher); Ethanol (C₂H₅OH) (Fisher); Iron (II) sulfate (FeSO₄·7H₂O) (Acros Organics, Morris Plains, NJ, USA); Phenol (C₆H₅OH) (Fisher); Potassium hexachloropalladate (K₂PdCl₆, 99%) (Acros Organics); Potassium nitrate (KNO₃) (Acros Organics); Sodium borohydride (NaBH₄) (ICN Biomedicals, Aurora, OH); Sodium carboxymethyl cellulose (CMC, M.W. = 90,000, D.S. = 0.9) (Acros Organics); Sodium citrate (Na₃C₆H₅O₇·2H₂O) (Fisher); Sodium chloride (NaCl) (Fisher); Sodium hydroxide (NaOH) (Fisher); Sodium hyperchlorite (NaClO) (Fisher); Sodium nitrate (NaNO₃) (Fisher); Sodium nitrite (NaNO₂) (Fisher); Sodium nitroprusside (Na₂Fe(CN)₅(NO)·2H₂O) (Fisher).

CMC-stabilized ZVI nanoparticles were prepared following a procedure by He et al. (2007). In brief, the preparation was performed in a 250 mL flask attached to a vacuum line. Before use, deionized (DI) water was purged with purified N₂ for 30

minutes to remove dissolved oxygen (DO). $\text{FeSO}_4 \cdot 7\text{H}_2\text{O}$ (0.1 M) and CMC stock solutions (1%~2% w/w) were prepared freshly before use with N_2 -purged DI water. In a typical preparation, a $\text{FeSO}_4 \cdot 7\text{H}_2\text{O}$ stock solution was added to a CMC solution to yield a desired concentration of Fe (1 g/L) and CMC (0.2%~0.9%, w/w). The mixture was purged with N_2 for another 30 minutes to remove DO and to allow for formation of Fe-CMC complexes. Fe^{2+} ions were then reduced to Fe^0 by adding a stoichiometric amount of NaBH_4 into the mixture under hand-shaking. When gas (hydrogen) evolution ceased (after ~15 min), the ZVI nanoparticles were ready for use. To test the catalytic effect of palladium and/or copper, stabilized ZVI nanoparticles in select cases were loaded with Pd and/or Cu by adding Pd^{2+} and/or Cu^{2+} to the nanoparticle suspension (He and Zhao, 2005). For comparison, non-stabilized ZVI particles were also prepared following the same procedure but without a stabilizer. In all cases, the nanoparticles were used or tested within 30 minutes of preparation.

Batch kinetic tests of CMC-stabilized nanoparticles for nitrate reduction were conducted in 25 mL amber glass vials capped with Teflon Mininert valves. Nitrate reduction was initiated by adding a nitrate stock solution (2 g/L) to the freshly prepared ZVI nanoparticle suspensions to yield desired nitrate and ZVI concentrations. The dosage of ZVI is represented by the ZVI-to- NO_3^- molar ratio with a unit of mole/mole throughout this study. Dilute (0.1 N) HCl or NaOH were used to adjust the pH of the suspension, and in select cases, HEPES or MES buffer solution (0.05 M) was employed to maintain a constant pH. The vials were filled with nearly zero headspace, and the mixtures were mixed on a rotary shaker (40 rpm) operated at room temperature (~21 °C). At select time intervals, duplicate vials were sampled and ~0.5 mL sample was diluted

with acidified DI water (pH = 3) with 10~20 times to convert the remaining ZVI nanoparticles to soluble Fe^{2+} , and then analyzed for nitrate remaining in the aqueous phase and reduction products (e.g. nitrite, ammonium) as well. Control experiments (without the addition of ZVI nanoparticles) were carried out in parallel. All experiments were duplicated to assure data quality.

Nitrate and nitrite were analyzed using a Dionex Ion Chromatography (DX-120) equipped with an AS14 column, an AG14 guard column, and a 100 μL sample loop. A solution containing 3.5 mM sodium carbonate and 1.0 mM sodium bicarbonate was used as the eluent, and the eluent flow rate was set at 1.0 mL/min. The detection limit for nitrate and nitrite was 0.01 mg/L and 0.08 mg/L, respectively. Ammonium was measured following the standard phenate method (Clesceri et al., 1998) with a detection limit of 0.02 mg/L.

4.3 Results and Discussion

4.3.1 Nitrate reduction with CMC-stabilized and non-stabilized ZVI nanoparticles

Figure 4-1 compares nitrate reduction rates for non-stabilized and CMC-stabilized ZVI nanoparticles under otherwise identical conditions. In all cases, the solution pH was kept at 7.0~7.5 with a 0.05 M HEPES buffer solution. The stabilized monometallic ZVI nanoparticles displayed much improved kinetics than non-stabilized ZVI nanoparticles. In the initial 10 min of reaction, the stabilized ZVI nanoparticles reduced nearly 80% of nitrate, compared to only ~50% reduced by the non-stabilized ZVI. At steady state (after ~90 min), the stabilized ZVI nanoparticles reduced more than 96% of nitrate, compared to only 77% for the non-stabilized ZVI particles. A control test using

the same concentrations of Fe^{2+} and NO_3^- (data not shown) indicated that there is no nitrate reduction by Fe^{2+} under pH 7.0~7.5 (0.05 M HEPES) after 24 hours.

The nitrate reduction kinetics for the CMC-stabilized nanoparticles also displayed a more distinguished two-phase profile, i.e. a rapid initial stage (<10 min) followed by a gradual reduction for over 1 h. This rate profile is in accord with the notion that the surface reactivity of the ZVI nanoparticles can be diminished due to formation of passivating iron hydroxide or iron oxide layers on the ZVI surface (Huang et al., 1998). Evidently, because of the greater reactivity, the CMC-stabilized nanoparticles became exhausted more rapidly than the non-stabilized ZVI particles.

To quantify the reaction rate, a pseudo-first-order reaction model, Eq. (4-3), was used to fit the observed kinetic data (Johnson et al., 1996):

$$\frac{d[NO_3^-]}{dt} = -k_{SA}a_s\rho_m[NO_3^-] = -k_{obs}[NO_3^-] \quad (4-3)$$

where $[NO_3^-]$ is the nitrate concentration (mg/L) in water at time t (min), k_{SA} is the specific reaction rate constant based on surface area of the nanoparticles (L/(min·m²)), a_s is the specific surface area of the nanoparticles (m²/g), ρ_m is the mass concentration of the nanoparticles (g/L), and k_{obs} is the observed pseudo-first-order rate constant (min⁻¹). In Eq. (4-3), $[NO_3^-]$, t , a_s and ρ_m were measured while k_{SA} and k_{obs} were fitted.

Because of the labile nature of the ZVI nanoparticles and the complexity of the system, only early stage ($t < 60$ min) data were fitted. Thus, the resultant rate constants only represent an operationally defined initial rate constant, which has been commonly used to facilitate reaction rate comparison.

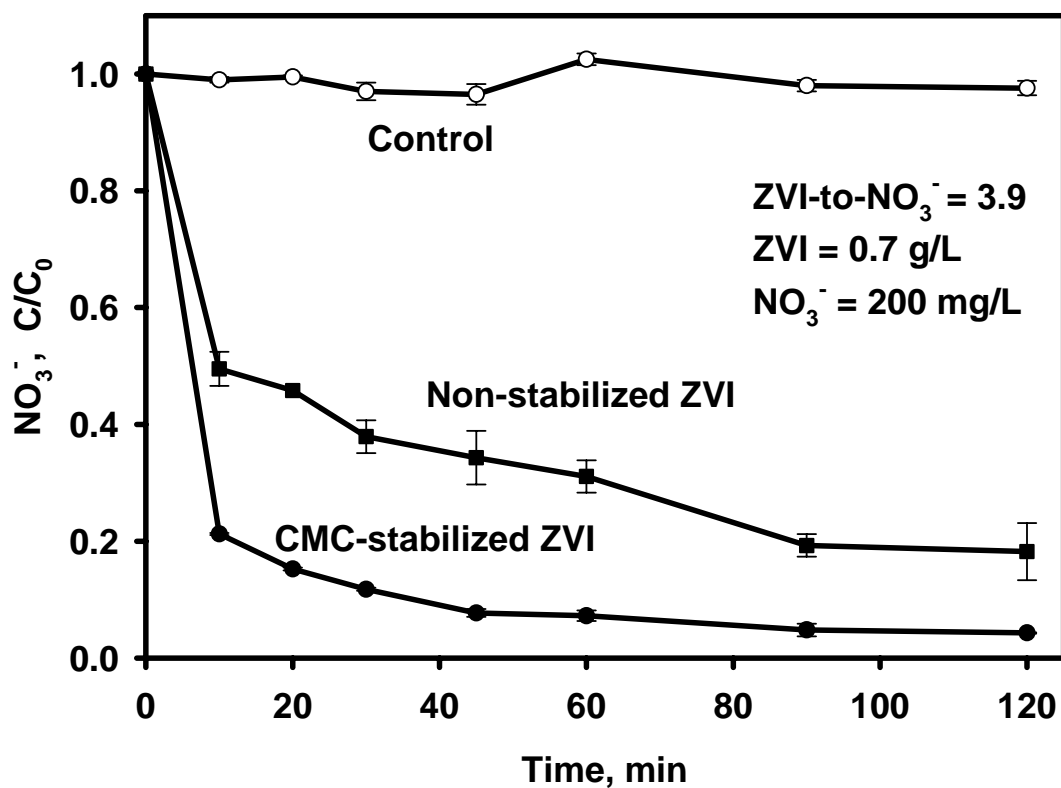


Figure 4-1. Reduction of nitrate by non-stabilized ZVI and CMC-stabilized ZVI nanoparticles. Initial nitrate concentration (C_0) = 200 mg/L, ZVI = 0.7 g/L ($\text{ZVI-to-NO}_3^- = 3.9$), CMC = 0.63% (w/w). Solution pH was controlled at 7.0~7.5 (initial and final) with a 0.05 M HEPES buffer. Data plotted as mean of duplicates.

Table 4-1 gives the best-fitted model parameters. Fairly good model fitting (R^2 0.90) was obtained for most of reactions except in two cases, one was at a lower ZVI dose (ZVI-to- NO_3^- molar ratio = 2.5), and the other was when the initial pH was extremely low ($\text{pH}_0 = 2.5$). This observation suggests that the pseudo-first model becomes less suitable when either ZVI supply is insufficient or when excess amounts of protons are present (note that H^+ accelerates ZVI corrosion as evidenced by the pH jump from the initial value of 2.5 to the final 8.6). As indicated by the observed k_{obs} values, the stabilized ZVI nanoparticles offered a 5.2 times greater reaction rate over the non-stabilized counterparts. In fact, the k_{obs} value (0.13 min^{-1}) of the CMC-stabilized ZVI nanoparticles (pH 7.0~7.5 with 0.05 M HEPES; ZVI-to- $\text{NO}_3^- = 3.9$) is more than 4 times greater than that ($k_{obs} = 0.014 \text{ min}^{-1}$) of microscale ZVI particles (pH 7.0 with 0.1 M HEPES; ZVI-to- $\text{NO}_3^- = 114$) (Cheng et al., 1997), or that ($k_{obs} = 0.03 \text{ min}^{-1}$; reaction order = 0.90) of non-stabilized ‘nanoscale’ ZVI particles (pH 3 with HCl; ZVI-to- $\text{NO}_3^- = 7.4$) (Yang and Lee, 2005), or that ($k_{obs} = 0.003 \text{ min}^{-1}$) of surfactant-stabilized ZVI nanoparticles (pH 7.0 with 0.1 M H_3PO_4 ; ZVI-to- $\text{NO}_3^- = 6.3$) (Chen et al., 2004) (**Table 4-2**). On the other hand, based on a specific surface area of $55.6 \text{ m}^2/\text{g}$ for the CMC-stabilized ZVI nanoparticles and $33.5 \text{ m}^2/\text{g}$ for non-stabilized ZVI nanoparticles (Wang and Zhang, 1997) (Note: The same method was used to prepare non-stabilized ZVI nanoparticles in this study and by other researchers who also found the specific surface area of non-stabilized ZVI nanoparticles around $33.5 \text{ m}^2/\text{g}$ (Choe et al., 2000; Liu et al., 2005; Yang and Lee, 2005)), the k_{SA} was calculated to be $3.34 \times 10^{-3} \text{ L}/(\text{min}\cdot\text{m}^2)$, $1.07 \times 10^{-3} \text{ L}/(\text{min}\cdot\text{m}^2)$, respectively, for CMC-stabilized and non-stabilized ZVI nanoparticles. The difference between these two k_{SA} values suggests that a stabilizer (CMC) not only

increased the surface area of the nanoparticles (because of the much smaller particle size), but also resulted in more reactive particle surface. A possible reason for the increased surface reactivity is that the presence of CMC prevents the formation of the passivating iron hydroxide or oxyhydroxides on the ZVI surface.

Table 4-1. Model-fitted pseudo-first-order rate constants of nitrate reduction under various experimental conditions.

ZVI/NO ₃ molar ratio	pH (initial ~final)	CMC, % (w/w)	Catalyst, % of Fe (w/w)	NaCl, % (w/w)	ρ_m , g/L	a_s , m ² /g	k_{obs} , min ⁻¹	k_{SA} , L/(min·m ²)	R ²
2.5	7.0~7.5	0.63	0	-	0.7	55.6	0.10	2.57×10^{-3}	0.74
3.9	7.0~7.5	0	0	-	0.7	33.5*	0.025	1.07×10^{-3}	0.94
3.9	7.0~7.5	0.63	0	-	0.7	55.6	0.13	3.34×10^{-3}	0.95
3.9	7.0~7.5	0.63	0.3 Pd	-	0.7	-	0.10	-	0.94
3.9	7.0~7.5	0.63	0.3 Cu	-	0.7	-	0.092	-	0.92
3.9	7.0~7.5	0.63	0.1 Pd & 0.4 Cu	-	0.7	-	0.095	-	0.90
3.9	7.0~7.5	0.63	0.4 Pd & 0.1 Cu	-	0.7	-	0.11	-	0.93
3.9	2.5~8.6	0.63	0	-	0.7	55.6	0.011	2.83×10^{-4}	0.74
3.9	7.0~8.7	0.63	0	-	0.7	55.6	0.0085	2.18×10^{-4}	0.96
3.9	6.1~6.4	0.63	0	-	0.7	55.6	0.41	1.05×10^{-2}	0.93
5.2	7.0~7.5	0.63	0	-	0.7	55.6	0.30	7.49×10^{-3}	0.99
5.2	7.0~7.5	0.63	0	1	0.7	55.6	0.29	7.24×10^{-3}	0.99
5.2	7.0~7.5	0.63	0	6	0.7	55.6	0.21	5.25×10^{-3}	0.95
5.2	7.0~7.5	0	0	-	0.7	33.5*	0.037	1.53×10^{-3}	0.90
5.2	7.0~7.5	0.14	0	-	0.7	-	0.20	-	0.98
5.2	7.0~7.5	0.36	0	-	0.7	-	0.26	-	0.99

* From Wang and Zhang (1997).

Table 4-2. Summary of nitrate reduction rate constants by various ZVI particles in the literature.

ZVI type	ZVI/NO ₃ ⁻ molar ratio	pH	ρ_m , g/L	a_s , m ² /g	k_{obs} , min ⁻¹	k_{SA} , L/(min·m ²)	Reference
Microscale (325 mesh)	114.3	7	80	-	0.014	-	Cheng et al., 1997
Nanoscale, non- stabilized	7.4	3	1.0	37.8	0.03	7.9×10^{-4}	Yang and Lee, 2005
Nanoscale, surfactant-stabilized	6.3	7	0.5	25.4	0.003	2.4×10^{-4}	Chen et al., 2004

4.3.2 Effect of ZVI-to-NO₃⁻ molar ratio on nitrate reduction rate and pathways

Based on the nitrate reduction stoichiometries given in Eqs. (4-1) and (4-2), it takes a minimum ZVI-to-NO₃⁻ molar ratio of 2.5 to reduce nitrate to N₂ and a ZVI-to-NO₃⁻ molar ratio of 4 to reach ammonium. Meanwhile, nitrate reduction to N₂ is thermodynamically more favorable than toward NH₄⁺, as indicated by ΔG^0 of Eqs. (4-1) and (4-2). Therefore, the ZVI-to-NO₃⁻ molar ratio can affect both the nitrate reduction rates and pathways and lead to different final products (N₂ versus NH₄⁺).

Figure 4-2 compares nitrate reduction rates at a ZVI-to-NO₃⁻ molar ratio of 2.5, 3.9 and 5.2, respectively. Note that the ZVI-to-NO₃⁻ molar ratio of 2.5 corresponds to the reaction stoichiometry of Eq. (4-2), whereas the ratio of 3.9 conforms to the pathway represented by Eq. (4-1). In all cases, the pH of the suspension was kept at 7.0~7.5 by using a 0.05 M HEPES buffer. At the ZVI-to-NO₃⁻ molar ratio of 2.5, the rate profile again displayed a rapid initial reduction followed by a slower stage after 15 minutes. However, a steady state was reached at ~50 minutes, when ~83% of nitrate was transformed. At a ZVI-to-NO₃⁻ molar ratio of 3.9, nearly 80% of nitrate was reduced rapidly in the first 10 minutes, after which an additional 16% was rather slowly reduced by the end of experiments (120 minutes). At a ZVI-to-NO₃⁻ molar ratio of 5.2 (i.e. 30% above the highest possible stoichiometric quantity), ~96% of nitrate was rapidly reduced within 10 minutes, and nearly complete reduction was achieved within 30 minutes.

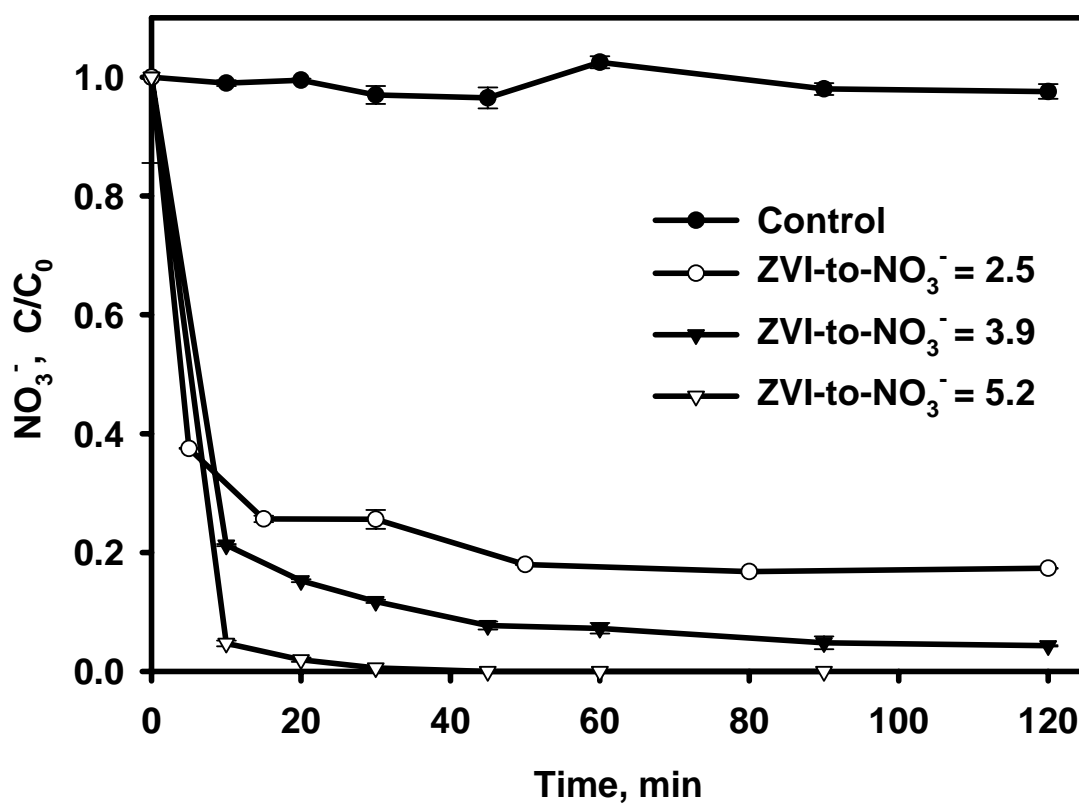


Figure 4-2. Effect of ZVI-to-NO₃⁻ molar ratios on nitrate reduction by CMC-stabilized ZVI nanoparticles. In all cases, ZVI = 0.7 g/L, CMC = 0.63%. Three initial nitrate concentrations were: NO₃⁻ = 310 mg/L, 200 mg/L, and 150 mg/L. Solution pH was controlled at 7.0~7.5 (initial and final) with a 0.05 M HEPES buffer. Data plotted as mean of duplicates.

The rate constant (k_{obs}) went up by 30% when the ZVI-to-NO₃⁻ molar ratio was increased from 2.5 to 3.9 (**Table 4-1**). However, when the ZVI-to-NO₃⁻ molar ratio was further raised from 3.9 to 5.2, the rate constant (k_{obs}) increased by a factor of 2.3. The latter remarkable increase in nitrate reduction rate is attributed to the presence of hydrogen atom or gas resulting from the reduction of water and/or protons in the presence of ‘excessive’ amounts of ZVI (i.e. greater than the maximum stoichiometric quantity of 4) as indicated by Eq. (4-4).



Siantar et al. (1996) and Huang et al. (1998) reported that pre-treating iron particles with H₂ resulted in substantial increase in nitrate reduction. A number of studies reported that hydrogen gas can effectively reduce nitrate to nitrogen or ammonium in the presence of a catalyst such as Pd-In and Pd-Cu (Lemaigen et al., 2002; Chen et al., 2003; Mikami et al., 2003). It was also reported that iron may activate sorbed H₂ similar to catalytic metals such as Pd (Grittini et al., 1995, Schreier and Reinhard, 1995). In our case, the transformation of nitrate can be catalyzed by the ZVI nanoparticles and/or their oxidized products (iron hydrous oxides), resulting in an additional pathway for nitrate reduction.

To evaluate the relative weight of the two reduction routes (i.e., Eqs. (4-1) and (4-2)), coupled nitrated reduction and production of ammonium were monitored. **Figure 4-3a** and **Figure 4-3b**, respectively, shows the nitrate reduction and ammonium production rates at a ZVI-to-NO₃⁻ molar ratio of 2.5 and 3.9. In both cases, no nitrite (NO₂⁻) was detected and control experiments showed that CMC and BH₄⁻ were unable to reduce nitrate.

It is evident from **Figure 4-3a** that the reduction of nitrate (as NO_3^- -N) was concerted with a rise in ammonium production (as NH_4^+ -N), which again indicates rapid conversion of nitrate. Although nitric oxide and nitrous oxide were reported to be possible products for nitrate or nitrite reduction (Sorenson and Thorling, 1991; Kielemoes et al., 2000) by ZVI powder or Fe^{2+} , nitrogen gas has been generally believed to account for the incomplete mass balance of total nitrogenous species for nitrate reduction by ZVI (Choe et al., 2000; Chen et al., 2003; Liou et al., 2005b). In this study, the conversion of nitrate to N_2 was calculated through mass balance calculations of the total nitrogen (i.e. NO_3^- -N + NH_4^+ -N) remaining in the system at a given time. **Figure 4-3a** shows that at steady state (after ~50 min), 18% of NO_3^- -N initially present in the system remained in the solution, 28% of the initial NO_3^- -N was converted to NH_4^+ -N via Eq. (4-1), and per mass balance calculations, 54% of NO_3^- -N was converted to N_2 -N via Eq. (4-2), i.e. N_2 -N accounted for two thirds (66%) of the nitrate reduction products. **Figure 4-3b** shows that when the ZVI dose was increased to the stoichiometric quantity of Eq. (4-1), nearly all (>98%) nitrate was reduced within two hours. However, this elevated ZVI-to- NO_3^- molar ratio seems to be more favorable to the formation of ammonium than N_2 . At the end of the 2-h reaction period, NH_4^+ -N accounted for 62% of the initial NO_3^- -N, i.e., only 36% of the reduced NO_3^- -N was converted to N_2 -N, which is 30% less than that of **Figure 4-3a**. Huang et al. (1998) reported that ammonia was the sole end product when nitrate was reduced by an iron powder (size: 6-10 μm) at a ZVI-to- NO_3^- molar ratio of 6.7. Yang and Lee (2005) reported that ammonium accounted for about 90% of the reduction products when nitrated was reduced by non-stabilized ZVI nanoparticles at a ZVI-to- NO_3^- molar ratio of 7.4 at acidic pH. Chen et al. (2004) observed that at a ZVI-to- NO_3^- molar ratio

6.3 and pH 4~7, microscale ZVI (size: 45 μm) powder converted 60% of nitrate after 6 h with ammonia being the sole end product; in contrast, a nanoscale ZVI prepared with a cationic surfactant as a dispersant was able to convert ~70% of nitrate under otherwise identical conditions with both ammonia and N_2 being the end products and ammonia accounting for 36.2%~45.3% depending on pH.

Evidently, ZVI dose not only affects nitrate reduction rate, but also strongly impacts the nitrate reduction pathway and final reduction products. For water or brine treatment, it is often preferable to completely remove nitrate by converting it to nitrogen gas rather than just transform it to ammonium. To this end, it is more advantageous to apply a ZVI dose in accord with the stoichiometry of Eq. (4-2).

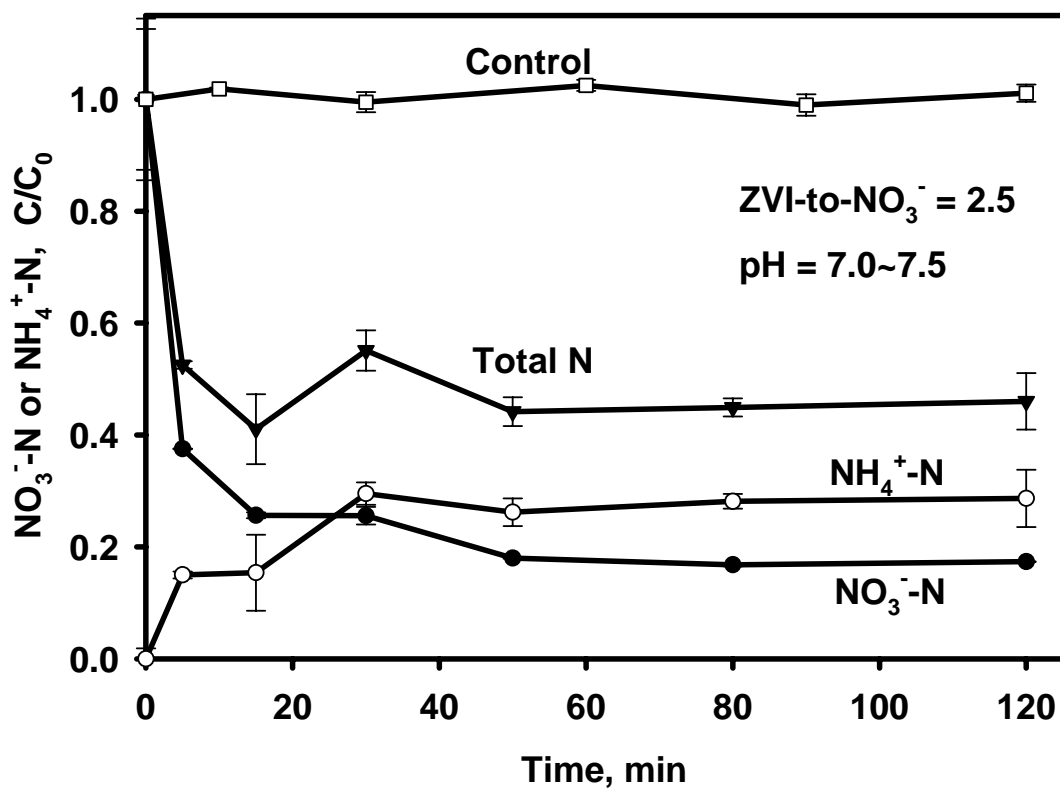


Figure 4-3a. Evolution of nitrate and ammonium concentrations (normalized to initial nitrate concentration, C_0) during nitrate reduction by CMC-stabilized ZVI nanoparticles at a ZVI-to- NO_3^- molar ratio of 2.5 (ZVI = 0.7 g/L; NO_3^- = 310 mg/L). CMC = 0.63% and solution pH was controlled at 7.0~7.5 (initial and final) with a 0.05 M HEPES buffer. Data plotted as mean of duplicates.

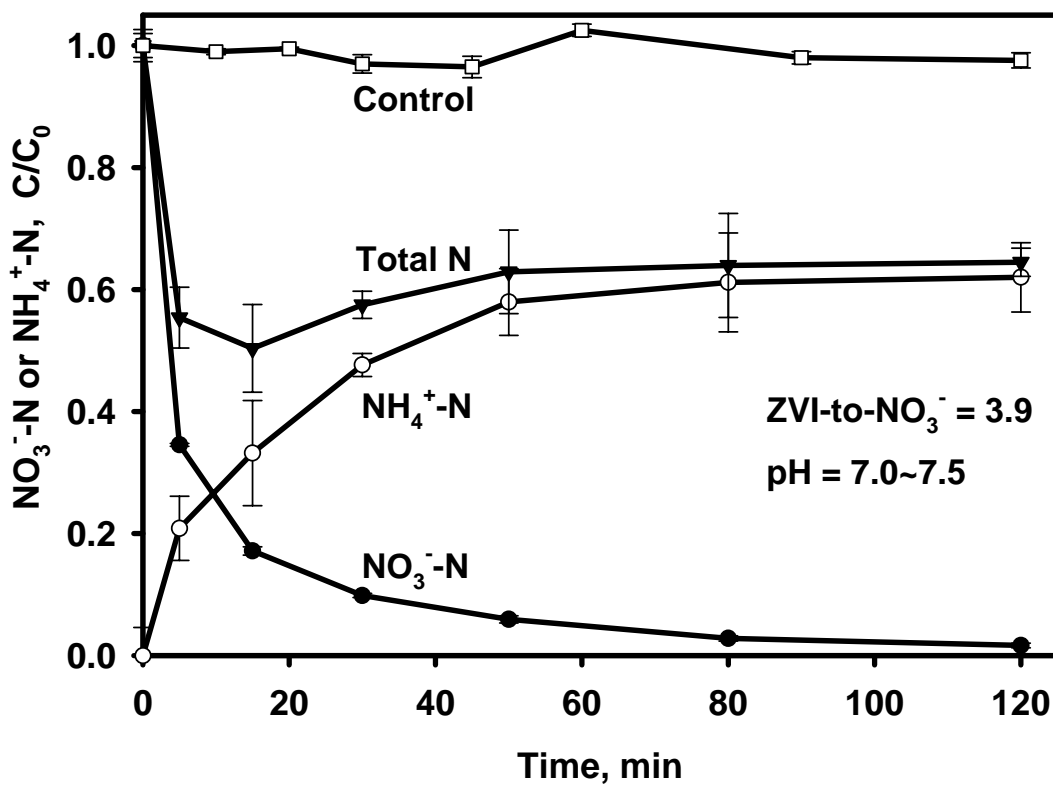
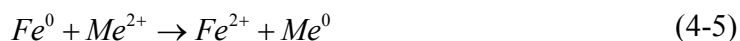


Figure 4-3b. Evolution of nitrate and ammonium concentrations (normalized to initial nitrate concentration, C_0) during nitrate reduction by CMC-stabilized ZVI nanoparticles at a ZVI-to- NO_3^- molar ratio of 3.9 (ZVI = 0.7 g/L; NO_3^- = 200 mg/L). CMC = 0.63% and solution pH was controlled at 7.0~7.5 (initial and final) with a 0.05 M HEPES buffer. Data plotted as mean of duplicates.

4.3.3 Effect of metal catalysts

Coating ZVI nanoparticles with a small fraction (e.g. 0.1% of Fe) of a catalytic metal (e.g. Pd) can substantially accelerate the reaction rate when used for dechlorination of chlorinated hydrocarbons (Wang and Zhang, 1997; Zhang et al., 1998; He and Zhao, 2005). Liou et al. (2005a; 2005b) reported that coating Cu (at 0.5%~20% of Fe) on nanoscale ZVI particles increased nitrate reduction rate by 2~5 times. Horold et al. (1993) and Chen et al. (2003) observed that a bimetallic catalyst Pd-Cu can affect the reduction pathway of nitrate by hydrogen, and a Pd-to-Cu mass ratio of 4-to-1 resulted in maximum nitrate reduction and minimum ammonium production. To test the effects of metal catalysts on the nitrate reduction rate and end products by stabilized ZVI nanoparticles, Pd and Cu were tested as either monometallic or bimetallic catalysts.

Figure 4-4 shows the nitrate reduction by the stabilized ZVI nanoparticles with or without the presence of metal catalysts. As shown in **Table 4-1**, the presence of additional metals did not help nitrate reduction rate. In fact, coating these metals on ZVI nanoparticles reduced the rate constant (k_{obs}) by 15%~29%. The metals were loaded to ZVI nanoparticles via the redox reaction,



where Me stands for metal such as Pd or Cu.

Because of the small fraction of the loaded metal catalysts relative to the amount of Fe, Eq. (4-5) should not decrease significantly, the reactivity of the ZVI nanoparticles. However, chemically, the presence of Pd and/or Cu may catalyze the oxidation of ZVI by water and/or protons (Huang et al., 1998) as indicated in Eq. (4-4). Although the resultant

H₂ may react with nitrate in the presence of a catalyst (Horold et al., 1993), the effect of Pd and/or Cu on this side reaction diminished the overall reduction of nitrate by ZVI nanoparticles.

On the other hand, mass balance calculations on the nitrogenous species during the nitrate reduction tests indicated that in the presence of monometallic Pd at 0.3% of Fe or Cu at 0.3% of Fe, the fraction of ammonium in the end products remained about the same (~62%) as the case when no catalyst was applied. However, the bimetallic catalysts Cu-Pd at Cu = 0.4% and Pd = 0.1% of Fe or Pd-Cu at Pd = 0.4% and Cu = 0.1% of Fe reduced the ammonium fraction to 54% and 55%, respectively. Although the reaction conditions and the recipe (concentration and metal ratio) of the catalysts were not optimized, this observation indicates that the presence of metal catalysts may affect the nitrate reduction pathway, and thus, allocation of ammonium and nitrogen gas in the products. However, the catalytic effect on the reduction of ammonium production was less profound compared to the finding of Chen et al. (2003), who observed an 82% conversion of NO₃⁻ to N₂ by H₂ with Pd-Cu as a catalyst.

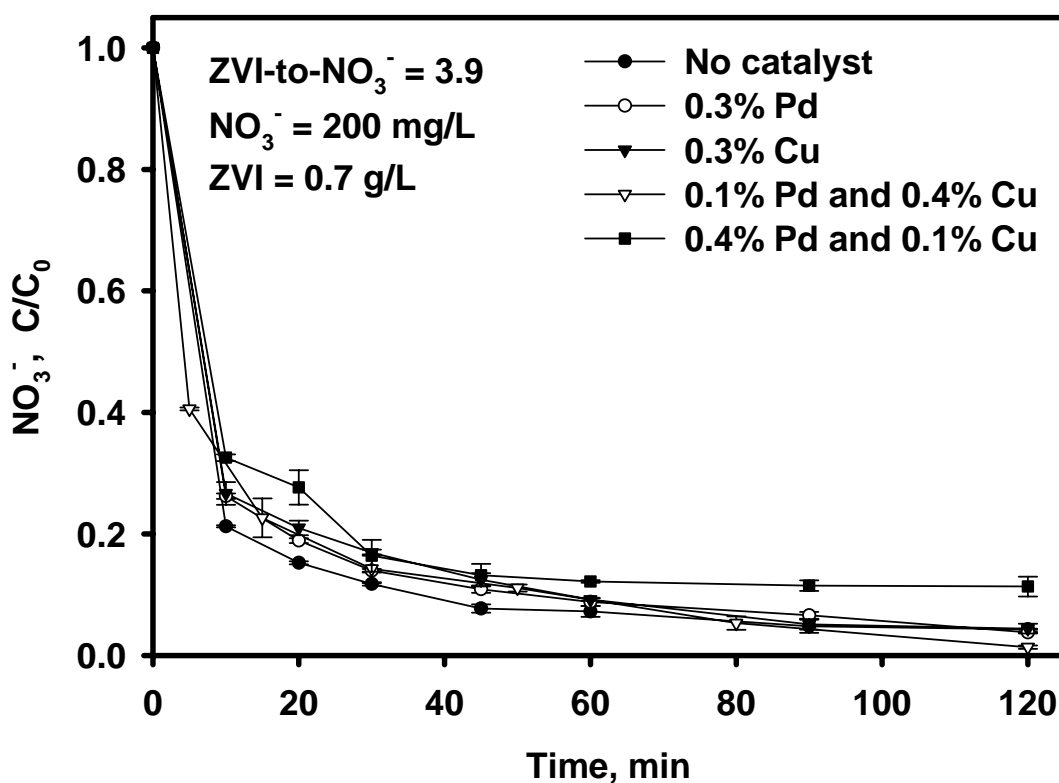


Figure 4-4. Effect of metal catalysts on nitrate reduction by CMC-stabilized ZVI nanoparticles at a ZVI-to- NO_3^- molar ratio of 3.9 ($\text{ZVI} = 0.7 \text{ g/L}$; $\text{NO}_3^- = 200 \text{ mg/L}$, CMC = 0.63%). Doses of catalysts are given as weight percentage of ZVI (w/w of Fe). Solution pH was controlled at 7.0~7.5 (initial and final) with a 0.05 M HEPES buffer. Data plotted as mean of duplicates.

4.3.4 Effect of stabilizer-to-ZVI molar ratio on reactivity of nanoparticles

As shown above, the use of CMC prevented ZVI nanoparticles from agglomerating and substantially enhanced the reactivity for nitrate reduction. Other prior work (He and Zhao, 2007a; 2007b) indicated that both particle stability and chemical reactivity can be affected by the concentration of stabilizer in relation to the ZVI concentration, i.e. the stabilizer-to-ZVI molar ratio. To determine the effect of the CMC-to-ZVI molar ratio on the nitrate reduction reactivity, batch kinetic tests of nitrate reduction were carried out at a fixed ZVI concentration of $0.7 \text{ g}\cdot\text{L}^{-1}$ and different CMC concentrations (0, 0.14%, 0.36%, 0.63%) to yield various CMC-to-ZVI molar ratios (0, 0.0012, 0.0032, 0.0056).

Figure 4-5 shows the nitrate reduction by non-stabilized ZVI or ZVI nanoparticles stabilized at various CMC-to-ZVI molar ratios (0.0012, 0.0032, 0.0056). Evidently, the rate and extent of nitrate reduction increased progressively as more CMC was used to stabilize the nanoparticles. At a CMC-to-ZVI molar ratio of 0.0056, nearly 100% of nitrate was reduced within 30 minutes compared to <65% for the non-stabilized ZVI particles, which amounted to an 8.1 times difference in k_{obs} and 4.9 times difference in k_{SA} (**Table 4-1**). Our recent studies (He et al., 2007; He and Zhao, 2007a) revealed that greater CMC-to-ZVI ratios lead to synthesis of finer ZVI nanoparticles. Evidently, the smaller ZVI nanoparticles not only offered greater reactive surface area, but also more reactive. It is also evident from **Figure 4-5** that at equilibrium ~10% and ~6% of nitrate remained intact for the non-stabilized ZVI or ZVI stabilized at a CMC-to-ZVI ratio of 0.0012, respectively, while 100% reduction was observed when the CMC-to-ZVI ratio

was higher. This observation suggests that a fraction of the ZVI electron donors in the larger ZVI particles were not available for nitrate reduction. Presumably, the more profound inactivation of ZVI in the particle cores is attributed to the formation of a thicker layer of iron oxides or iron hydroxides on the larger particles.

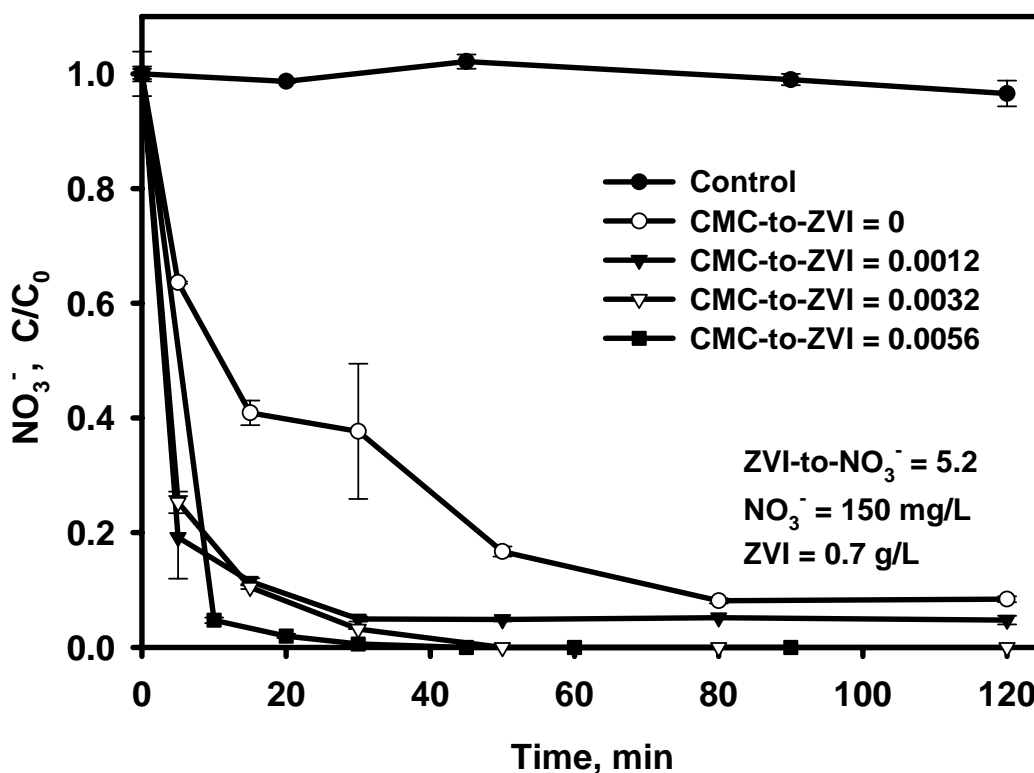


Figure 4-5. Effect of CMC concentrations (CMC-to-ZVI molar ratios) on nitrate reduction by CMC-stabilized ZVI nanoparticles. Initial nitrate concentration = 150 mg/L and ZVI = 0.7 g/L (ZVI-to-NO₃⁻ = 5.2). Solution pH was controlled at 7.0~7.5 (initial and final) with a 0.05 M HEPES buffer. Data plotted as mean of duplicates.

4.3.5 Effect of pH on nitrate reduction

Solution pH can affect both synthesis, and thus, the properties of the ZVI nanoparticles and the corrosion rate of the nanoparticles (He and Zhao, 2007a). Researchers (Cheng et al., 1997; Huang et al. 1998; Zhang and Huang, 2005) have reported that nitrate reduction by iron powder at near-neutral pH was negligible in a non-buffered system, and rapid nitrate reduction was observed only when the solution was buffered at $\text{pH} < 7.0$.

Figure 4-6a and **Figure 4-6b**, respectively, show nitrate reduction kinetics with stabilized ZVI nanoparticles at various pH conditions, and the pH evolution histories during the reactions. When the nanoparticle suspension was directly used for nitrate reduction without pH adjustment or addition of a buffer, the suspension pH experienced a quick rise from 7.0 to 8.2 within 5 minutes of the reaction (**Figure 4-6b**) and then a much slower increase from 8.2 to 8.7 by the end of the 120-min test period. In this case, nitrate was reduced slowly and incompletely with an observed rate constant $k_{obs} = 0.0085 \text{ min}^{-1}$ (**Table 4-1**) and only ~40% of nitrate reduced in the end. When the initial pH in the nanoparticle suspension was lowered to 2.5, the observed rate constant (k_{obs}) was increased to 0.011 min^{-1} , an increase by ~30% (**Figure 4-6a** and **Table 4-1**). On the other hand, **Figure 4-6b** shows that the pH level abruptly (within 5 minutes) rose up from 2.5 to 8.1 and then proceeded at a similar pH level as where no pH adjustment was exercised. Since pH was lowered after the nanoparticles were formed, the nanoparticles in the above two cases are essentially the same. Evidently, the high concentration of extra H^+ ions at the lower initial pH was rapidly reduced to H_2 by the ZVI nanoparticles through Eq. (4-4),

resulting in the sharp pH rebound. Based on electron balance calculations, the reduction of protons consumed ~ 0.089 g/L ZVI (i.e. $\sim 13\%$ of total ZVI added) and produced 1.58×10^{-3} M H_2 . Liou et al. (2005a) reported that treatment of an iron powder (<100 mesh) with H_2 doubled the nitrate reduction rate due to that the presence of H_2 enhanced the reactivity of the ZVI particles by removing the passive oxide layers deposited on the particle surface. In addition, it is also possible that the resultant H_2 acted as an additional reducing agent (in the presence of the ZVI nanoparticles), leading to the observed enhanced nitrate reduction kinetics.

Nitrate reduction tests were also carried out with the aid of a Good's buffer (0.05 M HEPES) to hold pH at 7.0~7.5 (initial and final pH). The pK_a of HEPES is 7.45 at 20 °C (Huang and Zhang, 2005). In this case, nearly 80% of nitrate was reduced in 10 min and $\sim 96\%$ reduced at the end of the test (2 h), and the observed rate constant (k_{obs}) was more than 15 times greater than that when pH was not adjusted. For comparison, 0.05 M of MES (another Good's buffer, $pK_a = 6.10$ at 25 °C) was also tested. In this case, pH was controlled in the range of 6.1~6.4 during the reaction (**Figure 4-6b**). Compared to the case of HEPES, the nitrate reduction with MES displayed an even faster initial rate, where $\sim 88\%$ of nitrate was reduced within the first 5 minutes (**Figure 4-6a**). Again, this faster nitrate reduction at lower pH is attributed to the greater production of H_2 , which in turn refreshing the surface reactivity of the nanoparticles. Moreover, the final amount of nitrate reduced in the lower pH case was slightly ($\sim 5\%$) less (**Figure 4-6a**). This observation suggests that although lower pH values enhanced the reaction rate, the increased conversion of the electron donor from ZVI to H_2 also results in a shift of the

nitrate reduction pathway. As a result, the equilibrium reduction of nitrate was lowered at a lower pH. Note that in all cases, the ZVI nanoparticles were initially the primary electron donors although some residual H_2 from the particle synthesis may also be present.

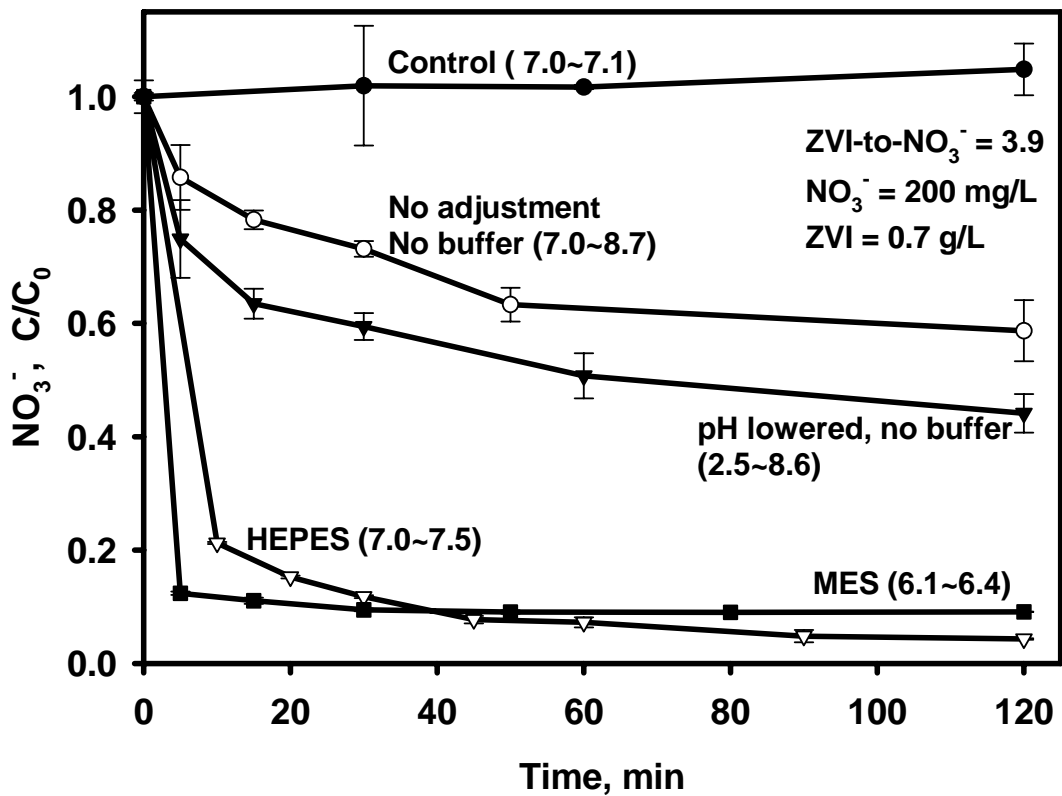


Figure 4-6a. Effect of solution pH on nitrate reduction by CMC-stabilized ZVI nanoparticles during nitrate reduction. Numbers in the parentheses refer to initial and

final pH values. ZVI = 0.7 g/L, $\text{NO}_3^- = 200 \text{ mg/L}$ ($\text{ZVI-to-NO}_3^- = 3.9$), $\text{CMC} = 0.63\%$.

Data plotted as mean of duplicates.

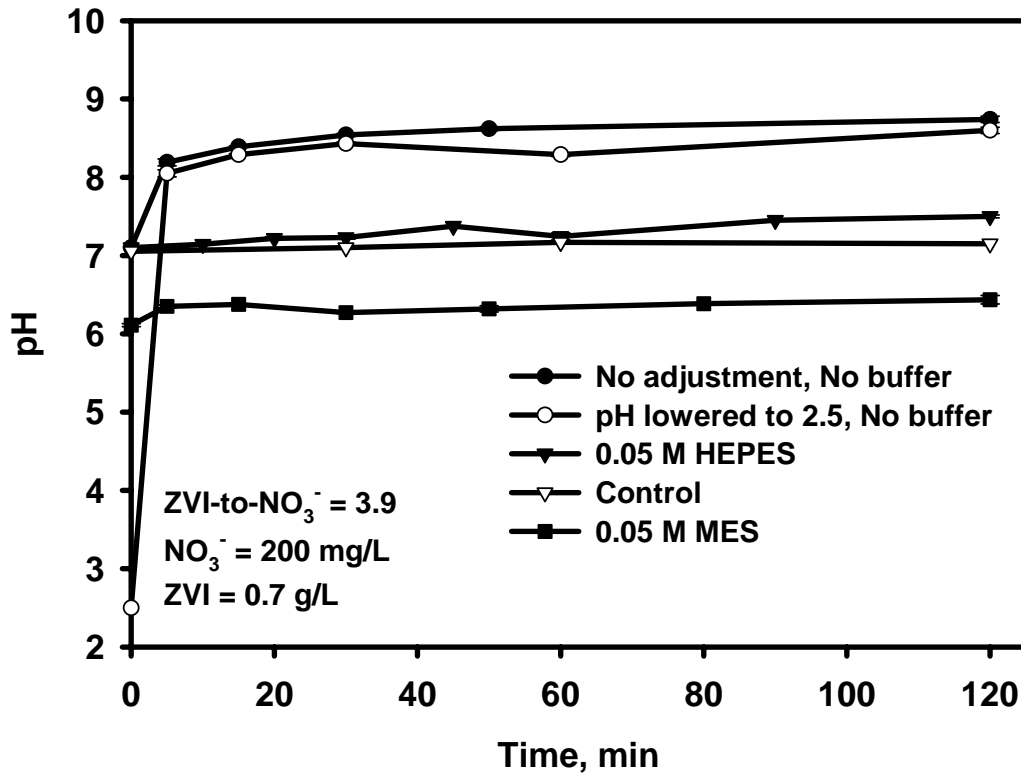


Figure 4-6b. pH evolution during nitrate reduction by CMC-stabilized ZVI nanoparticles.

ZVI = 0.7 g/L, $\text{NO}_3^- = 200 \text{ mg/L}$ ($\text{ZVI-to-NO}_3^- = 3.9$), $\text{CMC} = 0.63\%$. Data plotted as mean of duplicates.

4.3.6 Effect of salinity on nitrate reduction

As mentioned before, IX is a BAT for nitrate removal but is held back by the costs associated with regenerant brine (typically 4%~12% (w/w) NaCl) and brine disposal. From both economic and environmental viewpoints, it is highly desirable to treat and reuse the regenerant brine. From a practical standpoint, the advantage of the stabilized ZVI nanoparticles is best exploited when used for treating water or wastewater of highly concentrated nitrate in a confined volume such as spent nitrate-laden IX regeneration brine.

To test effects of high salinity on nitrate reduction effectiveness of the CMC-stabilized ZVI nanoparticles, batch kinetic tests were carried out in the presence of 1% and 6% (w/w) NaCl, respectively. **Figure 4-7** shows that nitrate reduction was slightly but progressively inhibited by the high concentrations of NaCl. Compared to the reaction without NaCl, the observed rate constant (k_{obs}) was reduced by 3.3% and 30%, respectively, by 1% and 6% of NaCl. He and Zhao (2007a) reported that the presence of high concentrations of cations promotes agglomeration of the CMC-stabilized nanoparticles. For instance, in the presence of 100 mM Na⁺ or 0.59% of NaCl, the primary (63%) particle size grew to 33.7 nm with the remaining 37% of particles being even greater than 50 nm. Consequently, the nitrate reduction rate was diminished due to the agglomeration and the reduced specific surface area of the ZVI nanoparticles. In addition, high concentrations of chloride may also compete with nitrate for the sorption/reaction sites on the ZVI surface, thereby further discounting the reduction rate. Nonetheless, **Figure 4-7** showed that nearly 100% of nitrate was reduced within 90 min

even in the presence of 6% NaCl, suggesting that the stabilized ZVI nanoparticles remain highly effective in reducing nitrate in highly saline water or spent IX brine.

Figure 4-8 shows the concentration histories of various nitrogenous species during nitrate reduction by the stabilized ZVI nanoparticles in the presence of 6% NaCl (w/w). Compared to the case with fresh water (**Figure 4-3**), trace concentrations (<0.95 mg/L) of nitrite-N were detected in the initial stage ($t < 80$ min), but it disappeared thereafter. A possible reason for the nitrite presence is that nitrite is an intermediate product of nitrate reduction (Huang et al., 1998; Alowitz and Schere, 2002) and high concentrations of Cl^- may slightly inhibit nitrite reduction by the stabilized ZVI nanoparticles. At the end, nitrate was transformed to ammonium (62%) and N_2 (38%).

As indicated by Eq. (4-1) and (4-2), as nitrate is reduced, Fe^0 is oxidized to Fe^{2+} . The resultant ferrous ions are non-toxic and can be either reused or removed. For example, new ZVI nanoparticles can be produced in situ by reducing the existing Fe^{2+} ions with borohydride. Given the fairly low solubility of Fe^{2+} (e.g. $44 \text{ mg}\cdot\text{L}^{-1}$ at pH 8.0), it can be removed, if desired, either by slightly raising the pH or converting it to even less insoluble Fe^{3+} under ambient conditions.

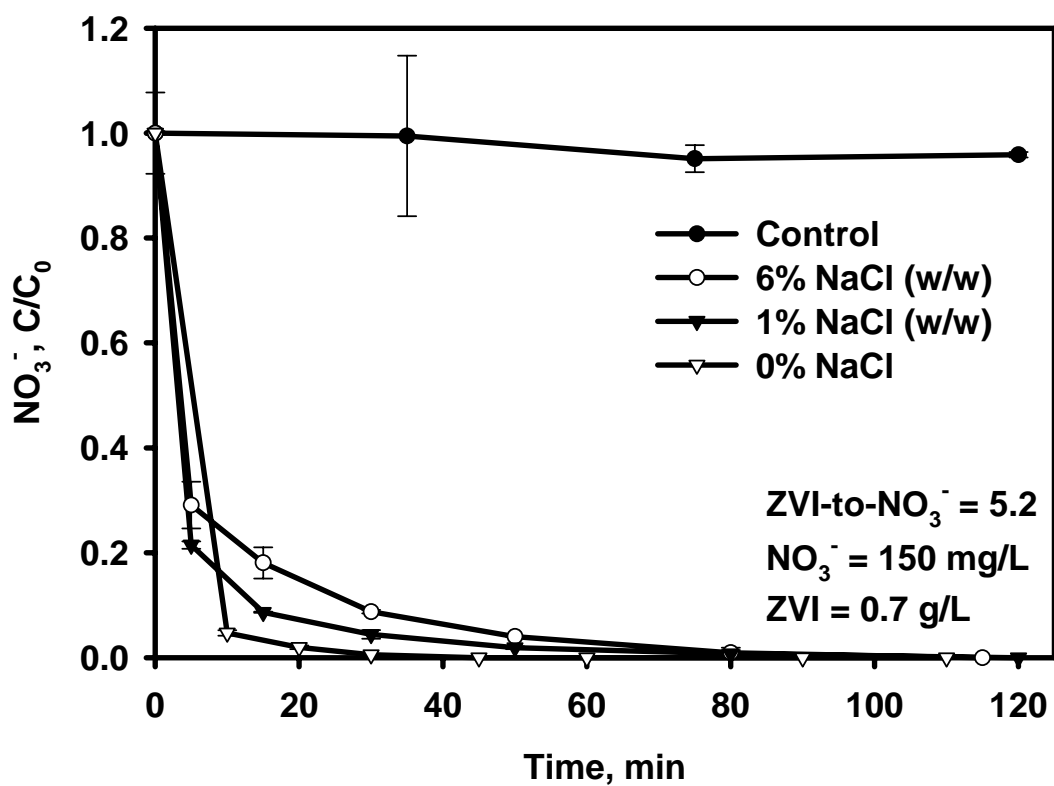


Figure 4-7. Nitrate reduction by CMC-stabilized ZVI nanoparticles in the presence of various concentrations of NaCl. Initial nitrate concentration = 150 mg/L, ZVI = 0.7 g/L ($\text{ZVI-to-NO}_3^- = 5.2$), CMC = 0.63%. Solution pH was controlled at 7.0~7.5 (initial and final) with a 0.05 M HEPES buffer. Data plotted as mean of duplicates.

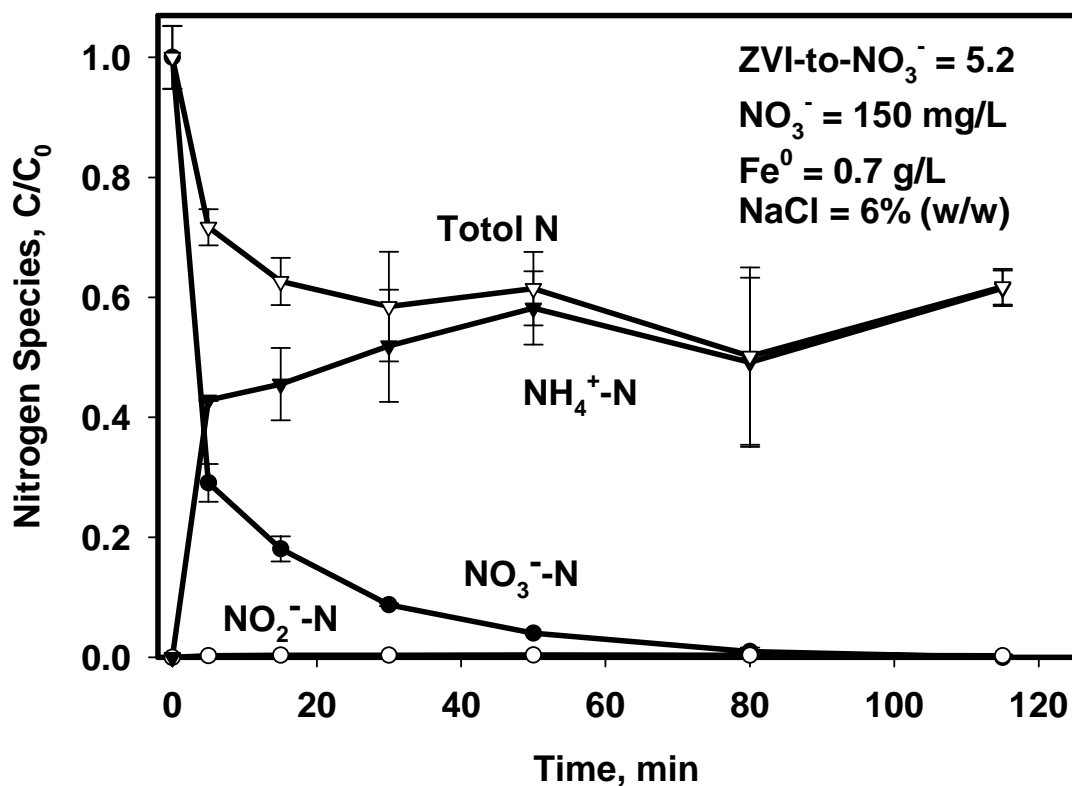


Figure 4-8. Concentration histories of various nitrogenous species during nitrate reduction by CMC-stabilized ZVI nanoparticles in the presence of 6% NaCl (w/w). Initial nitrate concentration = 150 mg/L, ZVI = 0.7 g/L (ZVI-to-NO₃⁻ = 5.2), CMC = 0.63%. All concentration was normalized to C₀. Solution pH was controlled at 7.0~7.5 (initial and final) with a 0.05 M HEPES buffer. Data plotted as mean of duplicates.

4.4 Summary and Conclusions

Major findings and conclusions from this study are summarized as follows:

1). Batch tests proved that ZVI nanoparticles were efficient for nitrate reduction. With a ZVI-to-NO₃⁻ molar ratio of 5.2 and a 0.05 M HEPES buffer, 150 mg/L nitrate was completely transformed within 60 minutes. The observed pseudo first-order rate constant (k_{obs}) for nitrate reduction with the stabilized ZVI nanoparticles was more than 5 times greater than that for non-stabilized ZVI particles. And the surface-area normalized reaction rate constants (k_{SA}) indicated that a stabilizer (CMC) not only increased the surface area of the nanoparticles, but also resulted in higher surface reactivity.

2). The ZVI-to-NO₃⁻ molar ratio not only affects nitrate reduction rate but also influences reaction pathways and final products, i.e. NH₄⁺ and N₂. The k_{obs} value was improved by about 3 times when the ZVI-to-NO₃⁻ molar ratio was increased from 2.5 to 5.2. With a ZVI-to-NO₃⁻ molar ratio of 2.5, N₂-N accounted for two thirds (66%) of the nitrate reduction products, 30% greater than that with a ZVI-to-NO₃⁻ molar ratio of 3.9.

3). Coating the stabilized ZVI nanoparticles with metals (Pd and Cu) reduced the rate constant (k_{obs}) by 15%~29% due to the oxidation of ZVI by water and/or protons. However, the bimetallic catalysts Cu-Pd at Cu = 0.4% and Pd = 0.1% of Fe or Pd-Cu at Pd = 0.4% and Cu = 0.1% of Fe reduced the ammonium fraction by 8% and 7%, respectively, compared to that without a catalyst.

4). The nitrate reduction rate increased progressively with the increase of the CMC-to-ZVI molar ratio. The observed rate constant (k_{obs}) with a CMC-to-ZVI molar ratio of 0.0056 was 8.1 times greater than that without CMC.

5). The nitrate reduction efficiency was strongly pH dependent and application of a 0.05 M HEPES buffer solution (pH 7.0~7.5) increased the k_{obs} value by 15 times compared to that without pH adjustment.

6). The presence of 6% NaCl (w/w) decreased k_{obs} by 30% compared to that in fresh water due to both the promotive effect of cations on the agglomeration of ZVI nanoparticles and the competition from chloride ions for reactive ZVI surface. However, 100% nitrate was removed within 2 hours in the saline water (6% NaCl), indicating that this technology can be used to treat nitrate in both fresh water and saline water such as IX brine.

CHAPTER 5. *IN-SITU* MERCURY IMMOBILIZATION IN SEDIMENT BY STABILIZED IRON SULFIDE NANOPARTICLES

Presented in this chapter is an innovative *in-situ* mercury (Hg) immobilization technology using stabilized iron sulfide (FeS(s)) nanoparticles that was investigated through a series of batch and column experiments. The FeS(s) nanoparticles are successfully prepared using a low-cost and food-grade cellulose (carboxymethyl cellulose, CMC) as the stabilizer and used for mercury (Hg) immobilization in sediment. It is shown that the stabilized FeS(s) nanoparticles are highly mobile in sediment and are very effective for mercury immobilization.

5.1 Introduction

Mercury (Hg) is one of the most pervasive and bio-accumulative contaminants. When it enters water and sediments, Hg undergoes a number of complex chemical and biological speciation and transformation processes, of which Hg methylation has been the primary environmental concern (U.S.EPA, 1997; UNEP, 2002). Methylmercury (MeHg) is a potent neuro-toxin (UNEP, 2002) and it can accumulate along the aquatic food chain, reaching its apex in predatory fish, where concentrations may be up to one million times greater than in the water column (Stein et al., 1996). As a result, even small concentrations of Hg in the water column (ng/L) can lead to significant concentrations of methylmercury in fish and waterfowl (Stein et al., 1996; Driscoll et al., 1994; Zillioux et

al., 1993). Triggered by the toxicity and bioaccumulation concerns, the U.S. EPA has identified Hg as one of its twelve priority persistent bio-accumulative toxins (PBTs).

Traditionally, remediation of Hg-contaminated soils or sediments employs excavation and subsequent disposal in a landfill (Barnett et al., 1997). However, this method is very costly and environmentally disruptive, and the landfilled Hg will very likely leach back to the environment. The estimated clean-up cost was more than one billion dollars using traditional methods (Barnett et al., 1998; 2001; Riddle et al., 2002). Recently, phytoremediation was explored to remove Hg from soils. For instance, some water hyacinths from South America are able to concentrate 4,435 µg/L Hg in their roots and 852 µg/L Hg in their shoots (Wagner-Döbler et al., 2000). However, this promising technology is held back by the common question of what to do with the Hg-saturated plants, which need further disposal. Biological conversion of methylmercury to elemental Hg was used to treat wastewater streams from Chlor Alkali plants (Benner et al., 1999). However, the de-methylation process is not favored in the subsurface environment. Permeable reactive barriers (PRBs) have been employed to remediate various contaminated sites. Typically scrap iron (i.e., Fe⁰) is employed to *in-situ* immobilize various redox active metals in soils and groundwater. However, because of the large particle size, the reaction kinetics is very limited. As a result, when applied to Hg immobilization, conventional PRBs have been seen to stimulate the growth of sulfate-reducing bacteria (SRB) (Gu et al., 1999; McMahon et al., 1999; Phillips et al., 2000), the primary culprits of Hg methylation.

In-situ immobilization of Hg using stabilized FeS(s) nanoparticles reported herein represents an innovative strategy. Mercury can be immobilized by addition of innocuous

iron sulfide nanoparticles and then mercury bioavailability will be reduced. Iron sulfide minerals have been shown as effective adsorbents for Hg(II) (Behra et al., 2001; Brown et al., 1979; Hyland et al., 1990; Jean and Bancroft, 1986; Bower, 2007). It was also reported that Hg(II) could be immobilized by nanosized (nonstabilized) FeS through adsorption or coprecipitation and neither adsorbed nor coprecipitated Hg was readily extracted by strongly complexing ligands, such as 0.1 M Na₄EDTA and 0.1 M NaCN (Jeong, 2005). Iron sulfide has also been shown to readily exchange Fe(II) with Hg(II) to form HgS(s) (Jeong, 2005; Morse and Luther, 1999; Svensson et al., 2006). The resultant HgS(s) can be either metacinnabar (cubic, black HgS(s)) or the thermodynamically more stable cinnabar (hexagonal, red HgS(s)) (Shi et al., 2006). Both forms of HgS(s) are extremely insoluble in water. In the absence of dissolved oxygen (DO), dissolution of HgS(s) is thermodynamically unfavorable. In the presence of DO, the HgS(s) dissolution turns thermodynamically favorable. However, HgS(s) dissolution is then limited by extremely slow oxidation kinetics (Barnett et al., 2001). Namely, once formed, HgS(s) may remain stable in the environment, even under oxidizing conditions, and HgS(s) has been proposed as the primary sink for mercury in the environment (Barnett et al., 2001). Compared to traditional approaches, this technology is likely more environmentally friendly and may result in substantial cost reduction.

To prepare FeS(s) nanoparticles that can be injected and well dispersed in soils or sediments to promote abiotic immobilization of Hg is the key to the success of *in-situ* immobilization of Hg. Various methods have been reported to prepare FeS(s) nanoparticles, including polymer-stabilized synthesis (Ha et al., 2005; Paknikar et al., 2005; Qian et al., 2001), chemical vapor condensation (CVC) process (Watson et al.,

1999), sulfate-reducing bacteria-assisted production (Watson et al., 2000; Chin et al., 2005), high-energy mechanical milling and mechanochemical process (Chadha et al., 1996), reverse micelle (Sarma and Chattopadhyay, 2004; Wilcoxon et al., 1996), and dendrimer stabilization (Shi et al., 2006). However, the preparation of functionalized FeS(s) nanoparticles using an environmentally friendly and cost-effective method still remains a great challenge.

Recently, water-soluble starch and cellulose were found to be effective stabilizers/dispersants to cap nanoparticles. Water-soluble starch was used to disperse Au nanoparticles in water (Sarma and Chattopadhyay, 2004), and used as a morphology-directing agent for tellurium nanowires (Lu et al., 2005). Cellulose acetate membranes were used as supports for preparation of Fe and Cu nanoparticles (Shim et al., 2001; 2002). Porous cellulose fibers were used for *in-situ* synthesis of noble metal nanoparticles such as Ag, Au, Pt, Pd (He et al., 2003). Sodium carboxymethyl cellulose (NaCMC) was used as a stabilizer in the preparation of superparamagnetic Fe (Si et al., 2004) and Ag nanoparticles (Magdassi et al., 2003). Polysaccharides were used as coating agents for preparing nanoparticles for drug delivery (He and Zhao, 2005). Water-soluble starch and NaCMC were also used to prepare ZVI nanoparticles for dechlorination (He et al., 2007; Zhao and He, 2004).

The objectives of this study are to synthesize a stable and dispersive iron sulfide (FeS(s)) nanoparticles using a low-cost, food-grade polysaccharides (e.g. CMC) as an effective and “green” stabilizer to yield FeS(s) nanoparticles suitable for *in-situ* injection uses and to use them as an *in-situ* remediation technology for mercury immobilization in sediment. The specific goals are 1) to synthesize a new class of stabilized FeS(s)

nanoparticles using CMC as a stabilizer; 2) to characterize the stabilized FeS(s) nanoparticles; 3) to investigate the efficiency of mercury immobilization by using the stabilized FeS(s) nanoparticles in sediment; 4) to study the mobility of the stabilized FeS(s) nanoparticles in sediment.

5.2 Materials and Methods

The following chemicals were used as received: ferrous sulfate ($\text{FeSO}_4 \cdot 7\text{H}_2\text{O}$) (Acros Organics, Morris Plains, NJ, USA); hydrochloric acid (HCl) (Fisher, Fair lawn, NJ, USA); hydroxylamine hydrochloride ($\text{NH}_2\text{OH} \cdot \text{HCl}$) (Fisher); mercury nitrate ($\text{Hg}(\text{NO}_3)_2 \cdot \text{H}_2\text{O}$) (Fisher); potassium bromide (KBr) (Fisher); potassium bromate (KBrO_3) (Fisher); sodium carboxymethyl cellulose (NaCMC) (M.W. = 90,000, D.S. = 0.7) (Acros Organics); sodium nitrate (NaNO_3) (Fisher); sodium sulfide ($\text{Na}_2\text{S} \cdot 9\text{H}_2\text{O}$) (Fisher); sodium thiosulfate ($\text{Na}_2\text{S}_2\text{O}_3$) (Fisher); stannous chloride ($\text{SnCl}_2 \cdot 2\text{H}_2\text{O}$) (Fisher).

The stabilized FeS(s) nanoparticles were prepared in a 250 mL flask attached to a vacuum line. A CMC stock solution (1%, w/w) was prepared by dissolving NaCMC with deionized (DI) water and the solution was purged with purified N_2 (>99%) for half an hour to remove dissolved oxygen (DO). Stock solutions of 0.1 M FeSO_4 and Na_2S were also prepared with N_2 -purged DI water. In a typical preparation, a FeSO_4 stock solution was mixed with a CMC stock solution through a burette to yield a desired concentration of iron and stabilizer. Based on our prior experiences preparing stabilized ZVI nanoparticles (He et al., 2007; Xiong et al., 2007a), 0.2% of CMC was used to stabilize 0.5 g/L FeS(s) nanoparticles in this study. Note the doses of FeS(s) and CMC were chosen here based on our prior experiences of preparing stabilized ZVI nanoparticles and

they are not optimized in this study. The mixture was then bubbled with purified N₂ for half an hour to remove DO and to complete the formation of Fe-CMC complexes. Fe²⁺ ions were then reacted with S²⁻ to form FeS(s) nanoparticles by adding Na₂S stock solution (the molar ratio of Fe-to-S = 1:1) to the mixture. The reactor system was operated under inert conditions through continuous vacuuming. The flask was hand-shaken intermittently during the preparation. For comparison, non-stabilized iron sulfide particles were also prepared following the same procedure but without adding a stabilizer. The particles were used within 30 minutes of preparation.

Transmission electron microscopy (TEM) images were obtained by using a Zeiss EM10 transmission electron microscope (Zeiss, Thornwood, NJ) operated at 60 kV. The TEM images were analyzed using a specialty image processing software named ImageJ to analyze the particle size. Dynamic light scattering (DLS) tests were performed with a Nicomp 380 Submicron Particle Sizer (PSS, Santa Barbara, CA) at a measurement angle of 90° (Internal He-Ne laser, wavelength 633 nm). The DLS data were processed and analyzed with a software package (CW380) to yield the number-weighted particle size distributions. The details of sample preparation and software operation have been reported (He and Zhao, 2005; He et al., 2007). X-ray diffraction (XRD) analysis on the stabilized iron sulfide nanoparticles was tried to characterize the nanoparticles using a Rigaku Miniflex Diffractometer using Cu-K α radiation (30 kV, 15 mA, 3° < 2 θ < 90°), but it is not successful so far because the nanoparticles can not be separated from the aqueous phase under even 60,000 rpm centrifuging. However, the synthetic FeS prepared by Jeong (2005) using the same method and similar conditions but without a stabilizer was found to consist mainly of poorly crystalline mackinawite with a small fraction of

greigite as an oxidation product. FeS(s) is used throughout this dissertation to represent the iron sulfide nanoparticles prepared in this study.

Clay loam sediment was obtained from a fishing pond in Auburn AL. The sediment was air-dried and sediment aggregates were broken by a mortar with pestle and sieved through a 2-mm screen. The sediment contains 30% of sand, 33% of silt, 37% of clay, 2.5% of organic matter. Hg was loaded to this sediment by following the procedure reported by Piao (2002). Briefly, 100-200 g sediment was mixed with 0.1-0.8 g $\text{Hg}(\text{NO}_3)_2 \cdot \text{H}_2\text{O}$ and 4-10 mL DI water. The mixture was mixed manually on a daily basis and was aged for one month. Two kinds of Hg-laden sediment were prepared in this study, i.e. high-content (3119.9 mg/kg) and low-content (177.2 mg/g) sediment. These two mercury concentrations were chosen because the U.S. EPA uses a value of 260 mg/kg as a threshold to categorize low-Hg content and high-Hg content mercury waste and they are comparable to those studied by other researchers (Biestel and Scholz, 1997; Biestel et al., 2000; Hintelmann et al., 1995; Jiang et al., 2006; Piao, 2002).

The aged sediments were digested following Appendix to the U.S. EPA Method 1631 to analyze the real mercury content. **Table 5-1** lists the composition of Hg-laden sediments used in this study.

Table 5-1. Composition of the mercury-laden sediments.

Sediment type	Desired Hg content, mg/kg	$\text{Hg}(\text{NO}_3)_2 \cdot \text{H}_2\text{O}$, g	Sediment, g	Water, mL	Real Hg content, mg/kg
High-Hg	5,000	0.80	92.86	4.6	3119.9
Low-Hg	350	0.12	196.70	10.0	177.2

Hg immobilization by stabilized FeS(s) nanoparticles was carried out in a series of Teflon vials. Typically, 3 g of Hg-laden sediment was added to 30 mL Teflon vials and certain volume of 0.5 g/L FeS(s) nanoparticles (stabilized with 0.2% CMC) and DI water were added to Teflon vials to yield desired doses of FeS(s) without leaving headspace. The mixtures were then rotated on an end-to-end rotator at 30 rpm in a glove box under a N₂:CO₂ (98:2) atmosphere (pCO₂ of 10^{-1.7} atm) at ambient temperature (22 ± 0.1 °C). The solution pH was kept at 7 ± 0.1 through intermittent adjustment with 0.1 N HNO₃ and/or 0.1 N NaOH. In about one week (a separate kinetic test showed that the reaction equilibrium arrived within one week), samples were taken and centrifuged with Accuspin 400 (Fisher) at 6000 g for 20 minutes and the supernatant was filtered through an Acrodisc syringe filter with a 0.2 µm Tuffryn membrane. Preliminary tests showed no mercury loss to Teflon vials or Acrodisc syringe filter. The filtrate was preserved with BCl (1%) for mercury analysis. Control tests were also carried out by using a solution containing 0.2% CMC and 0.1 M NaNO₃ under otherwise identical conditions.

Toxicity characteristic leaching procedure (TCLP) tests were performed following the U.S. EPA Method 1311. Briefly, 2.25 g of dried sediment was added to 45 ml TCLP fluid #1 in a Teflon vial without leaving headspace. The vials were mixed in an end-to-end rotator (30 rpm) for 18 hours and then centrifuged with Accuspin 400 (Fisher) at 6000 g for 20 minutes and the supernatant was filtered with an Acrodisc syringe filter with 0.2 µm Tuffryn membrane. The filtrates were preserved with BCl (1%) for mercury analysis.

The mobility test of the stabilized FeS(s) nanoparticles in a clay loam sediment column was carried out with an experiment set-up including a plexiglass column

(diameter = 10 mm, length = 100 mm, Omnifit, Cambridge, UK), a HPLC pump and a fraction collector (Eldex Laboratories, Napa, CA, USA). Typically, 5 g of Hg-laden sediment was wet-packed in the column yielding a porosity of 0.45. A stabilized FeS(s) nanoparticles suspension (FeS(s) = 0.5 g/L, CMC = 0.2%), a non-stabilized FeS(s) particles suspension (FeS(s) = 0.5 g/L), and a tracer solution (50 mg/L KBr) were passed downwardly through the sediment bed at an EBCT (Empty Bed Contact Time) of 30 minutes and a SLV (Superficial Liquid Velocity) of 0.13 cm/min. The effluent was collected by a fraction collector. The concentration of Br⁻ was analyzed to get the breakthrough history of KBr, while the concentration of total iron in the eluent was analyzed after the samples were dissolved with acidified DI water (pH=3) to represent the breakthrough history of the stabilized FeS(s) nanoparticles. A separate test using an eluent containing 0.2% CMC and 0.1 M NaNO₃ to wash the same sediment column showed that the iron concentration (<0.5 mg/L) in the effluent was negligible compared to that (318 mg/L maximum) for the 0.5 g/L FeS(s) nanoparticles suspensions.

Mercury immobilization column tests were conducted with the same experiment setup and procedure as described for the mobility tests. Briefly, 5 g of Hg-laden sediment was wet-packed in the column with a porosity of 0.45. An influent of 0.5 g/L FeS(s) nanoparticles stabilized with 0.2% CMC was passed downwardly through the sediment bed at an EBCT of 30 minutes and a SLV of 0.13 cm/min. The effluent was collected by a fraction collector. 0.2 mL BrCl was added to each sample to preserve mercury and the sampling tubes were sealed with parafilm immediately after the samples were collected. Control tests were also carried out by using a solution containing 0.2% CMC and 0.1 M NaNO₃ as the influent under otherwise identical conditions.

Total mercury was analyzed using cold vapor atomic absorption spectrometry (CVAAS-USEPA Methods 7470A and 7471A) (Varian SpectrAA 220FS Atomic Absorption Spectrometer) with SnCl_2 as a reductant. Mercury sample preparation and preservation was conducted similar to these two procedures and those described in EPA Method 1631. Prior to analysis, all samples were first preserved and oxidized with 1% BrCl , followed by 1% hydroxylamine hydrochloride to destroy the unreacted BrCl . All containers used in this study are made of Teflon to minimize mercury loss to containers walls. All the mercury concentrations included in this research are total mercury concentrations. All reagents for mercury analysis were prepared following the U.S. EPA Method 1631 C. The determination limit of total mercury was 0.5 $\mu\text{g/L}$. Br^- was analyzed using a Dionex Ion Chromatography (DX-120) equipped with an AS14 column. The detection limit for Br^- was 0.5 mg/L. Total iron concentration was analyzed with an atomic absorption spectrometer (Varian SpectrAA 220FS). The detection limit for total iron was 0.1 mg/L.

5.3 Results and Discussion

5.3.1 Characterization of stabilized FeS(s) nanoparticles and the role of stabilizer

Figure 5-1 shows TEM images of FeS(s) particles prepared without a stabilizer (a), and with 0.2% (w/w) CMC (b) under otherwise identical conditions. Without a stabilizer, FeS(s) particles appeared to be $>1 \mu\text{m}$ flocs. However, the stabilized FeS(s) nanoparticles appeared to be clearly discrete and well dispersed. Meanwhile, experimental observations indicated that non-stabilized FeS(s) particles agglomerated and precipitated within minutes while the stabilized FeS(s) nanoparticles remained suspended

in the water for more than 3 months. The formation of non-stabilized FeS(s) flocs can be attributed to the magnetic force and the Van der Waals force between individual FeS(s) particles, while the negatively charged CMC prevent them from agglomeration as discussed later on. Evidently, the presence of CMC prevented the aggregation of FeS(s) nanoparticles and thus can maintain the high surface area and reactivity.

The TEM images (4 different images) were used for particle size analysis following the method reported by He and Zhao (2005). **Figure 5-2** shows the particle size distribution of CMC-stabilized FeS(s) nanoparticles for a random sample of 247 particles. The particle size was in the range of 3-120 nm while the mean particle size was calculated to be 29.4 nm with a standard deviation of 24.9 nm. DLS tests were also conducted to get more accurate measurement of the particle size (He et al., 2007). The DLS results indicated a particle diameter of 38.5 nm with a deviation of 5.4 nm (99.9% particles by number) for freshly prepared CMC-stabilized FeS(s) nanoparticles, which agreed well with the TEM measurement.

After three months of storage in a refrigerator (4 °C), the stabilized FeS(s) nanoparticles remained suspended in water. And DLS measurement indicated that the particle size was found to be 31.4 nm with a standard deviation of 4.0 nm. This decrease in particle size by 18% in three months can be attributed to that some FeS(s) nanoparticles were dissolved in water or oxidized by residual DO in water.

The above results proved that CMC is highly effective in stabilizing FeS(s) nanoparticles. CMC is a cellulose derivative with carboxymethyl groups (-CH₂-COOH) bound to some of the hydroxyl groups of the glucopyranose monomers. The hydroxyl and carboxyl functional groups of CMC can form weak complex with Fe²⁺, which has been

well studied by He et al. (2007). Upon addition of Na_2S , FeS(s) nanoparticles are formed and coated with a thin layer of negatively charged CMC, which prevents FeS(s) nanoparticles from aggregation through the electrostatic repulsion and/or steric hindrance.

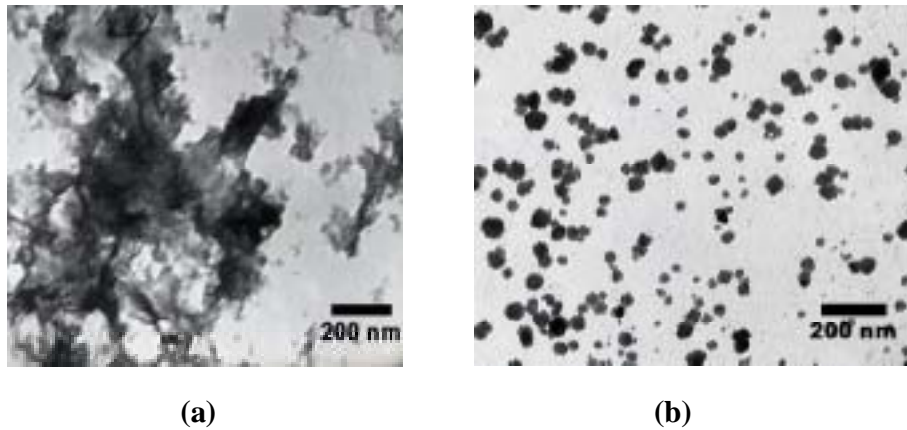


Figure 5-1. TEM images of FeS(s) particles prepared without a stabilizer **(a)**, and with 0.2% (w/w) CMC **(b)**. FeS(s) particles were prepared freshly in water and $\text{FeS(s)} = 0.5$ g/L in both cases. The scale bar represents 200 nm.

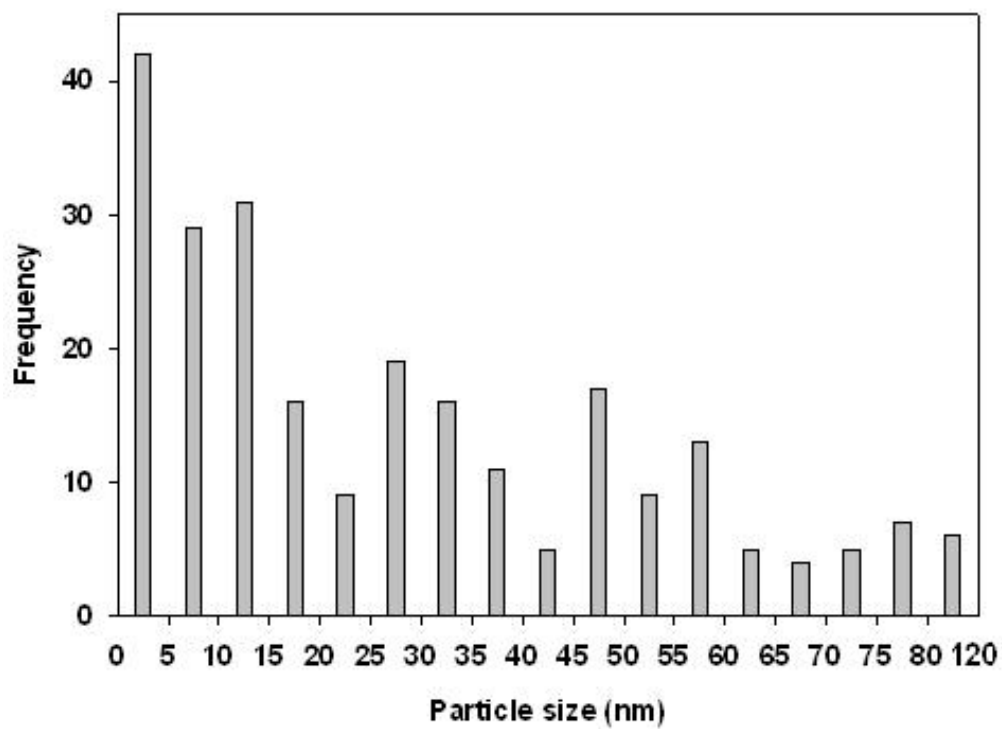


Figure 5-2. Histogram showing the size distribution of the CMC-stabilized FeS(s) nanoparticles for a random sample of 247 particles.

5.3.2 Immobilization of mercury by stabilized FeS(s) nanoparticles: batch tests

The effectiveness of stabilized FeS(s) nanoparticles for mercury immobilization in Hg-laden sediment was tested in a series of batch experiments. The low-Hg content sediment (**Table 5-1**) was used in the batch tests. **Figure 5-3** shows the mercury leached out in the aqueous phase from the Hg-laden sediment that was treated with various doses of CMC-stabilized FeS(s) nanoparticles at pH 7 ± 0.1 . The dose of stabilized FeS(s) nanoparticles was expressed by the molar ratio of stabilized FeS(s) nanoparticles added over the total Hg content in the sediment.

When there were no FeS(s) nanoparticles added to the mixture, 263.9 $\mu\text{g/L}$ of Hg leached out to the aqueous phase. Based on the mercury content (177.2 mg/kg) of the Hg-laden sediment, it was calculated that only 1.5% of total mercury in the sediment leached out. This is not surprising because the sediment was aged for one month before use and the organic matter was relatively high (2.5%), which was reported to form strong complexes with mercury (Lambertsson and Nilsson, 2006; Skyllberg et al., 2006). When the stabilized FeS(s) nanoparticles were added, the Hg concentration in the aqueous phase decreased dramatically. With a FeS(s)/Hg molar ratio of 2, the Hg concentration in the aqueous phase dropped by 73.2% compared to that without FeS(s) nanoparticles, and the Hg concentration in the aqueous phase decreased progressively as the FeS(s) dose increased. When a FeS(s)/Hg molar ratio of 26.5 was used, only 8.5 $\mu\text{g/L}$ of mercury leached out in the aqueous phase, a 96.8% drop compared to that without FeS(s) nanoparticles. Evidently, stabilized FeS(s) nanoparticles should be provided at molar quantities much higher than total mercury in the soil or sediment to be treated. Bower

(2007) observed that lowering the molar ratio of $(\text{Hg(II)}_0/\text{FeS(s)})$ only by a factor of 4 caused a significant increase in aqueous phase equilibrium Hg(II) concentrations (>2 orders of magnitude) when iron sulfide (99.9% metals basis, <100 mesh, Alfa Aesar) was used to remove mercury in water. Jeong (2005) examined mercury removal by synthesized FeS(s) in aqueous phase with a $\text{FeS(s)}/\text{Hg(II)}_0$ molar ratio of range of 25-2272 and found that the molar ratio of $\text{FeS(s)}/\text{Hg(II)}_0$ should be maintained as high as 50 to ensure the dominance of adsorption and a maximum sorption capacity of Hg(II) to FeS(s) of 0.23 mmol/g (46 mg/g) at pH 5.5-6.0 was calculated.

To further investigate the effectiveness of FeS(s) nanoparticles for Hg immobilization in sediment. The sediment samples that were treated with various doses of FeS(s) nanoparticles were air-dried and examined in TCLP extraction, which is used by the U.S. EPA as an operation measure of the leachability of sediment contaminants in response to mildly acidic (pH ~ 4.93), weak ligand extraction (acetate) conditions thought to be analogous to the leaching environment of municipal landfills. **Figure 5-4** shows the Hg concentrations in the TCLP extractant for sediments treated with various doses of FeS(s) nanoparticles. The Hg concentration in the TCLP extractant for the sediment without the treatment of FeS(s) nanoparticles was 211.82 $\mu\text{g/L}$. When the sediment was treated with FeS(s) nanoparticles, the Hg concentration in the TCLP extractant decreased progressively with the increase of the FeS(s) nanoparticles dose. With a $\text{FeS(s)}/\text{Hg}$ molar ratio of 2, the Hg concentration in the TCLP extractant dropped by 66.2% compared to that without the treatment of FeS(s) nanoparticles. When a $\text{FeS(s)}/\text{Hg}$ molar ratio of 26.5 was used, only 2 $\mu\text{g/L}$ of Hg was extracted in TCLP tests, a 99.1% drop compared to that without the treatment of FeS(s) nanoparticles. Meanwhile, Hg concentrations in TCLP

extractant for the sediment treated with stabilized FeS(s) nanoparticles were far below the regulated TCLP limit (0.2 mg/L), which is commonly used to classify hazardous wastes in the U.S. Apparently, the stabilized FeS(s) nanoparticles can greatly minimize Hg leachability.

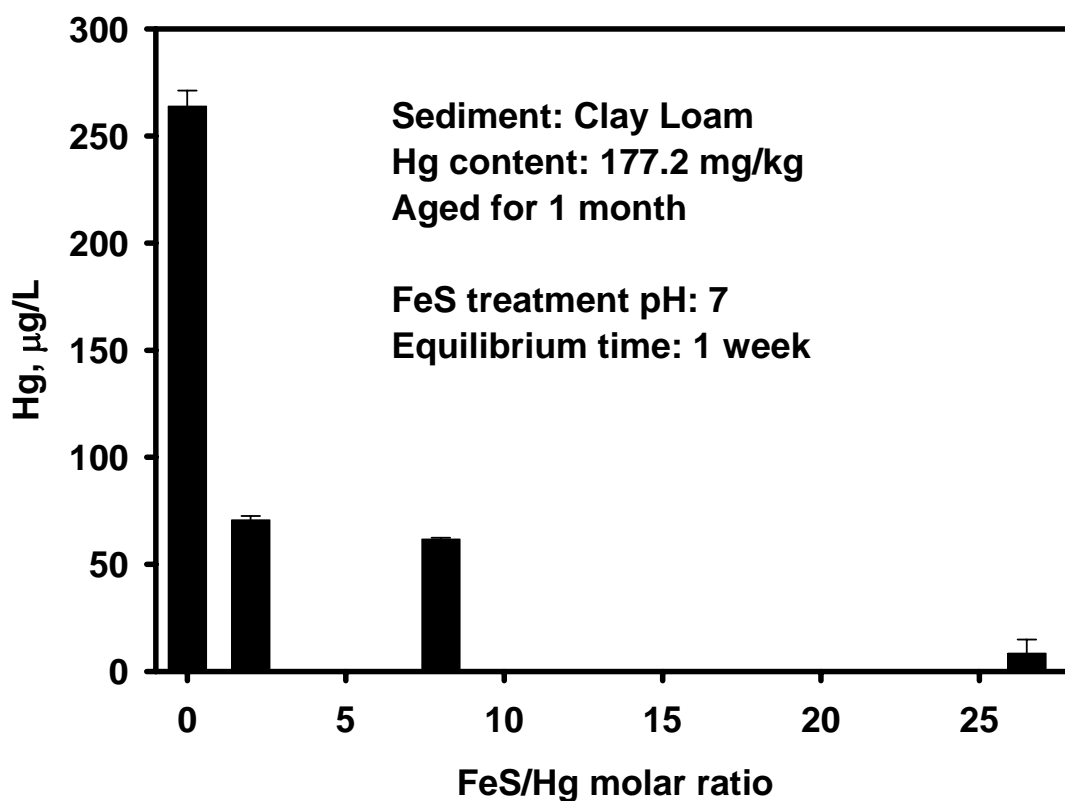


Figure 5-3. Mercury concentration in the aqueous phase when the Hg-laden sediment was treated with various doses (expressed as FeS(s)/Hg molar ratio) of the stabilized FeS(s) nanoparticles for 1 week. The pH was controlled at 7 with 0.1 N HCl and/or 0.1 N HNO₃. Control test was also carried out by using a solution containing 0.2% CMC and 0.1 M NaNO₃ but no FeS(s) nanoparticles. Data plotted as mean of duplicates.

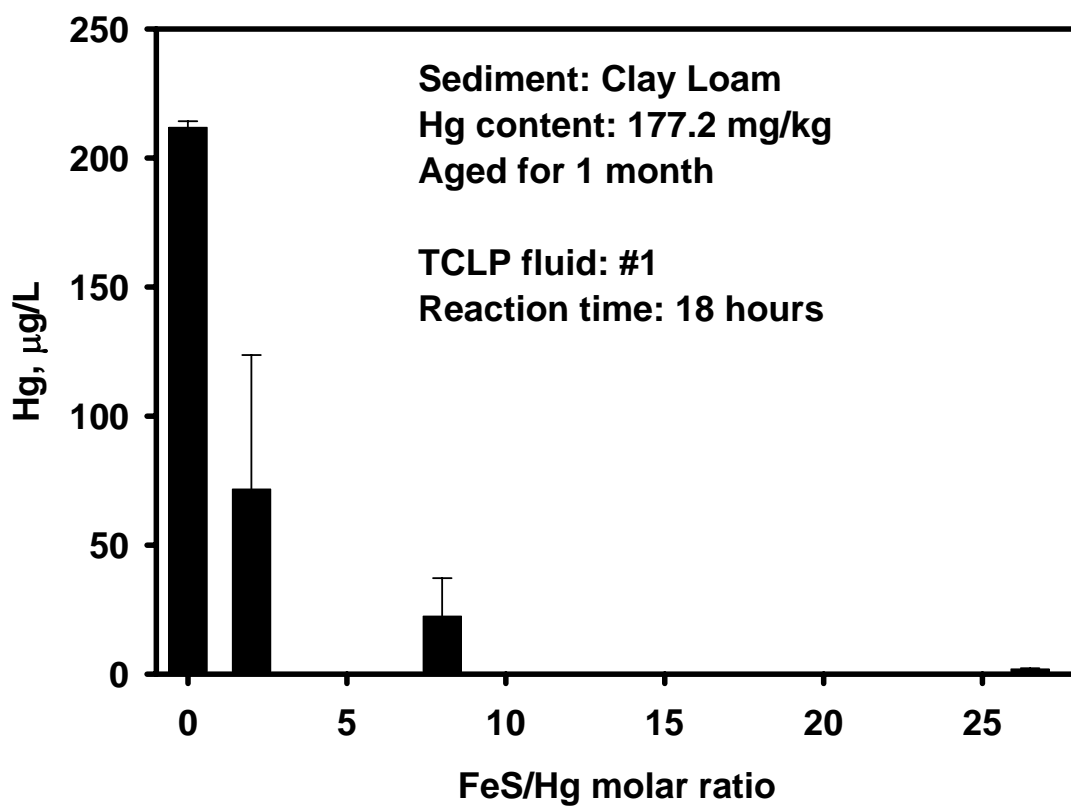


Figure 5-4. Mercury concentration in the TCLP extractant from the sediments that were treated with various doses of the stabilized FeS(s) nanoparticles. Data plotted as mean of duplicates.

The inhibition of Hg leachability from Hg-laden sediment by stabilized FeS(s) nanoparticles can be explained by the high affinity of Hg(II) to FeS(s). A number of researches have reported that iron sulfide minerals such as pyrite effectively immobilized mercury (Behra et al., 2001; Brown et al., 1979; Hyland et al., 1990; Jean and Bancroft, 1986; Jeong, 2005). The high affinity of Hg(II) for iron sulfides can be explained by the Lewis acid-base theory: Hg(II), a soft Lewis acid, forms strong covalent bonds with sulfides that are soft Lewis base (Jeong, 2005). Immobilization of mercury can occur by precipitation/coprecipitation, solid solution formation, or sorption as surface complexes on the metal sulfides (James and Macnaughton, 1977). Morse and Luther (1999) proposed the following reactions to describe the possible reactions for the incorporation of mercury into FeS(s):



in which *Me* stands for metal, such as Hg in this study.

Among these interactions, precipitation of HgS at the expense of FeS(s) is expected, based on thermodynamic and ion radii considerations: HgS is less soluble than FeS(s), and Hg(II) has a much larger ionic radius than Fe(II), both resulting in the favorable dissolution of FeS(s) and precipitation of HgS (Jeong, 2005). In fact, the formation of HgS(s) and subsequent deposition into soils and sediments is considered the dominant sink of Hg from the global Hg cycle (Stein et al., 1996). Meanwhile, HgS(s)

formation is generally desired over adsorption in terms of mercury mobility (Bower, 2007). Hyland et al. (1990) used ligands of differing Hg(II) complexing strength to desorb Hg(II) from Hg-sorbed Fe_{1-x}S and found that the sorbed Hg species are more readily desorbed than the coprecipitated crystalline phase (Fe-HgS phase substituted with Fe). The most weakly sorbed Hg is desorbed by Cl^- and SO_3^{2-} , more strongly bound Hg is removed by $\text{S}_2\text{O}_3^{2-}$, and CN^- removes all sorbed Hg. However, Jeong (2005) found that neither adsorbed nor coprecipitated Hg was readily desorbed from synthesized mackinawite, FeS(s) , by strong mercury complexing ligands such as EDTA and cyanide. The maximum mercury desorption was only $(3.8 \pm 0.1)\%$ by 0.1M Na_4EDTA solution and $(7.5 \pm 0.2)\%$ by 0.1 M NaCN solution.

It has been reported that the solubility of HgS(s) can be increased in the presence of high dissolved sulfide concentrations or zero-valent sulfur (S^0). Paquette and Helz (1997) found that HgS solubility is increased by S^0 through formation of bidentate polysulfide ligands and additional Hg solubility in S^0 saturated solutions up to pH 9.5 can be explained by: $\text{HgS (cinnabar)} + \text{SH}^- + (n-1)\text{S}^0(\text{rhomb}) = \text{Hg(S}_n\text{)SH}^-$, $\text{p}K = 3.97 \pm 0.17$. Jay et al. (2000) quantified a large increase in the solubility of cinnabar (HgS(s)) in the presence of elemental sulfur, particularly at high pH, and mercury complexes such as $\text{Hg(S}_x\text{)}_2^{2-}$, HgS_5 , and HgS_xOH^- were proposed to account the increase HgS(s) solubility. Although S^0 could be produced by FeS(s) oxidation (Lowson, 1982) and to increase HgS(s) solubility, no increase of mercury concentration in aqueous phase was observed in this study as the FeS(s) doses increased.

5.3.3 Mobility of stabilized FeS(s) nanoparticles in a sediment column

For *in-situ* application purpose, the FeS(s) nanoparticles are expected to be highly mobile and be able to pass through subsurface soil or sediment to ensure delivery to the targeted locations. The stabilized FeS(s) nanoparticles (FeS(s) = 0.5 g/L, CMC = 0.2%) were tested for their mobility in a clay loam sediment column. Total iron concentration in column effluent was analyzed in this experiment to indicate the breakthrough history of FeS(s) nanoparticles. Column tests showed that stabilized FeS(s) nanoparticles were highly mobile in a clay loam sediment and full breakthrough of 0.5 g/L FeS(s) nanoparticles occurred at 18.4 pore volumes (PV's) while the non-stabilized FeS(s) particles were separated at the top of the sediment bed (data not shown). As shown in **Figure 5-5**, the breakthrough of a tracer (KBr) happened at 3.4 PV's and relatively stable ($C/C_0 > 0.99$) iron concentrations were measured in the effluent after 18.4 PV's. By contrast, only ~0.3% of total iron was detected in the effluent when 18 PV's of the non-stabilized FeS(s) particles were applied (data not shown). Based on the breakthrough curve of 0.5 g/L stabilized FeS(s) nanoparticles, 32.5% of FeS(s) nanoparticles were lost to the sediment in the first 18.4 PV's of influent. The loss of stabilized FeS(s) nanoparticles is attributed to the adsorption or/and precipitation of FeS(s) nanoparticles to the sediment.

Clearly, the breakthrough history of the stabilized FeS(s) nanoparticles proved that they are highly mobile in the sediment and can be injected directly to the contaminated subsurface sediment/soil or groundwater. Meanwhile, the loss of FeS(s) nanoparticles to the sediment suggested that the transport of FeS(s) nanoparticles would be limited in a certain distance; the maximum distance that the stabilized FeS(s)

nanoparticles transport could be calculated under some dimensional assumptions, such as the depth and width of the transport zone. This unique mobility of FeS(s) nanoparticles helps to address the potential concern of the nanoparticles transport to biota or human body and the resulting toxicology of nanoparticles, which is attracting more and more attention recently (Wiesner et al., 2006).

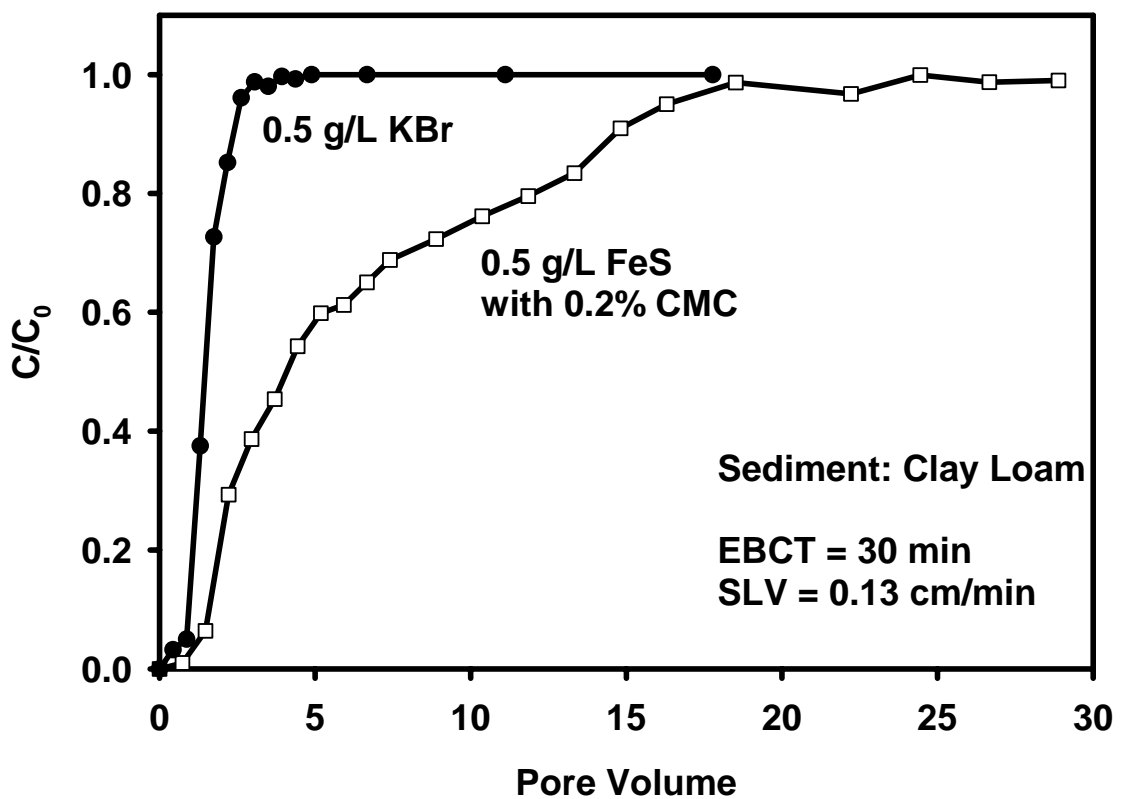


Figure 5-5. The breakthrough curves of a tracer (KBr) and FeS(s) nanoparticles in a clay loam sediment column. The initial KBr concentration was 0.05 g/L and the initial stabilized FeS(s) nanoparticles concentration was 0.5 g/L stabilized with 0.2% CMC. The Empty Bed Contact Time (EBCT) = 30 min and Superficial Liquid Velocity (SLV) = 0.13 cm/min.

5.3.4 Immobilization of mercury by stabilized FeS(s) nanoparticles: column tests

Mercury immobilization column tests were also conducted to simulate the *in-situ* application of the stabilized FeS(s) nanoparticles for mercury immobilization in Hg-laden sediments. Two different Hg-laden sediments were used, i.e. low-Hg (177.2 mg/kg) and high-Hg (3119.9 mg/kg) content sediment (**Table 5-1**). 0.5 g/L FeS(s) nanoparticles stabilized with 0.2% CMC were used to immobilize Hg in the sediment, while a solution containing 0.2% CMC and 0.1 M NaNO₃ was used as the influent in control tests.

Figure 5-6 and **Figure 5-7** show mercury washed off from a low-Hg and a high-Hg content clay loam sediment, respectively, by an influent with or without the presence of stabilized FeS(s) nanoparticles. In all cases, there is a similar mercury concentration profile, i.e. a Hg concentration peak in the effluent during the first 10-22 PV's followed by a relative stable trail. The Hg concentration in the effluent kept decreasing until it reached a relative constant value. In the control tests, Hg concentration remained around 58 µg/L after 110 PV's in **Figure 5-6** when a low-Hg content sediment was used, while Hg concentration reached a constant 6.2 mg/L after 45 PV's in **Figure 5-7** when a high-Hg content sediment was used. By comparing the mercury in 67 PV's of effluent to the total mercury content of the sediment, it was calculated that 3.8% and 14.7%, respectively, of total mercury was washed off from a low-Hg and a high-Hg content sediment in the control tests.

In the sediment, mercury was either attached to the binding sites, such as Fe/Mn oxide, amorphous organosulfur, or mineral lattice (Zhong and Wang, 2006), or dissolved in the pore water in the form of Hg(OH)₂⁰(aq), Hg(OH)₃⁻, Hg⁰ (aq) (Hamilton and Bowers, 1997). When the sediment was flushed with CMC solutions (control tests) or

FeS(s) nanoparticles suspensions (treatment tests), the dissolved mercury species in the pore water were firstly pushed out. Then the mercury species that attached to the weak binding sites such as Fe/Mn oxide, carboxyl and phenol functional groups (Drexel et al., 2002) were washed off and followed by the mercury species that are attached to the strong binding site such as thiol (R-SH), disulfide (R-SS-R), and disulfane (R-SSH) functional groups (Skylberg et al., 2006; Xia et al., 1999). These different mercury species in sediment/soil helped explain the mercury concentration peaks in the effluent in the beginning stage when the dissolved and/or weakly bonded Hg species were released.

The reason why it took more time for the effluent Hg concentration to reach a stable level for a low-Hg content sediment (110 PV's) than for a high-Hg content sediment (45 PV's) could be that mercury has been attached more strongly in the low-Hg content sediment than in the one with high-Hg content. When Hg-laden sediment was prepared, Hg was attached to binding sites in the sediment, such as thiol (R-SH), disulfide (R-SS-R), and disulfane (R-SSH) functional groups (Skylberg et al., 2006; Xia et al., 1999). For the same sediment, a low-Hg content means a greater binding site to Hg ratio, which results in stronger mercury adsorption. Consequently, Hg was more difficult to wash off from the low-Hg sediment than from the high-Hg sediment. This also explained why the percentage (14.7%) of total mercury washed off from the high-Hg sediment was more than 3 times greater than that (3.8%) from the low-Hg content sediment.

When the stabilized FeS(s) nanoparticles suspension was used as an influent, the Hg concentration peak heights were decreased and Hg concentrations in the effluent were reduced significantly. With stabilized FeS(s) nanoparticles, the highest Hg concentration in the effluent decreased by 11% and 35%, respectively, for the low-Hg and the high-Hg

content sediment compared to that in control tests. The mercury concentration in the effluent dropped to less than 5 ppb after 110 PV's in **Figure 5-6** and to less than 3 $\mu\text{g/L}$ after 33 PV's in **Figure 5-7**, a 91% and 99% decrease compared to that in the control tests, respectively. Based on the mercury content of the sediment, it was calculated that only 2.0% and 4.9%, respectively, of total mercury in the sediment was washed off from a low-Hg content sediment and a high-Hg content sediment, which was 46.4% and 66.6%, respectively, less than that in the control tests. In another word, 46.4% and 66.6%, respectively, of leachable Hg was immobilized by the stabilized FeS(s) nanoparticles in low-Hg and high-Hg content sediment. Evidently, the stabilized FeS(s) nanoparticles efficiently immobilized mercury in sediment.

The sediments that were treated with the stabilized FeS(s) nanoparticles and those from control tests were air-dried and further studied in TCLP tests. **Figure 5-8** compared the extracted Hg concentrations in TCLP solutions from the sediment with and without treatment of stabilized FeS(s) nanoparticles. As shown in **Figure 5-8**, the extracted Hg concentration from the low-Hg and high-Hg content sediment that was treated with 0.5 g/L stabilized FeS(s) nanoparticles was only 25.3% and 23.1%, respectively, of that from the sediment that was washed in control tests. Meanwhile, the extracted Hg concentration (10.3 $\mu\text{g/L}$) in the TCLP solution from the low-Hg content sediment treated with stabilized FeS(s) nanoparticles was much less than the regulated TCLP limit (200 $\mu\text{g/L}$). However, the extracted Hg concentration (820.6 $\mu\text{g/L}$) in the TCLP solution from the high-Hg content sediment was 4 times greater than the standard even it was treated with 67 PV's of 0.5 g/L stabilized FeS(s) nanoparticles. This result suggested that the high-Hg

content sediment need to be treated with more than 30 BV's of 0.5 g/L stabilized FeS(s) nanoparticles in order to satisfy TCLP standard.

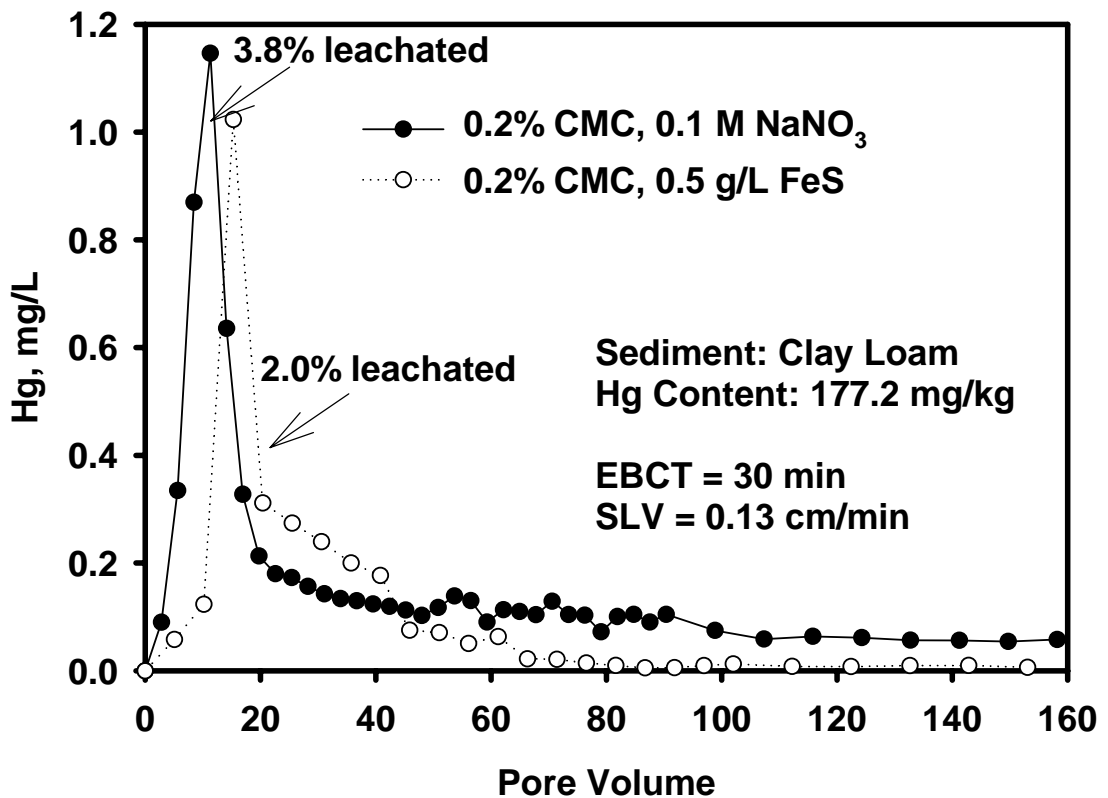


Figure 5-6. Mercury leached from a low-Hg content clay loam sediment by an influent with or without the presence of the stabilized FeS(s) nanoparticles. 0.5 g/L FeS(s) nanoparticles stabilized with 0.2% CMC were used to treat the sediment. A solution containing 0.2% CMC and 0.1 M NaNO₃ was used as a control. EBCT = 30 min and SLV = 0.13 cm/min.

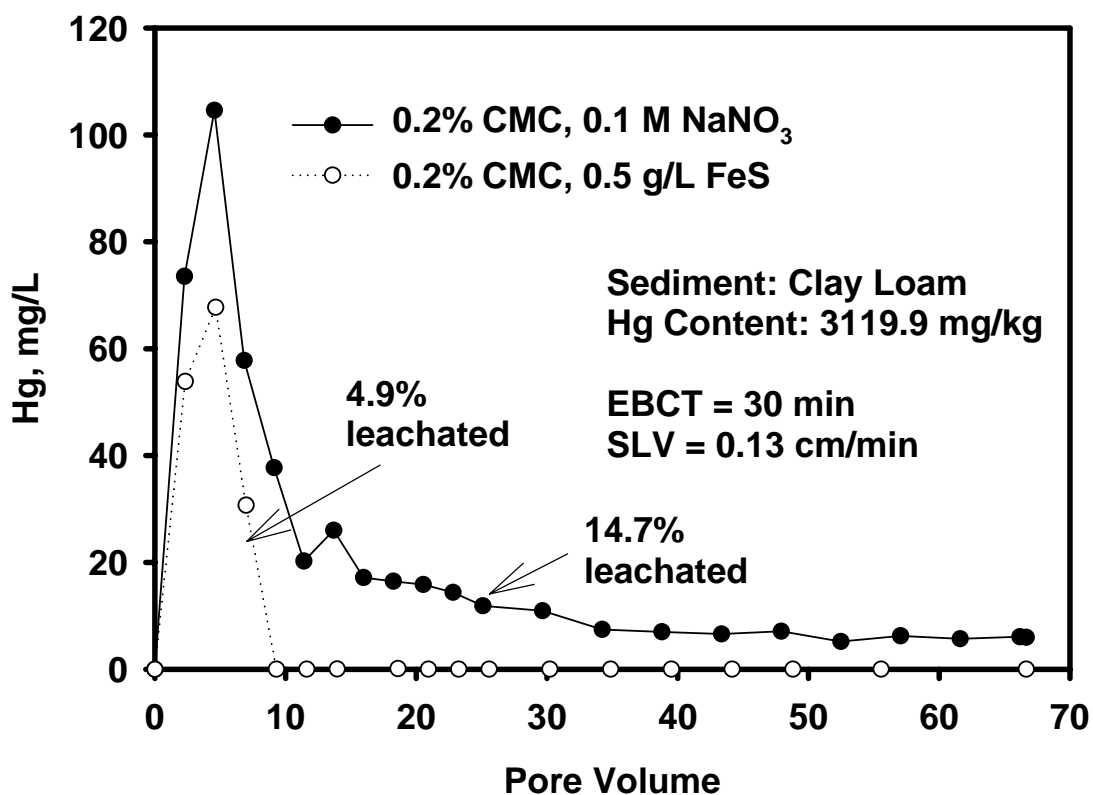


Figure 5-7. Mercury leached from a high-Hg content clay loam sediment by an influent with or without the presence of the stabilized FeS(s) nanoparticles. 0.5 g/L FeS(s) nanoparticles stabilized with 0.2% CMC were used to treat the sediment. A solution containing 0.2% CMC and 0.1 M NaNO₃ was used as a control. EBCT = 30 min and SLV = 0.13 cm/min.

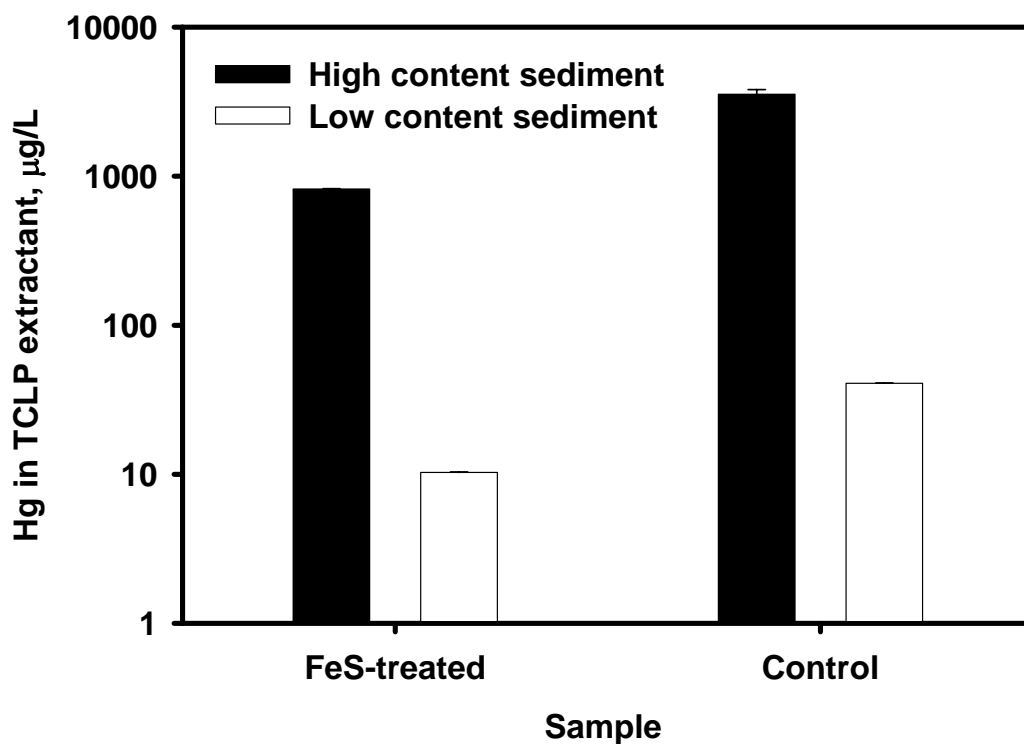


Figure 5-8. Mercury concentration in the TCLP extractant from a low-Hg and a high-Hg content clay loam sediments that was treated with the stabilized FeS(s) nanoparticles or from the control tests. TCLP fluid #1 was used as the extractant and the reaction time was 18 hours. Data plotted as mean of duplicates.

5.3.5 Implication to in-situ mercury remediation

This study has shown that the stabilized FeS(s) nanoparticles are very effective to immobilize mercury in the sediment and are highly mobile in sediment. Meanwhile, chemical cost for the stabilized FeS(s) nanoparticles is only \$10 per pound. These results indicate that the stabilized FeS(s) nanoparticles can be used as an effective and low-cost *in-situ* mercury immobilization technology. Since mercury methylation can be inhibited by reducing the availability of Hg (II) (Benoit et al., 2001; Drott et al., 2007), MeHg production may be decreased when the stabilized FeS(s) nanoparticles are applied to Hg-laden sediment. At the same time, the replaced Fe(II) in Eq. (5-3) can also inhibit mercury methylation by decreasing the activity of S^{2-} through the formation of FeS(s) (Mehrotra et al., 2003). Mehrotra and Sadlak (2005) reported that mercury methylation rates decrease was accomplished with iron amendment (25-30 mM). On the other hand, FeS(s) nanoparticles may be oxidized to zero-valent sulfur, which was found to increase the solubility of cinnabar (HgS(s)) (Jay et al., 2000; Paquette and Helz, 1997) and then boost mercury methylation. The effect of FeS(s) nanoparticles on mercury methylation is the focus of ongoing research.

5.4 Summary and Conclusion

An innovative *in-situ* mercury (Hg) immobilization technology using stabilized iron sulfide (FeS(s)) nanoparticles was investigated in this study through a series of batch and column experiments. The FeS(s) nanoparticles were successfully prepared using a low-cost and food-grade cellulose (CMC) as the stabilizer. The particle size of freshly prepared FeS(s) nanoparticles was measured to be 38.5 nm with a deviation of 5.4 nm.

Batch tests showed that the stabilized FeS(s) nanoparticles effectively immobilized Hg in the sediment. When the Hg-laden sediment was treated by stabilized FeS(s) nanoparticles with a FeS(s)/Hg molar ratio of 26.5, the Hg concentration leached out in the aqueous phase was reduced by 96.8% and TCLP tests showed that Hg leachability was reduced by 99.1%. Column tests proved that the stabilized FeS(s) nanoparticles reduced mercury leachability of Hg-laden sediment by as much as 66.7% and the extracted Hg in TCLP solutions was reduced by 76.9% when the sediments was treated with 0.5 g/L stabilized FeS(s) nanoparticles. Column tests also proved that stabilized FeS(s) nanoparticles were highly mobile in a clay loam sediment and ~100% of FeS(s) nanoparticles passed through the sediment with 18.4 PV's of 0.5 g/L stabilized FeS(s) nanoparticles.

CHAPTER 6. CONCLUSIONS AND SUGGESTIONS FOR FUTURE RESEARCH

6.1 Summary and Conclusions

Perchlorate is a widespread contaminant that has been detected in surface water, groundwater, and drinking water. This research compares representative standard strong-base anion (SBA) and weak-base anion (WBA) exchangers, a bifunctional resin (A-530E), a class of polymeric ligand exchangers (PLE's), and an ion-exchange fiber (IXF) with respect to perchlorate sorption capacity, kinetics, and regenerability. While A-530E offered the greatest perchlorate capacity and selectivity, practically acceptable capacity was also observed for other styrenic SBA and WBA resins, PLE's, and IXF. Fixed-bed column runs showed that 12,388 bed volumes of perchlorate-free water can be obtained when DOW 3N-Cu, a PLE resin, was used to treat a simulated contaminated water containing 200 $\mu\text{g/L}$ perchlorate. In contrast, polyacrylic resins offered much lower perchlorate capacity. The greater capacity of styrenic resins is attributed to enhanced ion-pairing and Lewis acid-base interactions owing to the hydrophobic nature of polystyrene matrices and low hydration energy of perchlorate. Conversely, regeneration of polyacrylic resins was much more efficient, and A-530E was the least regenerable. IXF offered comparable perchlorate capacity to that of styrenic resins, yet, unparalleled kinetics (with a sorption equilibrium time of <1.5 hours), and much greater regeneration efficiency.

Although perchlorate can be effectively removed from contaminated water with IX materials, perchlorate will be concentrated in a small volume of IX regeneration brine after the exhausted IX materials are regenerated. And this IX byproduct with high level of perchlorate and salt needs further disposal. This research tested the feasibility of using a new class of stabilized ZVI nanoparticles for complete destruction of perchlorate in both fresh water or IX regeneration brine. Highly reactive stabilized ZVI nanoparticles were prepared using a low-cost and food-grade carboxymethyl cellulose (CMC) as the stabilizer and were used for perchlorate reduction. Batch kinetic tests showed that at a ZVI dose of 1.8 g/L and at moderately elevated temperatures (90-95 °C), ~90% of perchlorate in both fresh water and a simulated IX regeneration brine (NaCl=6% (w/w)) was destroyed within 7 hours. An activation energy (E_a) of 52.59±8.41 kJ/mol was determined for the reaction. Kinetic tests suggested that Cl(VII) in perchlorate was rapidly reduced to chloride without accumulation of any intermediate products. Based on the surface-area normalized rate constant k_{SA} , starch- and CMC-stabilized ZVI nanoparticles degraded perchlorate 1.8 and 3.3 times, respectively, faster than non-stabilized ZVI particles did. Addition of a metal catalyst (Co, Cu, Ni, Pd, or Re) did not show any reaction improvement. This technology provides an effective method for complete destruction of perchlorate in both contaminated water and brines.

The stabilized ZVI nanoparticles were also tested for reductive transformation of nitrate in both fresh water and ion-exchange regeneration brine. Batch kinetic tests showed that the observed pseudo first-order rate constant (k_{obs}) for nitrate reduction with the stabilized ZVI nanoparticles was more than 5 times greater than that for non-stabilized ZVI particles. The surface-area normalized rate constant (k_{SA}) indicated that a

stabilizer not only increased the surface area of the nanoparticles, but also resulted in more reactive particle surface. The molar ratio between the two nitrate reduction final products, NH_4^+ and N_2 , can be manipulated by varying the ZVI dose (or ZVI-to-nitrate molar ratio) and/or applying a metal catalyst. With a ZVI-to- NO_3^- molar ratio of 2.5, N_2 -N accounted for two thirds (66%) of the nitrate reduction products, 30% greater than that with a ZVI-to- NO_3^- molar ratio of 3.9. And the bimetallic catalysts Cu-Pd at Cu = 0.4% and Pd = 0.1% of Fe or Pd-Cu at Pd = 0.4% and Cu = 0.1% of Fe reduced the ammonium fraction by 8% and 7%, respectively, compared to that without a catalyst. The greater CMC-to-ZVI ratio leads to the faster nitrate reduction rate by stabilized ZVI nanoparticles and the k_{obs} value at a CMC-to-ZVI molar ratio of 0.0056 is 8.1 times greater than that without CMC. The nitrate reduction efficiency was strongly pH dependent and application of a 0.05 M HEPES buffer solution (pH 7.0~7.5) increased the k_{obs} value by 15 times compared to that without pH adjustment. The presence of 6% of NaCl decreased k_{obs} by 30% than that in fresh water. However, 100% nitrate was removed within 2 hours in the saline water, indicating that this technology can be used to treat nitrate in both fresh water and saline water such as IX regeneration brine.

An innovative *in-situ* mercury (Hg) immobilization technology using stabilized iron sulfide (FeS(s)) nanoparticles was investigated in this study through a series of batch and column experiments. The FeS(s) nanoparticles were successfully prepared using a low-cost and food-grade cellulose (CMC) as the stabilizer. The particle size of freshly prepared FeS(s) nanoparticles was measured to be 38.5 nm with a deviation of 5.4 nm. Batch tests showed that the stabilized FeS(s) nanoparticles effectively immobilized Hg in the sediment. When the Hg-laden sediment was treated by stabilized FeS(s) nanoparticles

with a FeS(s)/Hg molar ratio of 26.5, the Hg concentration leached out in the aqueous phase was reduced by 96.8% and the TCLP tests showed that the Hg leachability was reduced by 99.1%. Column tests proved that the stabilized FeS(s) nanoparticles reduced the mercury leachability of the Hg-laden sediment by as much as 66.7% and the extracted Hg in TCLP solutions was reduced by 76.9% when the sediments was treated with 0.5 g/L stabilized FeS(s) nanoparticles. Column tests also proved that stabilized FeS(s) nanoparticles were highly mobile in a clay loam sediment and ~100% of FeS(s) nanoparticles passed through the sediment with 18.4 PV's of 0.5 g/L stabilized FeS(s) nanoparticles.

6.2 Suggestions for Future Work

The specific recommendations for future work were made as follows:

1. Metal catalysts such as Rhenium have been well recognized to be able to catalyze perchlorate reduction through an oxygen transfer reaction (Cai and Espenson, 2005; Abu-Omar et al., 2000; 2006), but all the metal catalysts tested in this study did not help perchlorate reduction by ZVI nanoparticles. Further effort is suggested to search for a catalyst that can catalyze perchlorate reduction by ZVI nanoparticles.
2. Catalyst for nitrate reduction pathway control is another interesting research area. Between the two final nitrate reduction products, N_2 (g) and NH_4^+ , N_2 (g) is a more desirable final product. It was found in this research that the bimetallic catalysts Cu-Pd at Cu = 0.4% and Pd = 0.1% of Fe or Pd-Cu at Pd = 0.4% and Cu = 0.1% of Fe reduced the ammonium fraction by 8% and 7%, respectively,

compared to that without a catalyst. It is interesting to find other catalysts that can better control nitrate reduction pathways in the favor of formation $N_2(g)$.

3. Mercury methylation is of major environmental concern because methylmercury is the most toxic mercury species. Since mercury has been found to be effectively immobilized in sediment with the treatment of FeS(s) nanoparticles. It is of interest to see how effective FeS(s) nanoparticles are to inhibit mercury methylation. Biological Hg methylation with and without the presence of FeS(s) nanoparticles can be monitored and compared in batch and column configurations.
4. X-ray diffraction (XRD), x-ray photoelectron spectroscopy (XPS), and extended x-ray absorption fine structure (EXAFS) tests on FeS(s) nanoparticles before or after reaction with Hg can be carried out to provide more evidence to elucidate mercury immobilization mechanisms.
5. Environmental fate and impacts of ZVI and FeS(s) nanoparticles is another interesting research area. The ultimate fate of spent nanoparticles as well as the capping agents, the impact of the nanoparticles to the soil/sediment chemistry (pH, ORP, and DO) and to the subsurface microbial community when injected in soil, and the secondary contamination such as accumulation of toxic by-products and/or dissolution of other contaminants are interesting research topics that require future work.

REFERENCES

- Abu-Omar, M.M., McPherson, L.D., Arias, J., Bereau, V.M., 2000. Clean and efficient catalytic reduction of perchlorate. *Angewandte Chemie*. 39 (23), 4310-4313.
- Abu-Omar, M.M., 2006. Metal mediated perchlorate reduction. Preprints of extended abstracts presented at the ACS National Meeting, American Chemical Society, Division of Environmental Chemistry. 46 (2), 413-415.
- Agency for Toxic Substances and Disease Registry (ATSDR), 1992. Toxicological profile for styrene. U.S. Public Health Service, U.S. Department of Health and Human Services, Atlanta, GA.
- Alkorta, I., Hernandez-Allica, J., Becerril, J.M., Amezaga, I., Albizu, I., Garbisu, C., 2004. Recent findings on the phytoremediation of soils contaminated with environmentally toxic heavy metals and metalloids such as zinc, cadmium, lead, and arsenic. *Reviews in Environmental Science and Bio/Technology*, 3 (1), 71-90.
- Alowitz, M.J., Scherer, M.M., 2002. Kinetics of nitrate, nitrite, and Cr(VI) reduction by iron metal. *Environ. Sci. Technol.* 36 (3), 299-306.
- An, B., Steinwinder, T.R., Zhao, D., 2005. Selective removal of arsenate from drinking water using a polymeric ligand exchanger. *Water Res.* 39 (20), 4993-5004.
- Bao, H.M., Gu, B., 2004. Natural perchlorate has a unique oxygen isotope signature. *Environ. Sci. Technol.* 38 (19), 5073-5077.

- Barnett, M.O., Harris, L.A., Turner, R.R., Stevenson, R.J., Henson, T.J., Melton, R.C., Hoffman, D.P., 1997. Formation of mercuric sulfide in soil. *Environ. Sci. Technol.* 31 (11), 3037-3043.
- Barnett, M.O., 1998. Formation and stability of mercuric sulfide in subsurface environments. Ph.D. dissertation. Department of Environmental Sciences and Engineering, University of North Carolina, Chapel Hill, North Carolina, U.S.A.
- Barnett, M.O., Turner, R.R., Singer, P.C., 2001. Oxidative dissolution of metacinnabar (b-HgS) by dissolved oxygen. *Appl. Geochem.* 16 (13), 1499-1512.
- Barron, R.E., Fritz, J.S., 1984. Effect of functional group structure on the selectivity of low-capacity anion exchangers for monovalent anions. *J. Chromatography.* 284 (1), 13-20.
- Batista, J.R., McGarvey, F.X., Viera, A.R., 2000. The removal of perchlorate from waters using ion-exchange resins. In: *Perchlorate in the Environment*. Urbansky, E.T. Kluwer Academic/Plenum Publishers: New York. 135-146.
- Behra, P., Bonnissel-Gissinger, P., Alnot, M., Revel, R., Ehrhardt, J.J., 2001. XPS and XAS study of the sorption of Hg(II) onto pyrite. *Environ. Sci. Technol.* 17 (13), 3970-3979.
- Benner, S.G., Blowes, D.W., Gould, W.D., 1999. Geochemistry of a permeable reactive barrier for metals and acid mine drainage. *Environ. Sci. Technol.* 33 (16), 2793-2799.
- Benoit, J.M., Gilmour, C.C., Mason, R.P., 2001. The influence of sulfide on solid-phase mercury bioavailability for methylation by pure cultures of *Desulfobulbus propionicus* (1pr3). *Environ. Sci. Technol.* 35 (1), 127-132.

- Biester, H., Scholz, C., 1997. Determination of mercury binding forms in contaminated soils: Mercury pyrolysis versus sequential extractions. *Environ. Sci. Technol.* 31 (1), 233-239.
- Biester, H., Gosar, M., Covelli, S., 2000. Mercury speciation in sediments affected by dumped mining residues in the drainage area of the Idrija mercury mine, Slovenia. *Environ. Sci. Technol.* 34 (16), 3330-3336.
- Blount, B.C., Pirkle, J.L., Osterloh, J.D., Valentin-Blasini, L., Caldwell, K.L., 2006. Urinary perchlorate and thyroid hormone levels in adolescent and adult men and women living in the United States. *Environ. Health Perspect.* 114 (12), 1865-1871.
- Bonnesen, P.V., Brown, G.M., Alexandratos, S.D., Bavoux, L.B., Preseley, D.J., Patel, V., Ober, R., Moyer, B.A., 2000. Development of novel bifunctional anion-exchange resins with improved selectivity and sorptive kinetics for pertechnetate: Batch-equilibrium experiments. *Environ. Sci. Technol.* 34 (17), 3761-3766.
- Bower, J.M., 2007. Immobilization of mercury using iron sulfide minerals. M.S. Thesis, Department of Civil Engineering, Auburn University, Auburn, AL.
- Brown, J.R., Bancroft, G.M., Fyee, W.S., Mclean, R., 1979. Mercury removal from water by iron sulfide minerals – Electron-spectroscopy for chemical analysis (ESCA) study. *Environ. Sci. Technol.* 13 (9), 1142-1144.
- Brown, G.M., Bonnesen, P.V., Moyer, B.A., Gu, B., Alexandratos, S.D., Patel, V., Ober, R., 2000. Efficient treatment of perchlorate(ClO_4^-)-contaminated groundwater with bifunctional anion exchange resins. In: *Perchlorate in the Environment*. Urbansky, E.T. Kluwer Academic/Plenum Publishers: New York. 155-164.

- Cai, Y., Espenson, J.H., 2005. Catalysis by methyltrioxorhenium(VII): Reduction of hydronium ions by europium(II) and reduction of perchlorate ions by europium(II) and chromium(II). *Inorg. Chem.* 44 (3), 489-495.
- Cang, Y., Roberts, D.J., Clifford, D.A., 2004. Development of cultures capable of reducing perchlorate and nitrate in high salt solutions. *Water Res.* 38 (14-15), 3322-3330.
- Cao, J., Elliott, D., Zhang, W.X., 2005. Perchlorate reduction by nanoscale iron particles. *J. Nanopart. Res.* 7 (4-5), 499-506.
- Chadha, A., Sharma, R.K., Stinespring, C.D., Dadyburjor, D.B., 1996. Iron, sulfide catalysts for coal liquefaction prepared using a micellar technique. *Ind. Eng. Chem. Res.* 35 (9), 2916-2919.
- Charles, M., 2002. Historical background of mercury in the environment. Presentation at the mercury forum in Mobile on May 20-21, 2002. http://www.masgc.org/mercury/ppt/Moore-ppt_files/frame.htm. (accessed September 2005).
- Chen, X.Y., Zhang, Y., Chen, G.H., 2003. Appropriate conditions or maximizing catalytic reduction efficiency of nitrate into nitrogen gas in groundwater. *Water Res.* 37, 2489-2495.
- Chen, S.-S., Hsu, H.-D., Li, C.-W., 2004. A new method to produce nanoscale iron for nitrate removal. *J. Nanoparticle Res.* 6 (6), 639-647.
- Chen, W., Cannon, F.S., Rangel-Mendez, J.R., 2005. Ammonia-tailoring of GAC to enhance perchlorate removal. II: Perchlorate adsorption. *Carbon.* 43 (3), 581-590.
- Cheng, I.F., Muftikian, R., Fernando, Q., Korte, N., 1997. Reduction of nitrate to ammonia by zero-valent iron. *Chemosphere.* 35 (11), 2689-2695.

- Chin, P.P., Ding, J., Yi, J.B., Liu, B.H., 2005. Synthesis of FeS₂ and FeS nanoparticles by high-energy mechanical milling and mechanochemical processing. *J. Alloys Compd.* 390 (1-2), 255-260.
- Choe, S., Chang, Y.-Y., Hwang, K.-Y., Khim, J., 2000. Kinetics of reductive denitrification by nanoscale zero-valent iron. *Chemosphere.* 41 (8), 1307-1311.
- Chu, B., Whitney, D.C., Diamond, R.M., 1962. On anion-exchange resin selectivities. *J. Inorg. Nucl. Chem.* 24, 1405-1415.
- Clesceri, L.S., Greenberg, A.E., Eaton, A.D., 1998. Standard methods for the examination of water and wastewater, 20th ed. American Public Health Association, Washington, D.C., U.S.
- Clifford, D., Weber, W.J. Jr., 1983. The determinants of divalent/monovalent selectivity in anion exchangers. *Reactive Polymers, Ion Exchangers, Sorbents.* 1 (2), 77-89.
- Clifford, D.A., Liu, X., 1993a. Ion exchange for nitrate removal. *J. AWWA.* 85 (4), 135-143.
- Clifford, D.A., Liu, X., 1993b. Biological denitrification of spent regenerant brine using a sequencing batch reactor. *Water Res.* 27 (9), 1477-1484.
- Clifford, D.A., 1999. Ion exchange and inorganic adsorption, Chapter Nine in *Water Quality and Treatment Fifth Edition*, Ray Letterman, McGraw Hill, Inc., New York.
- Cox, J.L., Hallen, R.T., Lllga, M.A., 1994. Thermochemical nitrate destruction. *Environ. Sci. Technol.* 28 (3), 423-428.
- Crank, J., 1975. *The mathematics of diffusion* (second ed). Clarendon Press: Oxford, UK.

- Czarra, F., 2003. Fresh water: Enough for you and me?. *The American Forum For Global Education*. 174, 1-15.
- Dasgupta, P.K., Martinelango, P.K., Jackson, W.A., Anderson, T.A., Tian, K., Tock, R.W., Rajagopalan, S., 2005. The origin of naturally occurring perchlorate: The role of atmospheric processes. *Environ. Sci. Technol.* 39 (6), 1569-1575.
- Dasgupta, P.K., Dyke, J.V., Kirk, A.B., Jackson, W.A., 2006. Perchlorate in the United States: Analysis of relative source contribution to the food chain. *Environ. Sci. Technol.* 40 (21), 6608-6614.
- Dillo, M.S., Falconer, K., Johnson, J.H. Jr., Goddard, W.A. III, 2007. Dendritic anion hosts: Perchlorate uptake by G5-NH₂ poly(propyleneimine) dendrimer in water and model electrolyte solutions. *Environ. Sci. Technol.* 41 (18), 6521-6527.
- Diamond, R.M., 1963. The aqueous solution behavior of large univalent ions. A new type of ion pairing. *J. Phys. Chem.* 67 (12), 2513-2516.
- Drexel, R.T., Haitzer, M., Ryan, J.N., Aiken, G.R., Nagy, K.L., 2002. Mercury(II) sorption to two Florida everglades peats: Evidence for strong and weak binding and competition by dissolved organic matter released from the peat. *Environ. Sci. Technol.* 36 (19), 4058-4064.
- Driscoll, C.T., Yan, C., Scheffeld, C.L., Munson, R., Holsapple, J., 1994. The mercury cycle and fish in the Adirondack Lakes. *Environ. Sci. Technol.* 28 (3), A136-A143.
- Drott, A., Lambertsson, L., Bjorn, E., Skyllberg, U., 2007. Importance of dissolved neutral mercury sulfides for methyl mercury production in contaminated sediments. *Environ. Sci. Technol.* 41 (7), 2270-2276.

- Ellington, J.J., Wolfe, N.L., Garrison, A.W., Evans, J.J., Avants, J.K., Teng, Q., 2001. Analysis of perchlorate in tobacco plants and tobacco products. *Environ Sci. Technol.* 35 (15), 3213-3218.
- Fan, A.M., Steinberg, V.E., 1996. Health implications of nitrate and nitrite in drinking water: An update on methemoglobinemia occurrence and reproductive and developmental toxicity. *Regul. Toxicol. Pharmacol.* 23 (1), 35-43.
- Gingras, T.M., Batista, J.R., 2002. Biological reduction of perchlorate in ion exchange regenerant solutions containing high salinity and ammonium levels. *J. Environ. Monit.* 4 (1), 96-102.
- Glass, C., Silverstein, J., 1999. Denitrification of high-nitrate, high-salinity wastewater. *Water Res.* 33 (1), 223-229.
- Glavce, G.N., Klabunde, K.J., Sorensen, C.M., Hadjipanayis, G.C., 1995. Chemistry of borohydride reduction of iron(II) and iron(III) ions in aqueous and nonaqueous media. Formation of nanoscale Fe, FeB, and Fe₂B powders. *Inorg. Chem.* 34, 28-35.
- Gotpagar, J., Lyuksyutov, S., Cohn, R., Grulke, E., Bhattacharyya, D., 1999. Reductive dehalogenation of trichloroethylene with zero-valent iron: Surface profiling microscopy and reagent enhancement studies. *Langmuir.* 15, 8412-8420.
- Greer, M.A., Goodman, G., Pleus, R.C., Greer, S.E., 2002. Health effects assessment for environmental perchlorate contamination: The dose response for inhibition of thyroidal radioiodine uptake in humans. *Environ. Health Persp.* 110 (9), 927-937.

- Grittini, G., Malcomson, M., Fernando, Q., Korte, N., 1995. Rapid dechlorination of polychlorinated biphenyls on the surface of a Pd/Fe bimetallic system. *Environ. Sci. Technol.* 29 (11), 2898-2900.
- Gu, B., Phelps, T.J., Liang, L., 1999. Biogeochemical dynamics in zero-valent iron columns: implications for permeable reactive barriers. *Environ. Sci. Technol.* 33 (13), 2170-2177.
- Gu, B., Brown, G.M., Spiro, D.A., Robert, O., James, A.D., Steven, P., 2000. Efficient treatment of perchlorate(ClO_4^-)-contaminated groundwater with bifunctional anion exchange resins. In: *Perchlorate in the Environment*. Urbansky, E.T. Kluwer Academic/Plenum Publishers: New York. 165-176.
- Gu, B., Brown, G.M., Maya, L., Lance, M.J., Moyer, B.A., 2001. Regeneration of perchlorate (ClO_4^-)-loaded anion exchange resins by a novel tetrachloroferrate (FeCl_4^-) displacement technique. *Environ. Sci. Technol.* 35 (16), 3363-3368.
- Gu, B., Dong, W., Brown, G.M., Cole, D.R., 2003. Complete degradation of perchlorate in ferric chloride and hydrochloric acid under controlled temperature and pressure. *Environ. Sci. Technol.* 37 (10), 2291-2295.
- Gu, B., Ku, Y-K., Brown, G.M., 2005. Sorption and desorption of perchlorate and U(VI) by strong-base anion-exchange resins. *Environ. Sci. Technol.* 39 (3), 901-907.
- Gu, B., Brown, G.M., 2006. Recent advances in ion exchange for perchlorate treatment, recovery and destruction. In: *Perchlorate, Environmental Occurrence, Interactions and Treatment*. Gu, B., Coats, J.D. Springer Science+Business Media, Inc. New York. 209-249.

- Gu, B., Bonnesen, G.P., Sloop, F.V., Brown, G.M., 2006. Titanium catalyzed perchlorate reduction and applications. In: Perchlorate, Environmental Occurrence, Interactions and Treatment. Gu, B., Coats, J.D. Springer Science+Business Media, Inc. New York. 373-386.
- Gu, B., Brown, G.M., Chiang, C.-C., 2007. Treatment of perchlorate-contaminated groundwater using highly selective, regenerable ion-exchange technologies. Environ. Sci. Technol. 41 (17), 6277-6282.
- Gurol, M.D., Kim, K., 2000. Investigation of perchlorate removal in drinking water sources by chemical methods. In: Perchlorate in the environment. Urbansky, E.T., Kluwer Academic/Plenum Publishers. New York. 99-108.
- Ha, J-K., Cho, K-K., Kim, K-W., Kim, J-U., Kim, Y-Y., 2006. Structure and electrochemical properties of FeS_x nanoparticles synthesized by chemical vapor condensation process. Mater. Sci. Forum. 510-511, 950-953.
- Hamilton, W.P., Bowers, A.R., 1997. Determination of acute Hg emissions from solidified/stabilized cement waste forms. Waste Manage. 17 (1), 25-32.
- Hansch, C., Leo, A., Hoekman, D., 1995. Exploring QSAR - Hydrophobic, electronic, and steric constants. American Chemical Society: Washington, DC.
- Hansel, J., 2002. EPA fish consumption advisories. Presentation at the mercury forum in Mobile on May 20-21, 2002. U.S. http://www.masgc.org/mercury/ppt/Hansel_ppt_files/frame.htm (accessed September 2005).
- Hatzinger, P.E., 2005. Perchlorate biodegradation for water. Environ. Sci. Technol. 39 (11), 239A-247A.

- Hazardous Waste Consultant, 1996. Remediating soil and sediment contaminated with heavy metals. Nov/Dec, Elsevier Science, Netherlands.
- He, F., Zhao, D., 2005. Preparation and characterization of a new class of starch-stabilized bimetallic nanoparticles for degradation of chlorinated hydrocarbons in water. *Environ. Sci. Technol.* 39 (9), 3314-3320.
- He, F., Zhao, D., Liu, J., Roberts, C.B., 2007. Stabilization of Fe-Pd nanoparticles with sodium carboxymethyl cellulose for enhanced transport and dechlorination of trichloroethylene in soil and groundwater. *Ind. Engr. Chem. Res.* 46 (1), 29-34.
- He, F., Zhao, D., 2007a. Manipulating the size and dispersibility of zero-valent iron nanoparticles by use of carboxymethyl cellulose stabilizers. *Environ. Sci. Technol.* 41 (17); 6216-6221.
- He, F., Zhao, D., 2007b. Hydrodechlorination of trichloroethene using stabilized Fe/Pd nanoparticles: Reaction mechanism and effects of stabilizer and reaction conditions. *Water Res.* In review.
- He, J., Kunitake, T., Nakao, A., 2003. Facile in-situ synthesis of noble metal nanoparticles in porous cellulose fibers. *Chem. Mater.* 15 (23), 4401-4406.
- Helfferich, F., 1962. *Ion Exchange*. McGraw-Hill: New York.
- Henry, W.D., Zhao, D., Lange, C., SenGupta, A.K., 2004. Preparation and characterization of a new class of polymeric ligand exchangers for selective removal of trace contaminants from water. *React. Funct. Polym.* 60, 109-120.
- Hintelmann, H., Hempel, M., Wilken, R.D., 1995. Observation of unusual organic mercury species in soils and sediments of industrially contaminated sites. *Environ. Sci. Technol.* 29 (7), 1845-1850.

- Horold, S., Vorlop, K.-D., Tacke, T., Sell, M., 1993. Development of catalysts for a selective nitrate and nitrite removal from drinking water. *Catal. Today*. 17 (1-2), 21-30.
- Huang, C-P., Wang, H-W., Chiu, P-C., 1998. Nitrate reduction by metallic iron. *Water Res.* 32 (8), 2257-2264.
- Huang, Y.H., Zhang, T.C., 2004. Effects of low pH on nitrate reduction by iron powder. *Water Res.* 38 (11), 2631-2642.
- Huang, Y.H., Zhang, T.C., 2005. Enhancement of nitrate reduction in Fe⁰-packed columns by selected cations. *J. Environ. Eng.* 131 (4), 603-611.
- Hurley, K.D., Shapley, J.R., 2007. Efficient heterogeneous catalytic reduction of perchlorate in water. *Environ. Sci. Technol.* 41 (6), 2044-2049.
- Hyland, M.M., Jean, G.E., Bancroft, G.M., 1990. XPS and AES studies of Hg(II) sorption and desorption reactions on sulfide minerals. *Geochim. Cosmochim. Ac.* 54 (7), 1957-1967.
- James, R.O., Macnaughton, M.G., 1977. Adsorption of aqueous heavy metals on inorganic minerals. *Geochim. Cosmochim. Ac.* 41 (11), 1549-1555.
- Jay, J.A., Morel, F.M.M., Hemond, H.F., 2000. Mercury speciation in the presence of polysulfides. *Environ. Sci. Technol.* 34 (11), 2196-2200.
- Jean, G.E., Bancroft, G.M., 1986. Heavy metal adsorption by sulfide mineral surfaces. *Geochim. Cosmochim. Ac.* 50 (7), 1455-1463.
- Jeong, H.Y., 2005. Removal of heavy metals and reductive dechlorination of chlorinated organic pollutants by nanosized FeS. Ph.D. dissertation. Department of Civil and

Environmental Engineering, University of Michigan, Ann Arbor, Michigan,
U.S.A.

Jiang, G.-B., Shi, J.-B., Feng, X.-B., 2006. Mercury pollution in China. *Environ. Sci. Technol.* 40 (12), 3672-3678.

Johnson, T.L., Fish, W., Gorby, Y.A., Tratnyek, P.G., 1998. Degradation of carbon tetrachloride by iron metal: Complexation effects on the oxide surface. *J. Contam. Hydrol.* 29 (4), 379-398.

Johnson, T.L., Scherer, M.M., Tratnyek, P.G., 1996. Kinetics of halogenated organic compound degradation by iron metal. *Environ. Sci. Technol.* 30 (8), 2634-2640.

Johnson Matthey, 2006. Johnson Matthey SMOPEX® metal scavenger fibres.
<http://www.chemicals.matthey.com/pdfs/news/110.pdf> (accessed December 2006).

Kanel, S.R., Greneche, J.M., Choi, H., 2006. Arsenic(V) removal from groundwater using nano scale zero-valent iron as a colloidal reactive barrier material. *Environ. Sci. Technol.* 40 (6), 2045-2050.

Kielemoes, J., De Boever, P., Verstraete, W., 2000. Influence of denitrification on the corrosion of iron and stainless steel powder. *Environ. Sci. Technol.* 34 (4), 663-671.

Kim, J., Benjamin, M.M., 2004. Modeling a novel ion exchange process for arsenic and nitrate removal. *Water Res.* 38 (8), 2053-2062.

Kirk, A.B., Martinelango, P.K., Tian, K., Dutta, A., Smith, E.E., Dasgupta, P.K., 2005. Perchlorate and iodide in dairy and breast milk. *Environ. Sci. Technol.* 39 (7), 2011-2017.

- Korchev, A.S., Shulyak, T.S., Slaten, B.L., Gale, W.F., Mills, G., 2005. Sulfonated poly(ether ether ketone)/poly(vinyl alcohol) sensitizing system for solution photogeneration of small Ag, Au, and Cu crystallites. *J. Phys. Chem. B*, 109 (16), 7733-7745.
- Labelle, M.A., Juteau, P., Jolicoeur, M., Villemur, R., Parent, S., Comeau, Y., 2005. Seawater denitrification in a closed mesocosm by a submerged moving bed biofilm reactor. *Water Res.*, 39 (14), 3409-3017.
- Lambertsson, L., Nilsson, M., 2006. Organic material: the primary control on mercury methylation and ambient methyl mercury concentrations in estuarine sediments. *Environ. Sci. Technol.* 40 (6), 1822-1829.
- Langwaldt, J.H., Puhakka, J.A., 2000. On-site biological remediation of contaminated groundwater: A review. *Environmental Pollution*, 107 (2), 187-197.
- Lemaigen, L., Tong, C., Begon, V., Burch, R., Chadwick, D., 2002. Catalytic denitrification of water with palladium-based catalysts supported on activated carbons. *Catal. Today.* 75 (1-4), 43-48.
- Li, P., SenGupta, A.K., 1998. Genesis of selectivity and reversibility for sorption of synthetic aromatic anions onto polymeric sorbents. *Environ. Sci. Technol.* 32 (23), 3756-3766.
- Liou, Y.H., Lo, S.L., Lin, C.J., Hu, C.Y., Kuan, W.H., Weng, S.C., 2005a. Methods for accelerating nitrate reduction using zerovalent iron at near-neutral pH: Effects of H₂-reducing pretreatment and copper deposition. *Environ. Sci. Technol.* 39 (24), 9643-9648.

- Liou, Y.H., Lo, S.L., Lin, C.J., Kuan, W.H., Weng, S.C., 2005b. Chemical reduction of an unbuffered nitrate solution using catalyzed and uncatalyzed nanoscale iron particles. *J. Haz. Mater.* 127 (1-3), 102-110.
- Liu, R., Guo, J., Tang, H., 2002. Adsorption of fluoride, phosphate and arsenate ions on a new type of ion exchange fiber. *J. Colloid Interface Sci.* 248 (2), 268-274.
- Liu, Y., Majetich, S.A., Tilton, R.D., Sholl, D.S., Lowry, G.V., 2005. TCE dechlorination rates, pathways, and efficiency of nanoscale iron particles with different properties. *Environ. Sci. Technol.* 39 (5), 1338-1345.
- Logan, B.E., 2000. Assessing the outlook for perchlorate remediation. *Environ. Sci. Technol.* 35 (23), 482A-487A.
- Logan, B.E., Wu, J., Unz, R., 2001. Biological perchlorate reduction in high-salinity solutions. *Water Res.* 2001, 35 (12), 3034-3038.
- Logan, B.E., LaPoint, D., 2002. Treatment of perchlorate- and nitrate-contaminated groundwater in an autotrophic, gas phase, packed-bed bioreactor. *Water Res.* 36 (14), 3647-3653.
- Lowry, G.V., Liu, Y., 2006. Nanoiron: reactant or catalyst? In: Proceedings of the Division of Environmental Chemistry for the 232nd ACS National Meeting, San Francisco, CA, September 10-14, 2006.
- Lowson, R.T., 1982. Aqueous oxidation of pyrite by molecular oxygen. *Chem. Rev.* 82 (5), 461-497.
- Lu, Q., Gao, F., Komarneni, S., 2005. A green chemical approach to the synthesis of tellurium nanowires. *Langmuir.* 21 (13), 6002-6005.

- Magdassi, S., Bassa, A., Vinetsky, Y., Kamyshny, A., 2003. Silver nanoparticles as pigments for water-based ink-jet inks. *Chem. Mater.* 15 (11), 2208-2217.
- McMahon, P.B., Dennehy, K.F., Sandstrom, M.W., 1999. Hydraulic and geochemical performance of a permeable reactive barrier containing zero-valent iron. *Ground Water.* 37 (3), 396-404.
- Mehrotra, A.S., Horne, A.J., Sedlak, D.L., 2003. Reduction of net mercury methylation by iron in *Desulfobulbus propionicus* (1pr3) cultures: Implications for engineered wetlands. *Environ. Sci. Technol.* 37 (13), 3018-3023.
- Mehrotra, A.S., Sedlak, D.L., 2005. Decrease in net mercury methylation rates following iron amendment to anoxic wetland sediment slurries. *Environ. Sci. Technol.* 39 (8), 2564-2570.
- Mendiratta, S.K., Dotson, R.L., Brooker, R.T., 2000. Perchloric acid and perchlorates, Kirk-Othmer, *Encyclopedia of Chemical Technology*.
- Michel, K., Roose, M., Ludwig, B., 2007. Comparison of different approaches for modelling heavy metal transport in acidic soils. *Geoderma.* 140, 207-214.
- Mikami, I., Sakamoto, Y., Yoshinaga, Y., Okuhara, T., 2003. Kinetic and adsorption studies on the hydrogenation of nitrate and nitrite in water using Pd-Cu on active carbon support. *Appl. Catal.* 44 (1), 79-86.
- Min, B., Evans, P.J., Chu, A.K., Logan, B.E., 2004. Perchlorate removal in sand and plastic media bioreactors. *Water Res.* 38 (1), 47-60.
- Mishra, D., Farrell, J., 2005. Understanding nitrate reactions with zerovalent iron using Tafel analysis and electrochemical impedance spectroscopy. *Environ. Sci. Technol.* 39 (2), 645-650.

- Moore, A.M., De Leon, C.H., Young, T.M., 2003. Rate and extent of aqueous perchlorate removal by iron surfaces. *Environ. Sci. Technol.* 37 (14), 3189-3198.
- Moore, A.M., Young, T.M., 2005. Chloride interactions with iron surfaces: Implications for perchlorate and nitrate remediation using permeable reactive barriers. *J. Environ. Engr.* 131 (6), 924-933.
- Morse, J.W., Luther, G.W., 1999. Chemical influences on trace metal-sulfide interactions in anoxic sediments. *Geochim. Cosmochim. Ac.* 63 (19-20), 3373-3378.
- Mueller, D.K., Helsel, D.R., 1996. Nutrients in the nation's waters-too much of a good thing? U.S. Geological Survey: Reston, VA, U.S.
- National Research Council (NRC), 1994. Alternatives for ground water cleanup. National Academy Press, Washington, DC.
- Natural Resources Defense Council (NRDC), 2003. EPA's mercury proposal: More toxic pollution for a longer time. <http://www.nrdc.org/media/pressreleases/031205.asp> (accessed July 2005).
- Nolan, B.T., Ruddy, B.C., Hitt, K.J., Helsel, D.R., 1997. Risk of nitrate in groundwaters of the United States-A national perspective. *Environ. Sci. Technol.* 31 (8), 2229-2236.
- Nuhoglu, A., Pekdemir, T., Yildiz, E., Keskinler, B., Akay, G., 2002. Drinking water denitrification by a membrane bio-reactor. *Water Res.* 36 (5), 1155-1166.
- Oh, S.Y., Chiu, P.C., Kim, B.J., Cha, D.K., 2006a. Enhanced reduction of perchlorate by elemental iron at elevated temperatures. *J. Hazard. Mater.* 129 (1-3), 304-307.

- Oh, S.Y., Cha, D.K., Chiu, P.C., Kim, B.J., 2006b. Zero-valent iron treatment of RDX-containing and perchlorate-containing wastewaters from an ammunition-manufacturing plant at elevated temperatures. *Water Sci. Technol.* 54 (10), 47-53.
- Okeke, B.C., Giblin, T., Frankenberger, W.T., 2002. Reduction of perchlorate and nitrate by salt tolerant bacteria. *Environmental Pollution*. 118 (3), 357-363.
- Paknikar, K.M., Nagpal, V., Pethkar, A.V., Rajwade, J.M., 2005. Degradation of lindane from aqueous solutions using iron sulfide nanoparticles stabilized by biopolymers. *Sci. Technol. Adv. Mat.* 6 (3-4), 370-374.
- Paquette K.E., Helz, G.R., 1997. Inorganic speciation of mercury in sulfidic waters: The importance of zero-valent sulfur. *Environ. Sci. Technol.* 31 (7), 2148-2153.
- Parette, R., Cannon, F.S., Weeks, K., 2005. Removing low ppb level perchlorate, RDX, and HMX from groundwater with cetyltrimethylammonium chloride (CTAC) pre-loaded activated carbon. *Water Res.* 39 (19), 4683-4692.
- Passouaud, M., Bollinger, J.C., Laccour, S., 2000. Water nitrate removal with ion-exchanger grafted textiles. *Environ. Technol.* 21 (7), 745-753.
- Peel, J.W., Reddy, K.J., Sullivan, B.P., Bowen, J.M., 2003. Electrocatalytic reduction of nitrate in water. *Water Res.* 37 (10), 2512-2519.
- Peyton, B.M., Mormile, M.R., Petersen, J.N., 2001. Nitrate reduction with halomonas Campisalis: Kinetics of denitrification at pH 9 and 12.5 % NaCl. *Water Res.* 35 (17), 4237-4242.
- Phillips, D.H., Gu, B., Watson, D.B., 2000. Performance evaluation of a zerovalent iron reactive barrier: mineralogical characteristics. *Environ. Sci. Technol.* 34 (19), 4169-4176.

- Piao, H., 2002. Stabilization of Mercury-containing waste using sulfide. Ph. D. dissertation. Department of Civil and Environmental Engineering, University of Cincinnati, Cincinnati, Ohio, U.S.A.
- Piver, W.T., 1992. Contamination and restoration of groundwater aquifers. *Environ. Health. Perspect.* 100, 237-247.
- Prinz, H., Strehblow, H.H., 1998. Investigations on pitting corrosion of iron in perchlorate electrolytes. *Corros. Sci.* 40 (10), 1671-1683.
- Pye, V., Patrick, R. 1983. Ground water contamination in the United States. *Science.* 221 (4612), 713-718.
- Qian, X.F., Yin, J., Yang, Y.F., Lu, Q.H., Zhu, Z.K., Lu, J., 2001. Polymer-inorganic nanocomposites prepared by hydrothermal method: Preparation and characterization of PVA-transition-metal sulfides. *J. Appl. Polym. Sci.* 82 (11), 2744-2749.
- Rautenbach, R., Kopp, W., Hellekes, R., Teter, R., Van Opbergen, G., 1986. Separation of nitrate from well water by membrane processes (reverse osmosis/electrodialysis reversal). *Aqua.* 5, 279-282.
- Riddle, S.G., Tran, H.H., Dewitt, J.G., Andrews, J.C., 2002. Field, laboratory, and X-ray absorption spectroscopic studies of mercury accumulation by water hyacinths. *Environ. Sci. Technol.* 36 (9), 1965-1970.
- Rikken, G.B., Kroon, A.G.M., vanGinkel, C.G., 1996. Transformation of (per)chlorate into chloride by a newly isolated bacterium: Reduction and dismutation. *Appl. Microbiol. Biotechnol.* 45 (3), 420-426.

- Sanchez, C.A., Crump, K.S., Krieger, R.I., Khandaker, N.R., Gibbs, J.P., 2005. Perchlorate and nitrate in leafy vegetables of North America. *Environ. Sci. Technol.* 39 (24), 9391-9397.
- Sanchez, C.A., Krieger, R.I., Khandaker, N., Valentin-Blasini, L., Blount, B.C., 2006. Potential perchlorate exposure from Citrus sp. irrigated with contaminated water. *Anal. Chim. Acta.* 567 (1), 33-38.
- Sarma, T.K., Chattopadhyay, A., 2004. Reversible encapsulation of nanometer-size polyaniline and polyaniline-Au-nanoparticle composite in starch. *Langmuir*, 20 (11), 4733-4737.
- Schreier, C.G., Reinhard, M., 1995. Catalytic hydrodehalogenation of chlorinated ethylenes using palladium and hydrogen for the treatment of contaminated water. *Chemosphere*, 31 (6), 3475-3487.
- SenGupta, A.K., Clifford, D., 1986. Some unique characteristics of chromate ion exchange. *React. Polym.* 4 (2), 113-130.
- Shi, X., Sun, K., Balogh, L.P., Baker, J.R. Jr., 2006. Synthesis, characterization, and manipulation of dendrimer-stabilized iron sulfide nanoparticles. *Nanotechnology*, 17 (18), 4554-4560.
- Shim, I.W., Choi, S., Noh, W.T., Kwon, J., Cho, J.Y., Chae, D.Y., Kim, K.S., 2001. Preparation of iron nanoparticles in cellulose acetate polymer and their reaction chemistry in the polymer. *Bull. Korean Chem. Soc.* 22 (7), 772-774.
- Shim, I.W., Noh, W.T., Kwon, J., Cho, J.Y., Kim, K.S., Kang, D.H., 2002. Preparation of copper nanoparticles in cellulose acetate polymer and the reaction chemistry of copper complexes in the polymer. *Bull. Korean Chem. Soc.* 23 (4), 563-566.

- Si, S., Kotal, A., Mandal, T., Giri, S., Nakamura, H., Kohara, T., 2004. Size-controlled synthesis of magnetite nanoparticles in the presence of polyelectrolytes. *Chem. Mater.* 16, 3489-3496.
- Siantar, D.P., Schreier, C.G., Chou, C.-S., Reinhard, M., 1996. Treatment of 1,2-dibromo-3-chloropropane and nitrate-contaminated water with zero-valent iron or hydrogen/palladium catalysts. *Water Res.* 30 (10), 2315-2322.
- Skyllberg, U., Bloom, P.R., Qian, J., Lin, C.-M., Bleam, W.F., 2006. Complexation of mercury(II) in soil organic matter: EXAFS evidence for linear two-coordination with reduced sulfur groups. *Environ. Sci. Technol.* 40 (13), 4174-4180.
- Smith, P.N., Yu, L., McMurry, T., Anderson, T.A., 2004. Perchlorate in water, soil, vegetation, and rodents collected from the Las Vegas wash Nevada, USA. *Environ. Pollut.* 132 (1), 121-127.
- Smith, R.L., Buckwalter¹, S.P., Repert, D.A., Miller, D.N., 2005. Small-scale, hydrogen-oxidizing-denitrifying bioreactor for treatment of nitrate-contaminated drinking water. *Water Res.* 39 (10), 2014-2023.
- Snyder, S.A., Vanderford, B.J., Rexing, D.J., 2005. Trace analysis of bromate, chlorate, iodate, and perchlorate in natural and bottled waters. *Environ. Sci. Technol.* 39 (12), 4586-4593.
- Sohn, K., Kang, S.W., Ahn, S., Woo, M., Yang, S.-K., 2006. Fe(0) nanoparticles for nitrate reduction: Stability, reactivity, and transformation. *Environ. Sci. Technol.* 40 (17), 5514-5519.
- Sorenson, J., Thorling, L., 1991. Stimulation by lepidocrocite (γ -FeOOH) of Fe(II)-dependent nitrite reduction. *Geochim. Cosmochim. Acta.* 55, 1289-1294.

- Sridhar, S., Collette, T.W., Garrison, A.W., Wolfe, N.L., McCutcheon, S.C., 1999. Perchlorate identification in fertilizers. *Environ. Sci. Technol.* 33 (19), 3469-3472.
- Stein, E.D., Cohen, Y., Winer, A.M., 1996. Environmental distribution and transformation of mercury compounds. *Crit. Rev. Env. Sci. Technol.* 26 (1), 1-43.
- Su, C., Puls, R.W., 2004. Nitrate reduction by zerovalent iron: Effects of formate, oxalate, citrate, chloride, sulfate, borate, and phosphate. *Environ. Sci. Technol.* 38 (9), 2715-2720.
- Susalar, S., Collette, T.W., Garrison, A.W., Wolfe, N.L., McCutcheon, S.C., 1999. Perchlorate identification in fertilizers. *Environ. Sci. Technol.* 33 (19), 3469-3472.
- Sznopak, J.L., Goonan, T.G., 2002. The materials flow of mercury in the economies of the United States and the world. Presentation at the mercury forum in Mobile on May 20-21, 2002. http://www.masgc.org/mercury/ppt/Moore-ppt_files/frame.htm (accessed September 2005).
- Tripp, A.R., Clifford, D.A., 2000. The treatability of perchlorate in groundwater using ion-exchange technology. In: *Perchlorate in the Environment*. Urbansky, E.T. Kluwer Academic/Plenum Publishers: New York. 123-134.
- Tripp, A.R., Clifford, D.A., 2004. Selectivity considerations in modeling the treatment of perchlorate using ion-exchange processes. *Ion Exchange and Solvent Extraction*. 16, 267-338.
- Tripp, A.R., Clifford, D.A., 2006. Ion exchange for the remediation of perchlorate-contaminated drinking water. *J. AWWA*. 98 (4), 105-114.

- United Nation Environmental Programme (UNEP), 2002. Global mercury assessment. Report no.54790.01. <http://www.chem.unep.ch/mercury/report/1stdraft-report.htm>, assessed on 12 April 2007
- Urbansky, E.T., 1998. Perchlorate chemistry: Implications for analysis and remediation. *Biorem. J.* 2 (2), 81-95.
- Urbansky, E.T., Magnuson, M.L., Kelty, C.A., Brown, S.K., 2000. Perchlorate uptake by Salt Cedar (*Tamarix ramosissima*) in the Las Vegas wash riparian ecosystem. *Sci. Total Environ.* 256 (2-3), 227-232.
- United States Environmental Protection Agency (U.S. EPA), 1995. Drinking water regulations and health advisories. Washington, DC.
- United States Environmental Protection Agency (U.S. EPA), 1997. Mercury report to congress. EPA-452/R-97-005, Office of Air Quality Planning and Standards, Office of research and development, Washington, DC.
- United States Environmental Protection Agency (U.S. EPA), 2005. EPA sets reference dose for perchlorate. <http://yosemite.epa.gov/opa/admpress.nsf/b1ab9f485b098972852562e7004dc686/c1a57d2077c4bfda85256fac005b8b32!OpenDocument> (accessed December 2005).
- United States Environmental Protection Agency (U.S. EPA), 2007. Groundwater contamination. <http://www.epa.gov/superfund/students/wastsite/grndwatr.htm> (accessed August 2007).
- U.S. Government Accountability Office (U.S. GAO), 2005. Perchlorate: A system to track sampling and cleanup results is needed. GAO-05-462. <http://www.gao.gov/cgi-bin/getrpt?GAO-05-462> (accessed August 2006).

- U.S. Government Accountability Office (U.S. GAO), 2006. Perchlorate: A system to track sampling and cleanup results is needed. <http://www.gao.gov/cgi-bin/getrpt?GAO-05-462> (accessed August 2006).
- Van der Hoek, J.P., Latour, P.J.M., Klapwijk, A., 1987. Denitrification with methanol in the presence of high salt concentrations and at high pH levels. *Appl. Microb. Biotech.* 27 (2), 199-205.
- Van der Hoek, J.P., Van der Hoek, W.F., Klapwijk, A., 1988. Nitrate removal from ground water: use of a nitrate selective resin and a low concentrated regenerant. *Water Air Soil Poll.* 37 (1-2), 41-53.
- Wagner-Döbler, I., von Canstein, H., Li, Y., Timmis, K.N., Deckwer, W.D., 2000. Removal of mercury from chemical wastewater by microorganisms in technical scale. *Environ. Sci. Technol.* 34 (21), 4628-4634.
- Wang, C.B., Zhang, W.X., 1997. Synthesizing nanoscale iron particles for rapid and complete dechlorination of TCE and PCBs. *Environ. Sci. Technol.* 31 (7), 2154-2156.
- Ward, M.H., Mark, S.D., Cantor, K.P., Weisenburger, D.D., Correa-Villaseñor, A., Zahm, S.H., 1996. Drinking water nitrate and the risk of Non-Hodgkin's Lymphoma. *Epidemiology*, 7 (5), 465-471.
- Watson, J.H.P., Ellwood, D.C., Soper, A.K., Charnock, J., 1999. Nanosized strongly-magnetic bacterially-produced iron sulfide materials. *J. Magn. Magn. Mater.* 203 (1), 69-72.
- Watson, J.H.P., Cressey, B.A., Roberts, A.P., Ellwood, D.C., Charnock, J.M., Soper, A.K., 2000. Structural and magnetic studies on heavy-metal-adsorbing iron sulphide

- nanoparticles produced by sulphate-reducing bacteria. *J. Magn. Magn. Mater.* 214 (1-2), 13-30.
- Wiesner, M.R., Lowry, G.V., Alvarez, P., Dionysiou, D., Biswas, P., 2006. Progress and research needs towards assessing the risks of manufactured nanomaterials. *Environ. Sci. Technol.*, 40 (14), 4336-4345.
- Wilcoxon, J.P., Newcomer, P.P., Samara, G.A., 1996. Strong quantum confinement effects in semiconductors: FeS₂ nanoclusters. *Solid State Commun.* 98 (6), 581-585.
- Wilkin, R.T., Su, C., Ford, R.G., Paul, C.J., 2005. Chromium-removal processes during groundwater remediation by a zerovalent iron permeable reactive barrier. *Environ. Sci. Technol.* 39 (12), 4599-4605.
- Wolff, J., 1998. Perchlorate and the thyroid gland. *Pharmac. Rev.* 50 (1), 89-105.
- Xia, K., Skyllberg, U.L., Bleam, W.F., Bloom, P.R., Nater, E.A., Helmke, P.A., 1999. X-ray absorption spectroscopic evidence for the complexation of Hg(II) by reduced sulfur in soil humic substances. *Environ. Sci. Technol.* 33 (2), 257-261.
- Xiong, Z., Dimick, P., Zhao, D., Kney, A., Tavakoli, J., 2006. Removal of perchlorate from contaminated water using a regenerable polymeric ligand exchanger. *Separ. Sci. Tech.* 41 (11), 2555-2574.
- Xiong, Z., Zhao, D., Harper, W.F., 2007a. Sorption and desorption of perchlorate with various classes of ion-exchangers: A comparative study. *Ind. Eng. Chem. Res.* in press.
- Xiong, Z., Zhao, D., Pan, G., 2007b. Rapid and complete destruction of perchlorate in water and ion-exchange brine using stabilized zero-valent iron nanoparticles. *Water Res.* 41 (15), 3497-3505.

- Xiong, Z., Zhao, D., Pan, G., 2007c. Rapid transformation of nitrate in water and ion exchange brine by stabilized zero-valent iron nanoparticles. *J. Nanopart. Res.* in review.
- Xiong, Z., Zhao, D., He, F., Barnett, M.O., Harper, W.F., 2007d. *In-situ* mercury immobilization in sediment by stabilized iron sulfide nanoparticles. To be submitted to *Environ. Sci. Technol.*
- Xu, J., Song, Y., Min, B., Steinberg, L., Logan, B.E., 2003. Microbial degradation of perchlorate: Principles and applications. *Environ. Eng. Sci.* 20 (5), 405-422.
- Yang, G.C., Lee, H.L., 2005. Chemical reduction of nitrate by nanosized iron: Kinetics and pathways. *Water Res.* 39 (5), 884-894.
- Yoon, J., Yoon, Y., Amy, G., Cho, J., Foss, D., Kim, T.H., 2003. Use of surfactant modified ultrafiltration for perchlorate (ClO_4^-) removal. *Water Res.* 37 (9), 2001-2012.
- Zhang, W.X., Wang, C.B., Lien, H.L., 1998. Treatment of chlorinated organic contaminants with nanoscale bimetallic particles. *Catal. Today.* 40 (4), 387-395.
- Zhang, T.C., Huang, Y.H., 2005. Effects of selected Good's pH buffers on nitrate reduction by iron powder. *J. Environ. Eng.* 131 (3), 461-470.
- Zhao, D., 1997. Polymeric ligand exchange: A new approach toward enhanced separation of environmental contaminants. Ph.D. Dissertation, Department of Civil and Environmental Engineering, Lehigh University, Bethlehem, PA.
- Zhao, D., SenGupta, A.K., 1998. Ultimate removal of phosphate from wastewater using a new class of polymeric ion exchangers. *Water Res.* 32 (5), 1613-1625.
- Zhao, D., Sengupta, A.K., 2000. Ligand separation with a Cu(II)-loaded polymeric ligand

- exchanger. *Ind. Eng. Chem. Res.* 39 (2), 455-462.
- Zhao, D., He, F., 2004. Preparation and application of a new class of stabilized bimetallic nanoparticles for dechlorination of chlorinated hydrocarbons in soils and water. U.S. Patent Pending (# 60/584,063).
- Zhao, D., Steinwinder, T., An, B., Barnett, M.O., Kramer, T., 2006. Developing a new class of ion exchangers for selective removal of arsenic and exploring an engineered approach for treatment and reuse of spent regenerant brine and for enhanced stability of process waste Residuals, WERC and AWWA Research Foundation, Denver, CO.
- Zhong, H., Wang, W-X., 2006. Sediment-bound inorganic Hg extraction mechanisms in the gut fluids of marine deposit feeders. *Environ. Sci. Technol.* 40 (19), 6181-6186.
- Zillioux, E.J., Porcella, D.B., Benoit, J.M., 1993. Mercury cycling and effects in freshwater wetland ecosystems. *Environ. Toxicol. Chem.* 12 (12), 2245-2264.

APPENDIX A ADDITIONAL EXPERIMENTAL RESULTS

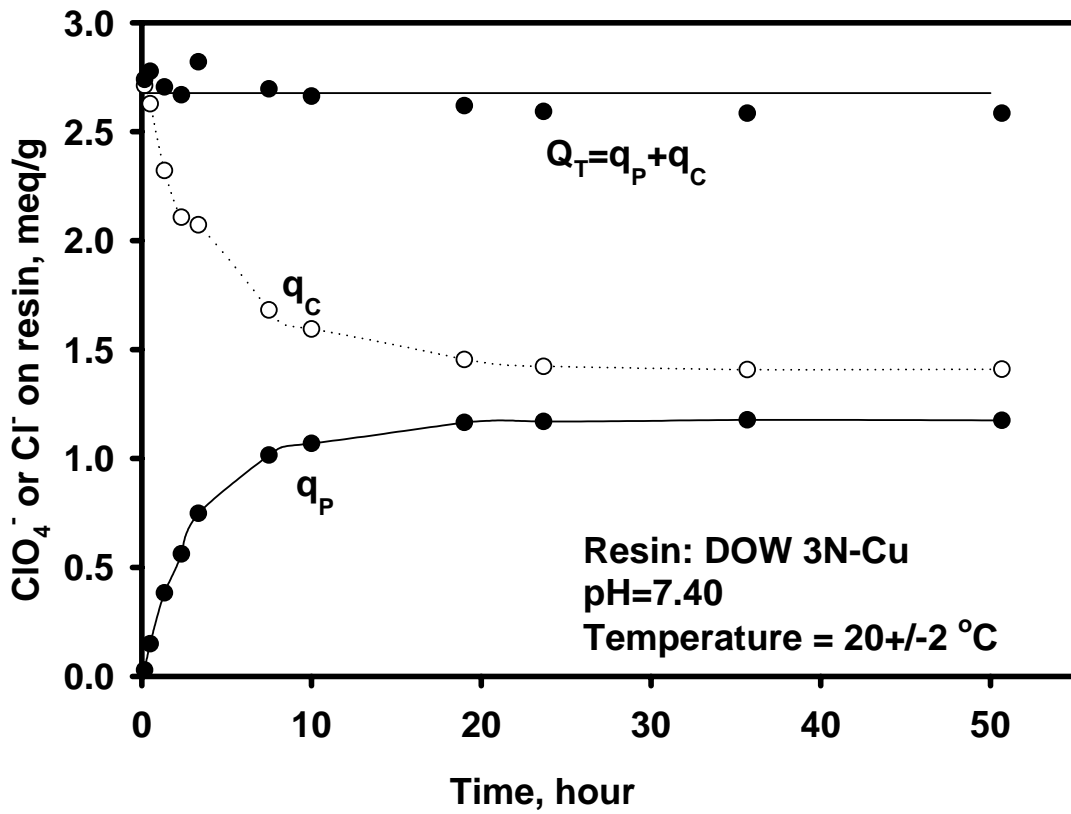


Figure A-1. Validation of ion-exchange stoichiometry with DOW3 N-Cu in perchlorate-chloride system.

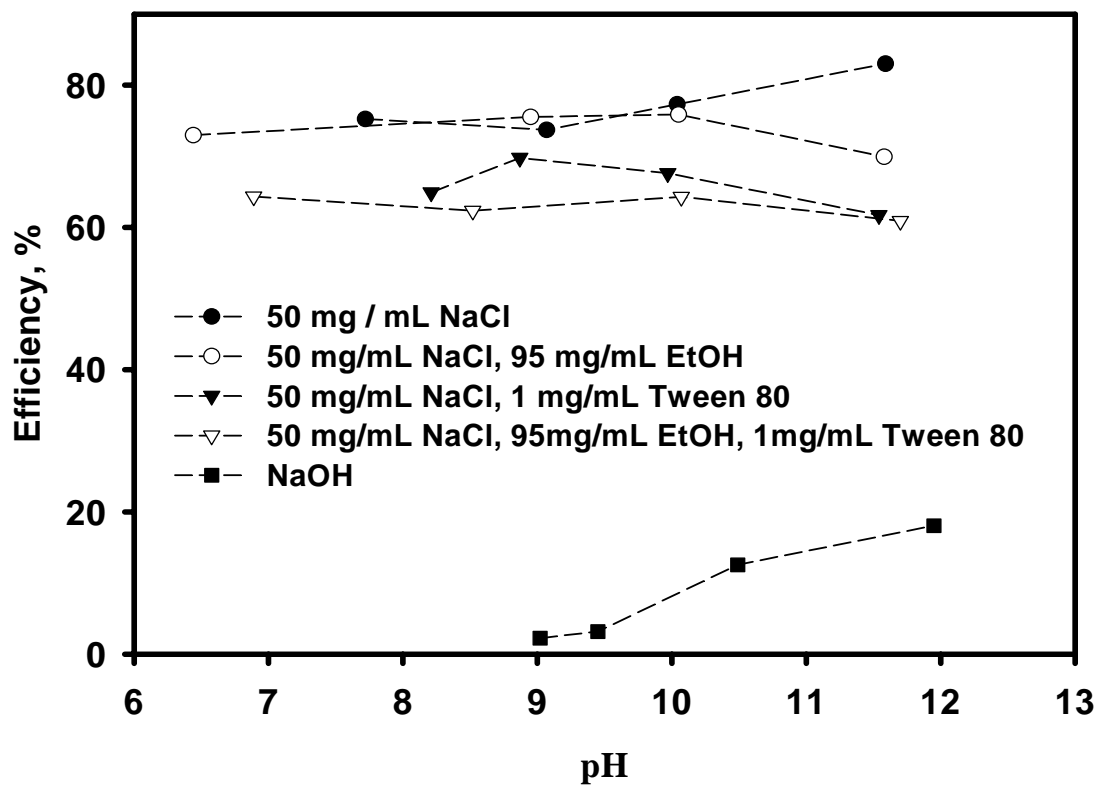


Figure A-2. Plot of regeneration efficiency of exhausted DOW 3N-Cu versus pH grouped by regenerant.

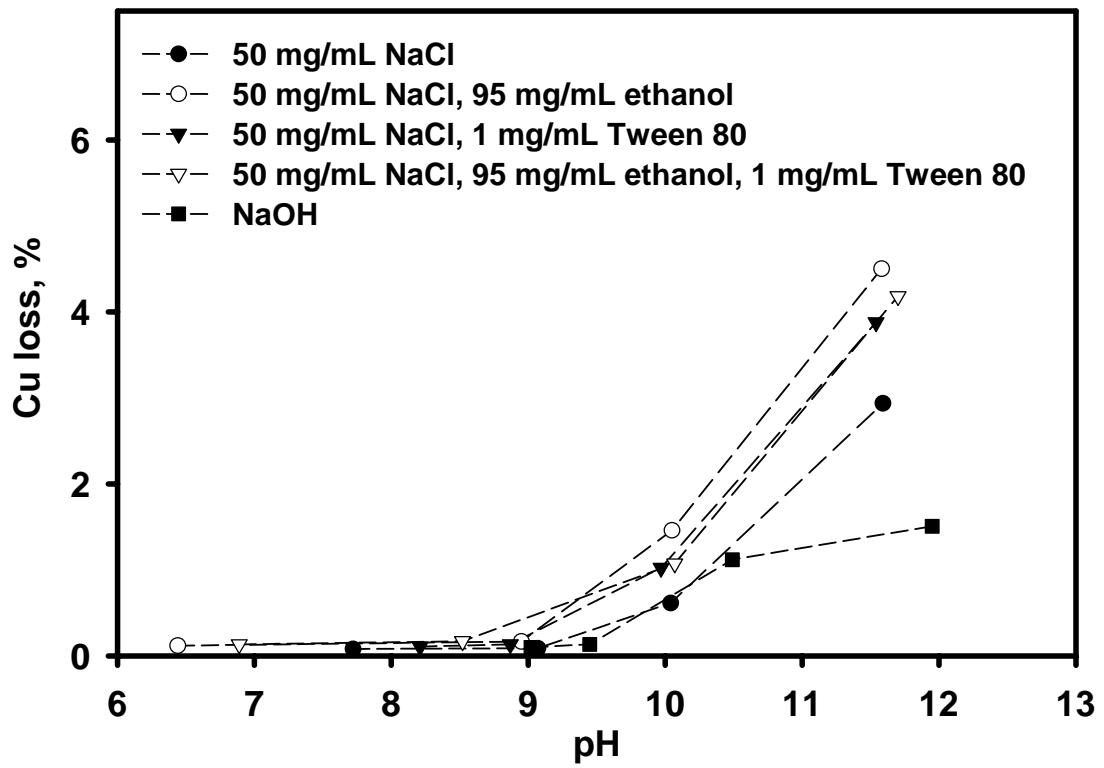


Figure A-3. Plot of percent Cu loss from DOW 3N-Cu versus pH for different regenerants.

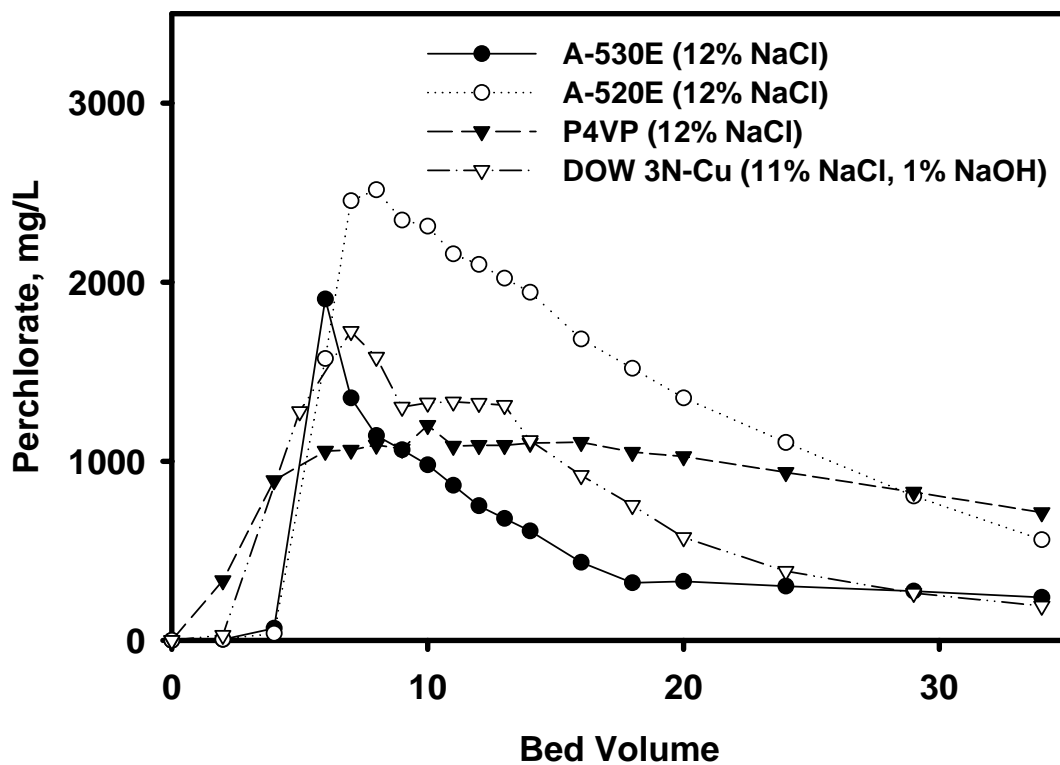


Figure A-4. Perchlorate elution curves for the regeneration of DOW 3N-Cu, A-530E, A-520E, and P4VP with 12% brines or 11% NaCl/1% NaOH at an EBCT of 21 ± 1 minutes.

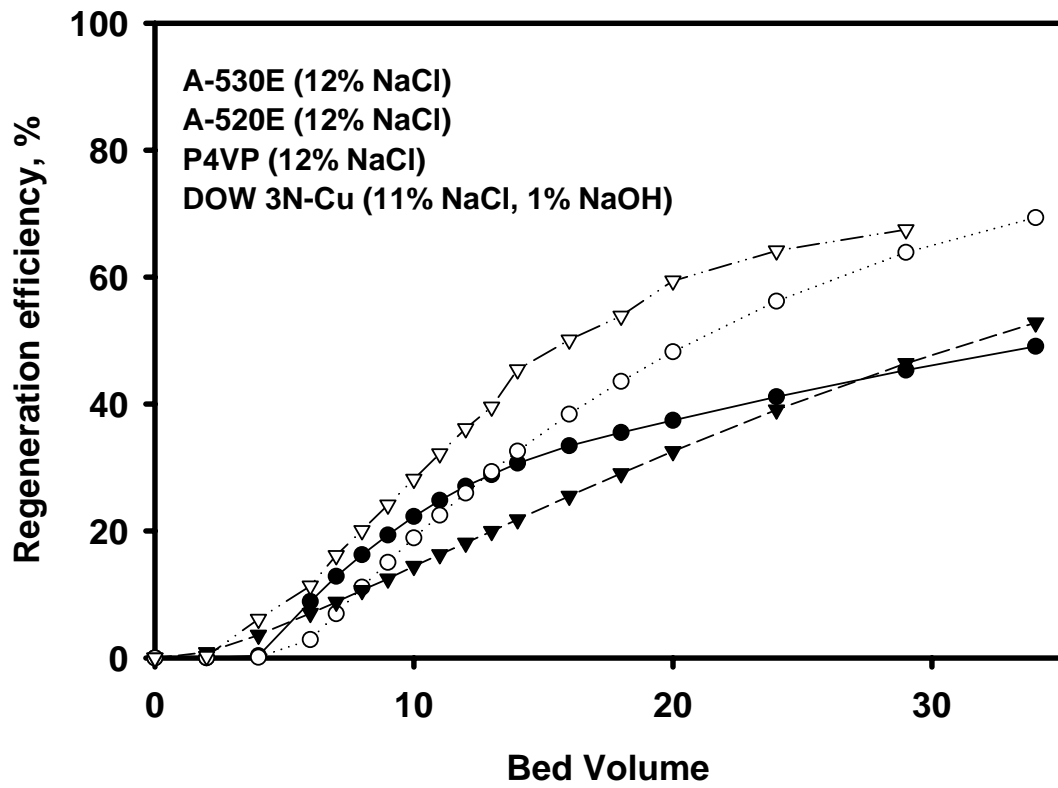


Figure A-5. Regeneration efficiency curves for DOW 3N-Cu, A-530E, A-520E, and P4VP with 12% brines and an EBCT of 21 ± 1 minutes.

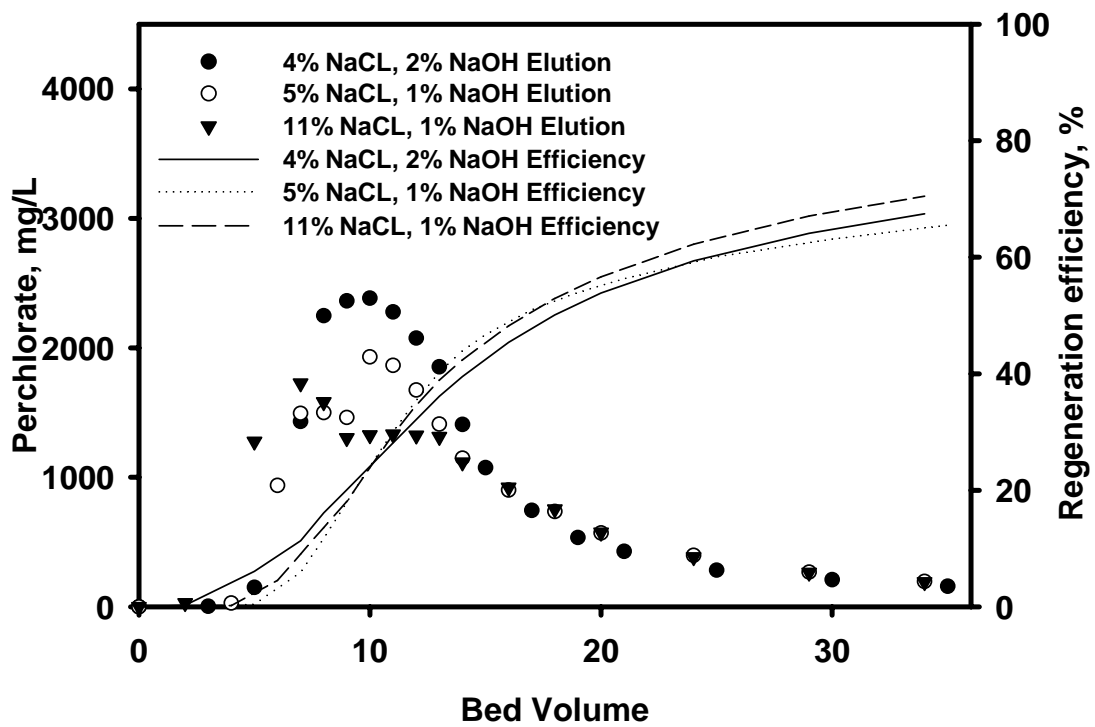


Figure A-6. DOW 3N-Cu regeneration breakthrough and efficiency curves varying salt brine composition regenerated at an EBCT of 20.4 ± 0.4 minutes.

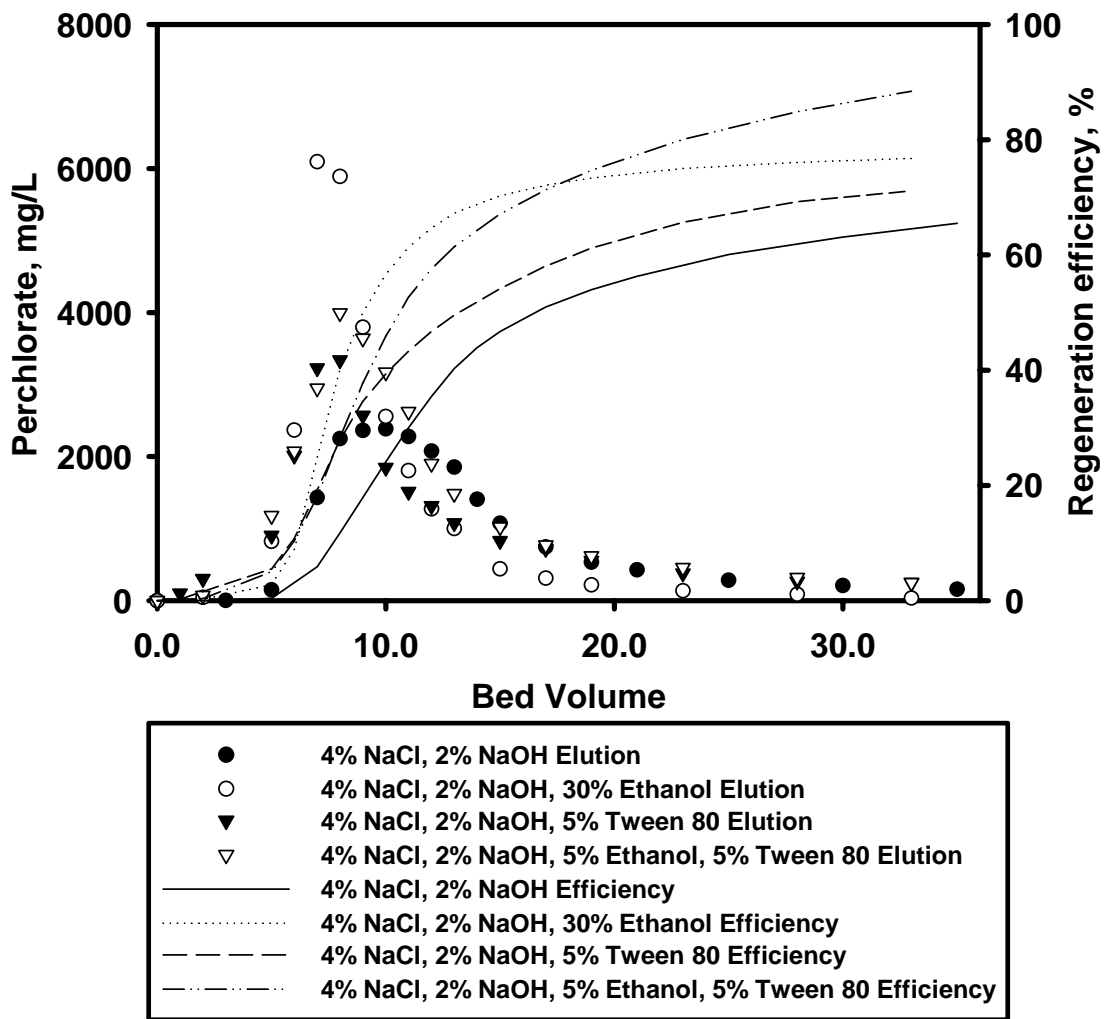


Figure A-7. Perchlorate elution and regeneration efficiency curves for DOW 3N-Cu with regenerate solutions composed of 4%NaCl, 2% NaOH and solvents containing a combination of water, Tween 80, and ethanol regenerated at an EBCT of 20.4 ± 0.4 minutes.

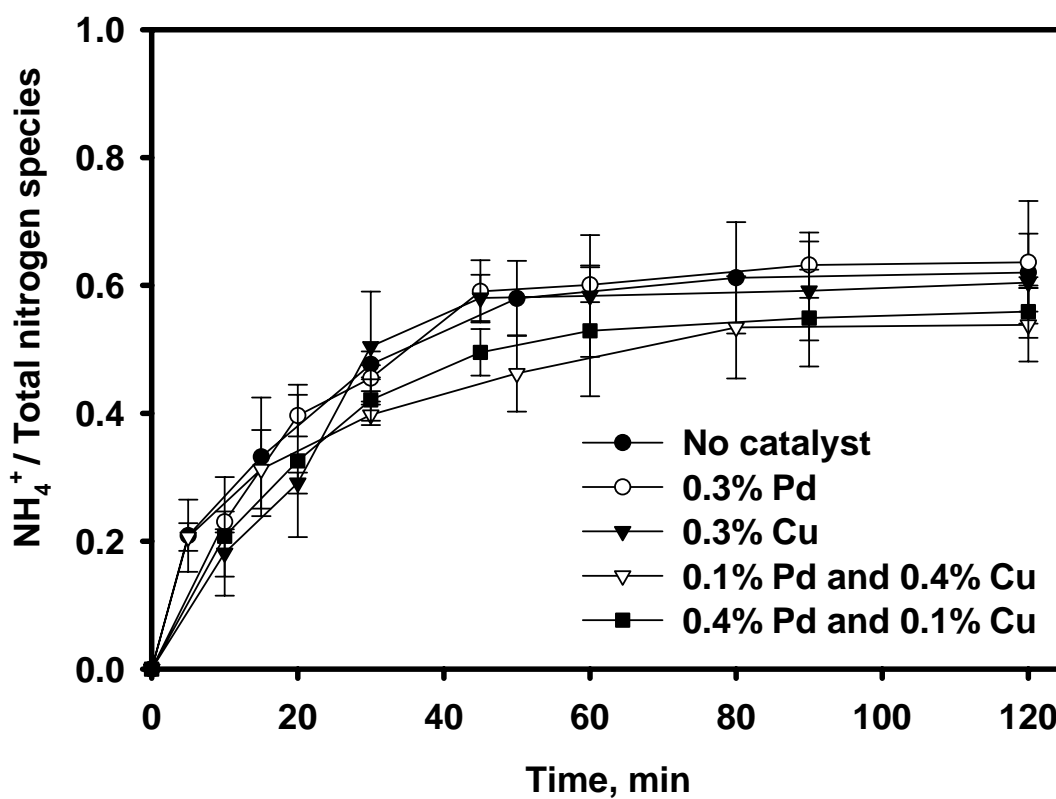


Figure A-8. Catalyst effect on ammonium production during nitrate reduction by CMC-stabilized ZVI nanoparticles. Initial nitrate concentration = 200 mg/L, ZVI = 0.7 g/L (ZVI-to- NO_3^- = 3.9), CMC = 0.63%. Solution pH was controlled at 7.0~7.5 (initial and final) with a 0.05 M HEPES buffer. Data plotted as mean of duplicates, and errors refer to standard deviation.

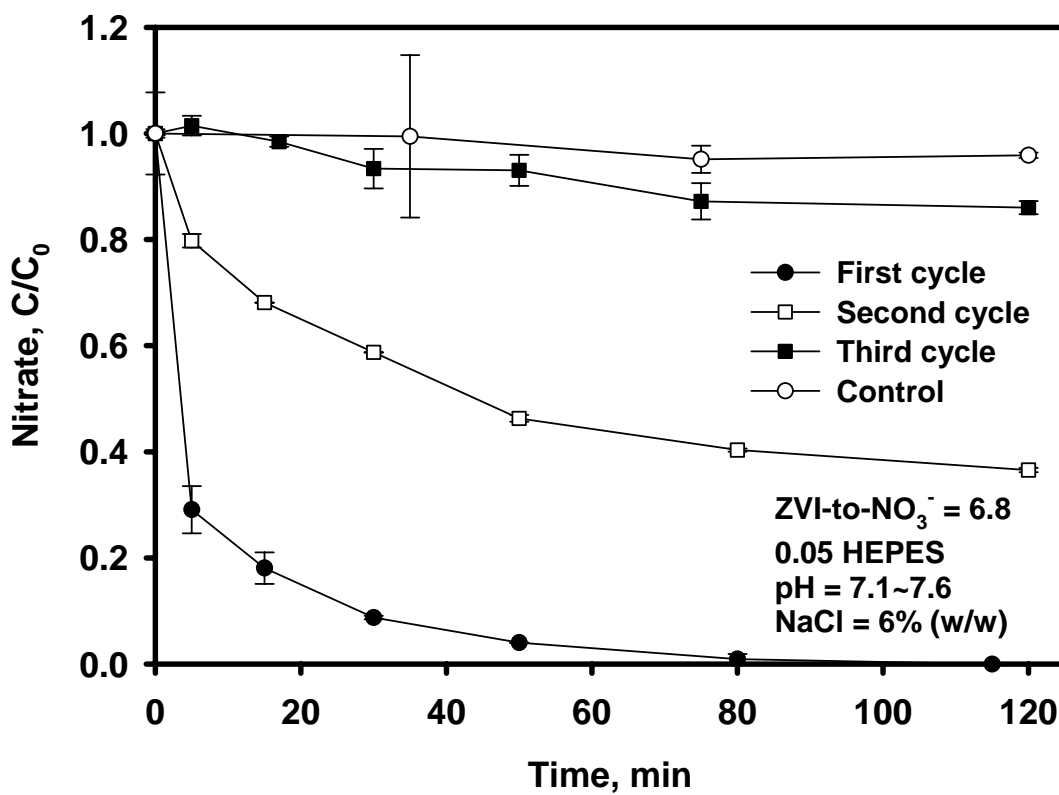


Figure A-9. Reuse of oxidized ZVI nanoparticles for nitrate reduction in the presence of 6% (w/w) NaCl. A stoichiometric amount of $NaBH_4$ was added to produce ZVI nanoparticles after each cycle.

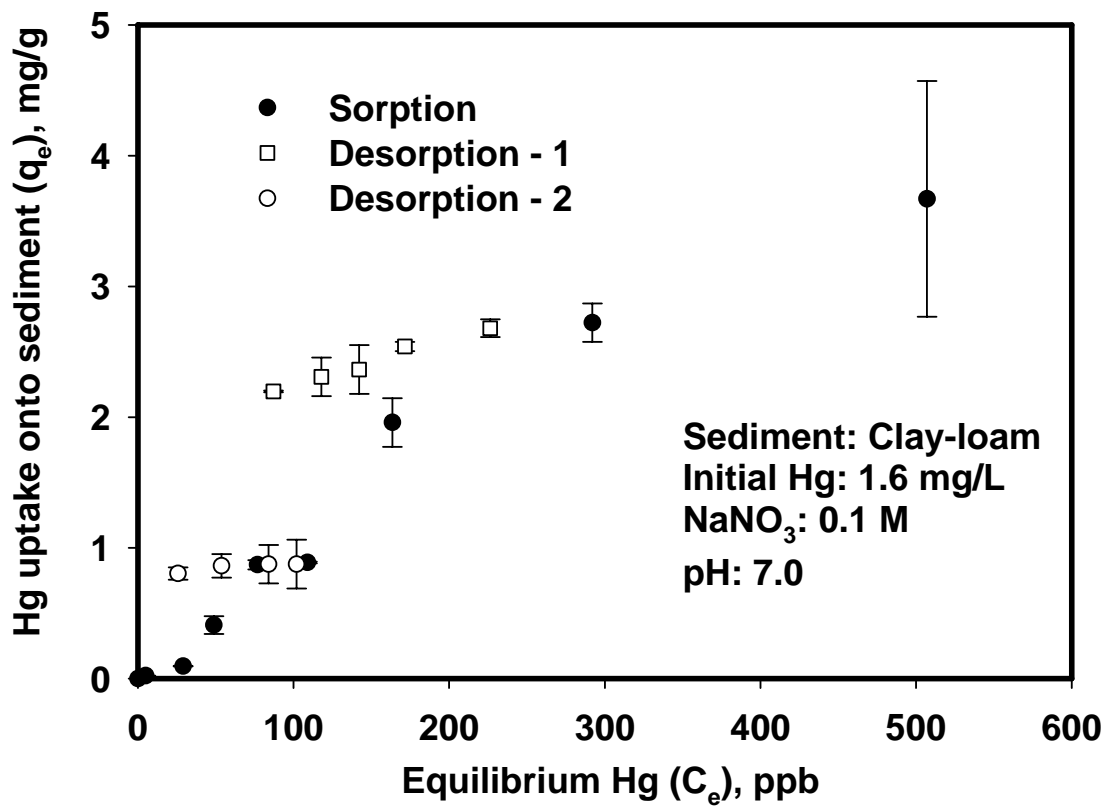


Figure A-10. Hysteresis of mercury adsorption onto clay-loam sediment.

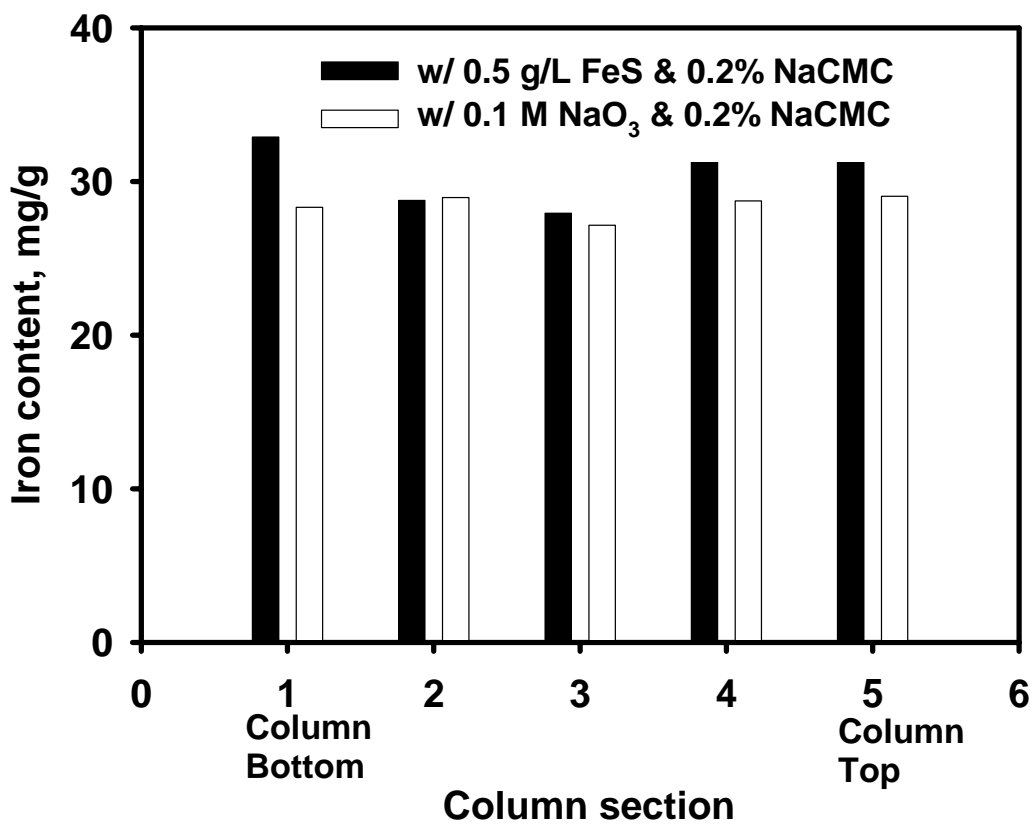


Figure A-11. Iron content in a clay-loam sediment column treated with 0.5 g/L FeS(s) stabilized with 0.2% NaCMC or a solution containing 0.1 M NaNO₃ and 0.2% NaCMC.

APPENDIX B KINETIC MODELING OF PERCHLORATE UPTAKE BY DOW 3N-

CU

Program DOW3NCu kinetic

! This program is to calculate the limited volume solution by Crank
! for DOW 3N-Cu in the presence of sulfate.
! Notation:
! PK: partition coefficient (q/C (mg/g)/(mg/L))
! Unit: q-mg/g; C-mg-P/L; D-cm²/min; t-min; a-cm ; V-L

integer m, k
real fmid, t, qn, qq, term, sum, root(1000), x1, dx
real x0, x2, alpha, Frac, M0, Mt, Ct, C0, V

Parameter (pi=3.141592694)

Data a/0.022/, D/2.5E-7/, alpha/0.5863/, M0/0.5792/, V/1.0/
Data C0/0.9188/

Fun(z)= tan(z)-3*z/(3+alpha*z**2)

! alpha=3*V/(4*pi*a**3*PK) use Minfinite/VC0=1/(1+alpha)

Open (Unit=100, FILE='OUTpaper0699.dat', STATUS='replace')

Write (10, *) 'Time (hour) Ct'

! Compute the roots using bisectional method

do 10 m=1, 1000

```

x1=float(2*(m-1)-1)*(pi/2)
if (m.eq.1) x1=0.
  x2=float(2*m-1)*(pi/2)
  root(m)=x1
  dx=x2-x1
  do 20 j=1, 200
dx=0.5*dx
  xmid=root(m)+dx
  fmid=Fun(xmid)
  if (fmid.lt.0.0) root(m)=xmid
  if (ABS(dx).lt.1e-10) goto 10
  if (fmid.eq.0.0) goto 10

20  continue

10  continue

!  the series solution

DO 50 k=0, 100, 1

sum=0.
  t=float(k)*60.0

  do 30 n=1, 500

    qn=root(n+1)
    qq=qn*qn
    term=6.0*alpha*(alpha+1.0)*exp(-D*qq*t/a**2.0)/(9.0+9.0*alpha+qq
& *alpha**2.0)

    sum=sum+term

    if (ABS(term).lt.ABS(sum/1.0E6)) goto 40

30  continue

40  Frac=1.0-sum

Mt=M0*Frac

if (k.LE.3) then

```

```

V=1.0-0.0015
elseif ((k.GT.3).AND.(k.LE.6)) then
V=1.0-0.003
elseif ((k.GT.6).AND.(k.LE.12)) then
V=1-0.0045
elseif ((k.GT.12).AND.(k.LE.20)) then
V=1-0.006
elseif ((k.GT.20).AND.(k.LE.30)) then
V=1-0.0075
elseif ((k.GT.30).AND.(k.LE.40)) then
V=1-0.0090
elseif ((k.GT.40).AND.(k.LE.50)) then
V=1-0.0105
elseif ((k.GT.50).AND.(k.LE.60)) then
V=1-0.0120
elseif ((k.GT.60).AND.(k.LE.80)) then
V=1-0.0135
elseif ((k.GT.80).AND.(k.LE.100)) then
V=1-0.0150
elseif ((k.GT.100).AND.(k.LE.120)) then
V=1-0.0165
elseif ((k.GT.120).AND.(k.LE.140)) then
V=1-0.0180
elseif ((k.GT.140).AND.(k.LE.160)) then
V=1-0.0195
elseif ((k.GT.160).AND.(k.LE.180)) then
V=1-0.021
elseif (k.GT.180) then
V=1-0.0225
endif

Ct=C0-Mt/V+0.003

write(10, '(1X, I5, F20.5)') k, Ct

50 continue

close (100)
end

```